UNIVERSIDAD AUTÓNOMA DE MADRID

DEPARTMENT OF MOLECULAR BIOLOGY

FACULTY OF SCIENCES

Study of the functions of mammalian PrimPol protein *in vivo*

Marcos Díaz Muñoz

Doctoral thesis

Madrid, October 2016

DEPARTMENT OF MOLECULAR BIOLOGY

FACULTY OF SCIENCES

UNIVERSIDAD AUTÓNOMA DE MADRID

Study of the functions of mammalian PrimPol protein *in vivo*

Marcos Díaz Muñoz

Graduate in Biotechnology

This thesis, submitted for the degree of Doctor of Philosophy at the Universidad Autónoma de Madrid, has been completed in the DNA Replication Group at the Spanish National Cancer Research Centre (CNIO) under the supervision of **Dr. Juan Méndez Zunzunegui**.

This Thesis was supported by a "Formación de personal investigador" (FPI) fellowship (Ministerio de Economía y Competitividad).

Madrid, October 2016

Dr Juan Méndez Zunzunegui, head of the DNA Replication Group at the Spanish National Cancer Research Centre (CNIO)

CERTIFIES

That Mr. **Marcos Díaz Muñoz**, Graduate in Biotechnology by the Universitat de Lleida, has completed his Doctoral Thesis "Study of the functions of mammalian PrimPol protein *in vivo*" and meets the necessary requirements to obtain the PhD degree in Molecular Biosciences. To this purpose, he will defend his doctoral thesis at the Universidad Autónoma de Madrid. The thesis has been carried out under my direction and I hereby authorize it to be defended in front of the appropriate Thesis Tribunal.

I hereby issue this certificate in Madrid on Semptember 30th 2016

Juan Méndez Zunzunegui

PhD thesis Director

AGRADECIMIENTOS

En primer lugar, quería agradecer a Juan Méndez por haberme dado la oportunidad de realizar la tesis doctoral en su laboratorio, así como por la mentoría científica durante estos cuatro años. Quiero darte las gracias por el tiempo dedicado, todas las técnicas que he aprendido durante este tiempo, todas las discusiones científicas, correcciones en los trabajos, permitirme la asistencia a congresos, además de hacerme ganar un poco más de confianza en mi trabajo y en mí mismo. Agradezco mucho tu comprensión y paciencia en los momentos más complicados, siempre con amabilidad y predisposición.

Me gustaría agradecer también a Luis Blanco por la estrecha colaboración científica, su opinión experta, sus valiosas observaciones y por contagiarnos con su entusiasmo por la ciencia. Además, a Patricia Calvo y Alberto Díaz por la estrecha colaboración realizada.

Por supuesto, quiero agradecer también a mis compañeros de laboratorio, a los presentes y a los que ya se han ido. Primero quiero agradecer a Silvana Mourón que fue quién empezó el trabajo con PrimPol y del cuál yo he obtenido muchas de las herramientas utilizadas durante el desarrollo de esta tesis. Además de por compartir toda tu experiencia en el mundo científico conmigo. Gracias a Sara Rodríguez por todas las aportaciones y asesoramiento en la realización de esta tesis. También agradezco esta tesis a Silvia Álvarez por dedicarme su tiempo a enseñarme a trabajar con ratones y mucho del trabajo de poyata. A Sergio, Karolina, Dani y Sabela por sus críticas siempre constructivas y por la ayuda incondicional prestada.

Quiero también agradecer a todo el grupo de Dinámica Cromósomica. Ana Losada por todas las observaciones, predisposición por ayudar y discusiones científicas realizadas durante el trascurso de esta tesis. Miriam, Miguel, Magali, Aleks, Ana, Carmen y Sam por vuestro imput científico en los lab meetings y toda la ayuda que me habéis dado.

Agradezco a las Unidades Técnicas del CNIO. A la Unidad de Histopatología, Citometría y Confocal, Alba de Martino, Lola Martínez y Diego Megías, sin vuestra ayuda esta tesis no hubiera salido adelante. También quiero agradecer por su trabajo fundamental a Soraya Ruiz e Isabel Blanco por la manipulación diaria de los ratones.

Finalmente, quiero agradecer a mi familia y amigos por vuestro apoyo constante a pesar de la distancia. Por compartir mis éxitos y mis frustraciones, GRACIAS!

A mis padres y hermano

ABSTRACT

PRESENTACIÓN

ABSTRACT

During eukaryotic DNA replication, the replisome machinery slows down when the template DNA is damaged by endogenous or exogenous elements. To minimize the risk of fork collapse, "DNA damage tolerance" (DDT) mechanisms facilitate progression of DNA replication through damaged templates. A classical DDT response involves the use of DNA polymerases specialized in "translesion synthesis". An alternative DDT mechanism consists in the reinitiation of DNA synthesis downstream of the damaged DNA, leaving a short unreplicated gap to be repaired post-replicatively. This mechanism requires the repositioning of the replisome and a new priming event. In 2013, mammalian PrimPol protein was identified as the enzyme that mediates fork restart after different types of DNA lesions, including thymine photodimers caused by UV light. PrimPol is a member of the archaeal-eukaryotic primase (AEP) superfamily and is included in a clade of AEP proteins that contain both primase and polymerase activities. Recent studies confirmed a similar role for PrimPol at natural obstacles or difficult-to-replicate sites. Despite these antecedents, the contribution of PrimPol to maintaining genomic stability and its possible protective function against UV-induced DNA damage remained to be investigated.

In this thesis we have studied the functions of mouse PrimPol *in vivo*. In a first approach, we participated in a structure-function study designed to understand the functional importance of several conserved amino acids in the PrimPol family, including two variants presumably associated to pathology: Y89D and Y100H. This study led to the identification of two amino acids located within a conserved WFYY motif that are indispensable for PrimPol functionality.

In the second part of the thesis, we have studied the physiological consequences of PrimPol ablation in mammals using a KO mouse model. PrimPol$^{-/-}$ mice are viable but hypersensitive to UV-induced DNA damage. Without PrimPol, skin healing after UV irradiation is compromised due to inefficient cell proliferation in the epidermis, which is necessary to replace cells with damaged DNA. The absence of PrimPol also caused a higher incidence of UV-induced papillomas, gender-specific alopecia, obesity and the development of aggressive tumors. Our results underscore the importance of mammalian PrimPol for the maintenance of genomic stability and strongly suggest a tumor suppression function *in vivo.*

PRESENTACIÓN

Durante la replicación del DNA eucariótico, la maquinaria replicativa se ralentiza cuando el DNA molde ha sido dañado por causas exógenas o endógenas. Para minimizar el riesgo de colapso en las horquillas de replicación, los mecanismos de tolerancia al daño en el DNA (DDT) facilitan el proceso de replicación a través de moldes dañados. Un mecanismo clásico de DDT implica el uso de DNA polimerasas especializadas en síntesis "translesiva". Un mecanismo alternativo consiste en la reiniciación de la síntesis de DNA tras la lesión dejando un segmento de DNA sin replicar que será reparado post-replicativamente. Este mecanismo requiere el reposicionamiento del replisoma y un nuevo evento de "primado". En 2013, la proteína PrimPol humana fue identificada como el enzima responsable del reinicio de las horquillas ante diferentes tipos de lesiones en el DNA, incluyendo fotodímeros de timina causados por la luz ultravioleta (UV). PrimPol pertenece a la superfamilia de primasas de archaea y eukarya (AEP) y se incluye en un clado de proteínas AEP que contienen actividades primasa y polimerasa. Estudios recientes han confirmado una función similar para PrimPol ante obstáculos naturales en el genoma o puntos difíciles de replicar. A pesar de estos antecedentes, la contribución de PrimPol al mantenimiento de la estabilidad genómica y su posible función protectora ante el daño inducido por UV todavía no habían sido investigadas.

En esta tesis hemos estudiado las funciones de la proteína PrimPol *in vivo*. En primer lugar, hemos participado en un estudio de estructura-función diseñado para comprender la relevancia funcional de varios aminoácidos conservados en la familia PrimPol, inlcuyendo dos variantes presuntamente asociadas a patologías humanas: Y89D y Y100H. Este estudio condujo a la identificación de dos aminoácidos, localizados en el motivo conservado WFYY, que son indispensables para la funcionalidad de PrimPol.

En la segunda parte de la tesis, hemos estudiado las consecuencias fisiológicas de la pérdida de PrimPol en mamíferos utilizando un modelo KO murino. Los ratones PrimPol$^{-/-}$ son viables pero hipersensibles al daño inducido por UV. Sin PrimPol, el proceso de curación de la piel tras haber recibido una dosis alta de UV se ve comprometido debido a la ineficiente proliferación celular en la epidermis, que es necesaria para reemplazar las células dañadas. La ausencia de PrimPol también causó una incidencia mayor de papilomas, alopecia, obesidad y desarrollo de tumores agresivos. Nuestros resultados muestran la importancia de PrimPol en el mantenimiento de la estabilidad genómica y sugieren una función supresora de tumores *in vivo*.

TABLE OF CONTENTS

TABLE OF CONTENTS

ABBREVIATIONS

ABBREVIATIONS

(6,4)-pp	(6-4)pyrimidine-pyrimidone
8-oxo-G	8-hydroxyguanine, 8-oxoguanine
BAT	Brown adipose tissue
BER	Base excision repair
BrdU	5-Bromo-2'-deoxyuridine
CldU	5-Chloro-2'-deoxyuridine
CPD	Cyclobutane pyrimidine dimer
DDR	DNA damage response
DDT	DNA damage tolerance
dNTP	Deoxyribonucleotide triphosphate
DSB	Double strand break
FACS	Fluorescence activated cell sorting
FR	Fork rate
HCC	Hepatocellular carcinoma or hepatocarcinoma
HF	Hair follicle
H&E	Hematoxylin and Eosin
HR	Homologous recombination
HU	Hydroxyurea
ICL	Inter-strand crosslink
IdU	5-Iodo-2'-deoxyuridine
IF	Immunofluorescence
IFE	Interfollicular epidermis
IHC	Immunohistochemistry
MEF	Mouse embryonic fibroblast
MMR	Mismatch repair
mtSSB	Mitochondrial single-strand binding protein
NER	Nucleotide excision repair
NHEJ	Non-homologous end-joining
PFA	Paraformaldehyde
Pol	Polymerase
RPA	Replication protein A
RS	Replicative stress

SCC	Squamous cell carcinoma
SCE	Sister Chromatid Exchange
TLS	Translesion synthesis
TPA	12-O-tetradecanoylphorbol 13-acetate
TS	Template switching
UTR	Untranslated region
UV	Ultraviolet
WAT	White adipose tissue

INTRODUCTION

INTRODUCTION

Preservation of genome integrity is essential for cell viability and tissue homeostasis. The process of DNA replication is frequently challenged by DNA lesions induced by endogenous or exogenous agents, or intrinsic replication-fork obstacles such as unusual DNA structures and collisions with the transcriptional machinery proteins or other protein-DNA complexes (reviewed in Berti and Vindigni, 2015). Replicative stress (RS) can be defined as any DNA replication disturbance that generates stretches of ssDNA that are rapidly covered by ssDNA-binding protein (RPA). Notably, persistent ssDNA is harmful as it may cause breakages in the genome (Lindahl *et al.*, 1993). Recently, a more general definition of RS has been proposed: slowing or stalling of replication fork progression and/or DNA synthesis (Zeman and Cimprich, 2014). The source, the extension and duration of RS determine the type of cellular response (reviewed in Muñoz and Méndez, 2016).

A first strategy to cope with RS is the use of specialized bypass mechanisms known as DNA damage tolerance (DDT) to continue with DNA replication across the blocking element, before repairing it. In addition, the DNA damage response (DDR) also facilitates recognition, bypass and repair of DNA lesions (reviewed in Sale, 2012). Remarkably, if repair were to occur at a stalled replication fork, it would increase the chance of generation of a double strand break (DSB) (reviewed in Jackson *et al.*, 2009). Therefore, DDT mechanisms are crucial to prevent fork breakages and to promote replication across lesions. Notably, those lesions that remain in the damaged template can be repaired postreplicatively. Both DDT and DNA repair require the use of DNA polymerases and primases, as it will be described in the next sections.

1. Eukaryotic DNA polymerases

DNA polymerases are enzymes that synthesize DNA. Their essential role takes part in genome duplication. During eukaryotic DNA replication, as the helicase MCM2-7 unwinds DNA, Polε duplicates DNA continuously on the leading strand, while the lagging strand is replicated discontinuously by Polα and Polδ. PCNA is the processivity factor of the replisome and has a role on tethering Polε and Polδ (Figure 1; Lujan *et al.*, 2016).

Besides DNA polymerases essential role in genome duplication, they are also crucial for protecting the cell against the effects of DNA damage. Remarkably, none of the known DNA polymerases are able to start DNA synthesis *de novo*; rather, they extend DNA from pre-existing "primer" molecule (DNA or DNA).

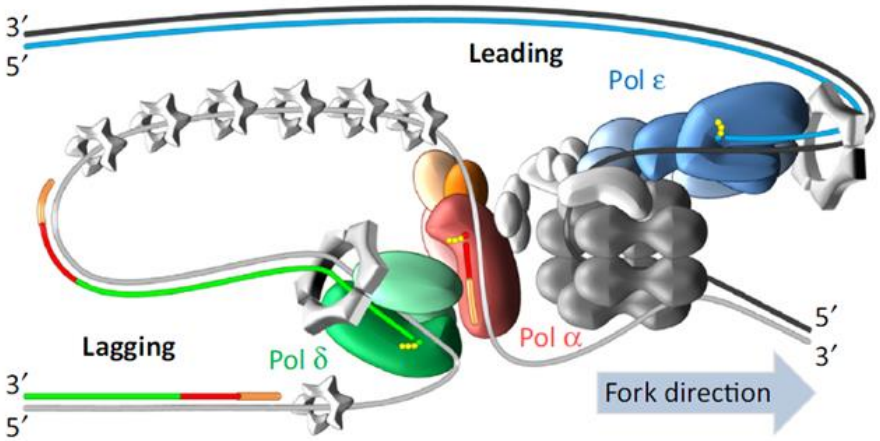

Figure 1. Central elements of the eukaryotic DNA replication fork. The schematic depicts the asymmetric nature of DNA synthesis. MCM, the DNA helicase (dark grey hexamer) along with its cofactors CDC45 and GINS, separates the two strands in the parental double helix. The 'leading strand' is replicated continuously by Polε, whereas the 'lagging strand' is replicated discontinuously. Polα/Prim1 synthesize short RNA primers (orange) that are inicially elongated by Polα (red) and then further elongated by Polδ (green). Small grey trimeric rings represent single-stranded DNA-binding protein RPA. Small yellow circles represent dNTPs (reproduced from Lujan *et al.*, 2016).

Based on sequence homology and structural similarities, eukaryotic DNA polymerases have been classically grouped in four families: A, B, X and Y (Ito and Braithwaite, 1991; reviewed in Lujan *et al.*, 2016). As of today, up to 16 DNA polymerases in higher eukaryotes perform distinct (and possibly redundant) functions (Table 1). All structurally polymerases share a common organization in three domains, called *finger*, *palm* and *thumb* that form a cavity. In the bottom of this cavity, the *palm* domain contains three acidic residues that coordinate the two divalent metallic ions required. The *fingers* are implicated in the union of the incoming nucleotide and the DNA template, whereas the *thumb* holds the emerging double helix of DNA. This "right hand" topology is conserved in all the phylogenetic families of DNA polymerases. In addition, Y-family polymerases can bypass specialized lesions in the DNA template because of an additional labile domain called *little finger* (Figure 2; Ollis *et al.* 1985; Steitz and Steitz, 1993; reviewed in Friedberg, 2005).

Family	DNA polymerase	Gene	Enzymatic activities	Proposed functions
B	Polα	POLA1	-	DNA replication, checkpoint activation and HR
B	Polε	POLE	3'-5' exonuclease	DNA replication, NER, MMR,HR and SHM
B	Polδ	POLD1	3'-5' exonuclease	DNA replication, NER, MMR, HR, SHM and TLS
B	Polζ	REV3L	-	TLS, mutagenesis, SHM and V(D)J
A	Polγ	POLG	3'-5' exonuclease 5'exonuclease	Mitochondrial DNA replication and repair
A	Polθ	POLQ	3'-5' exonuclease dRP lyase	NHEJ, ICL repair, TLS, SHM and regulation of replication timing
A	Polν	POLN	ATPase, helicase	ICL repair, NHEJ and TLS
Y	Polη	POLH	-	TLS and SHM
Y	Polι	POLI	dRP lyase	TLS, BER and SHM
Y	Polκ	POLK	-	TLS and NER
Y	Rev1	REV1	-	TLS and TLS polymerase "scaffold"
X	Polβ	POLB	dRP lyase, AP lyase	BER, meiotic recombination and TLS
X	Polλ	POLL	dRP lyase	BER, NHEJ, V(D)J, meiosis and TLS
X	Polμ	POLM	TdT	V(D)J, NHEJ and TLS
X	TDT	DNTT	-	Ig diversification
RT	TERT	TERT	-	Telomere maintenance

Table 1. Mammalian DNA polymerases. Most eukaryotic DNA polymerase proteins are named with Greek letters and the genes are named with the corresponding roman letter. It should be noted that Table 1 shows only the catalytic subunit gene. BER: Base excision repair; TLS: Translesion synthesis; NHEJ: Non-homologous end-joining; ICL: Interstrand crosslink; SHM: Somatic hypermutation; MMR: Mismatch repair; HR: Homologous recombination; dRP: 5'-deoxyribose phosphate.

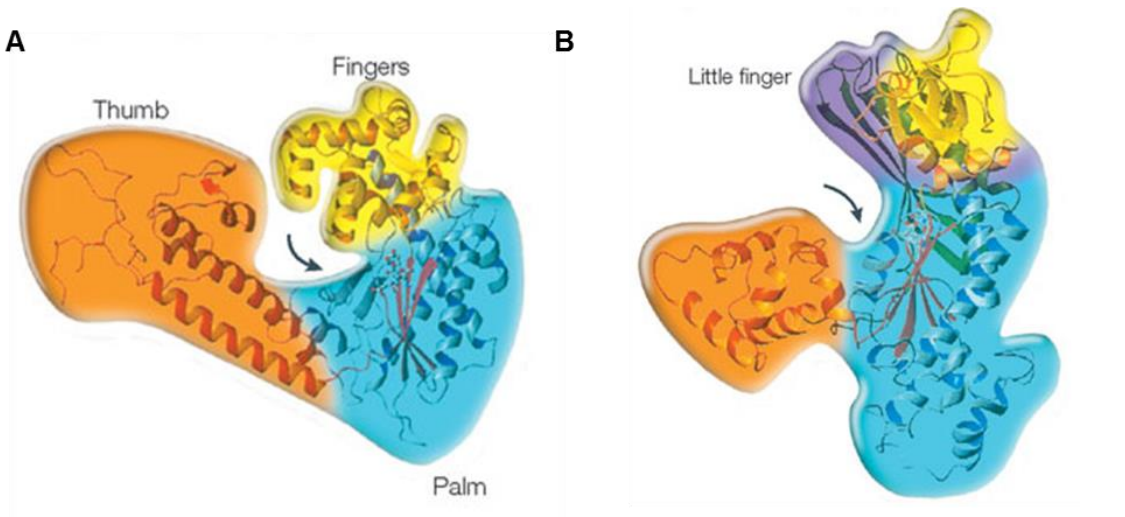

Figure 2. Common structural elements in eukaryotic DNA polymerases. Schematic representation of the crystal structure of (**A**) a canonical high-fidelity DNA polymerase and (**B**) a specialized DNA polymerase from the Y-family. Arrows indicate the catalytic site. Note the obvious difference in accessibility to both active sites. In addition to the canonical 'thumb' (orange), 'palm' (blue) and 'fingers' (yellow) domains, some specialized polymerases also have an extra domain known as 'little finger' (purple; reproduced from Friedberg, 2005).

1.1. DNA polymerases directly involved in DNA replication

1.1.1. Nuclear DNA replication

Nuclear DNA is replicated accurately by the coordinated action of DNA polymerases α, δ and ε. The catalytic subunit of Polα is not highly processive and lacks 3'→5' exonuclease proofreading activity. Polα is associated with a primase (Prim1) forming the Polα/primase complex that synthesizes and elongates RNA primers to initiate DNA synthesis (once per origin in the leading strand and once each Okazaki fragment in the lagging strand). Polε and Polδ are in charge of elongating these fragments in the leading and lagging strand, respectively. The rate of base substitution of both polymerases is approximately 10^{-5}, the lowest of all the characterized DNA polymerases, and misincorporated nucleotides usually removed by the 3'→5' exonuclease activity (Figure 1; reviewed in Lujan *et al.*, 2016). An alternative model for replication in yeast has been proposed, which Polδ replicates both strand, and a switch to Polε occurs only upon DNA damage in the leading strand template, linking DNA-damage detection to the essential role for polymerase ε and associated checkpoint proteins (Johnson *et al.*, 2015). However, this model has been contested (Burgers *et al.*, 2016) and it is unclear whether it will withstand the test of time.

Although not a conventional DNA polymerase, telomerase (TERT) adds telomere repeat sequences to the 3' end of telomeres in order to maintain chromosomal integrity. In humans, telomerase is active in stem cells but is normally absent in somatic cells (reviewed in Schmidt and Cech, 2015).

1.1.2. Mitochondrial DNA replication

The mitochondrial genome is replicated by a unique high-fidelity DNA polymerase, Polγ, which is encoded by the nuclear DNA (Wernette *et al.*, 1988; Hansen *et al.*, 2006). mtDNA is circular and composed by two strands referred as "heavy" and "light" chain, each one with its own origin of replication. The mechanism of initiation of mtDNA replication is poorly understood as there are three proposed replication models. In the asymmetric "strand displacement" model, one strand begins to replicate first, displacing the other strand. The second strand begins replicating in the opposite direction at the point when replication is completed on the first strand (Brown *et al.*, 2005). In a second model, mtDNA replicates symmetrically, with leading- and lagging-strand synthesis

progressing from bidirectional replication forks initiated at multiple points within large versions (Bowmaker *et al.*, 2003). The third model, RNA incorporation during mtDNA replication (RITOLS), which is a modification of the asynchronous model of replication (first model), argues that large regions of single stranded DNA do not exist, rather, the lagging-strand template is largely protected by RNA and subsequently converted into DNA (Yasukawa *et al.*, 2006). None of the models are totally accepted and therefore they are under debate, although in all the proposed models Polγ is suggested to be the mitochondrial replicative DNA polymerase. However, the protein implicated in the initiation or priming of the mtDNA replication is still unknown. Recently it was discovered that mitochondrial RNA polymerase (POLRMT) can initiate replication of mtDNA synthesizing primers from the light-strand origin of DNA replication on leading stran (Fuste *et al.*, 2010). However, the role of POLRMT only fits in the symmetrical replication model but does not explain primers synthesis on the lagging strand that is suggested as a major mechanism in the RITOLS model. This implies that there might be distinc mode of DNA priming and additional primases involved in the replication of the mtDNA.

1.2. DNA polymerases in DNA damage tolerance

There are two main DDT mechanisms that involve the use of DNA polymerases, and both are highly conserved throughout the eukaryotic kingdom. One involves the invasion of a homologous template strand, usually a sister chromatid, and is generally "error-free". The other involves the use of specialized DNA polymerases whose active site allows the insertion of nucleotides opposite the damaged template (reviewed in Branzei, 2011). Biochemically, translesion synthesis (TLS)-polymerases display low fidelity and for this reason, TLS is considered error-prone (Walker *et al.*, 2009). However, in some cases, TLS DNA polymerases are able to insert preferentially the correct nucleotide opposite to the lesion. The choice between the two modes of DDT is generally dictated by specific posttranslational modifications in PCNA (Figure 3; Hoege *et al.*, 2002). Notably, in eukaryotes, when ongoing forks stall, dormant origins may be activated to ensure completion of replication. Nevertheless, if two convergent forks stall, in regions lacking of back-up origins, cells must restart at least one of these forks to duplicate all the genome (Ge *et al.*, 2007; Ibarra *et al.*, 2008).

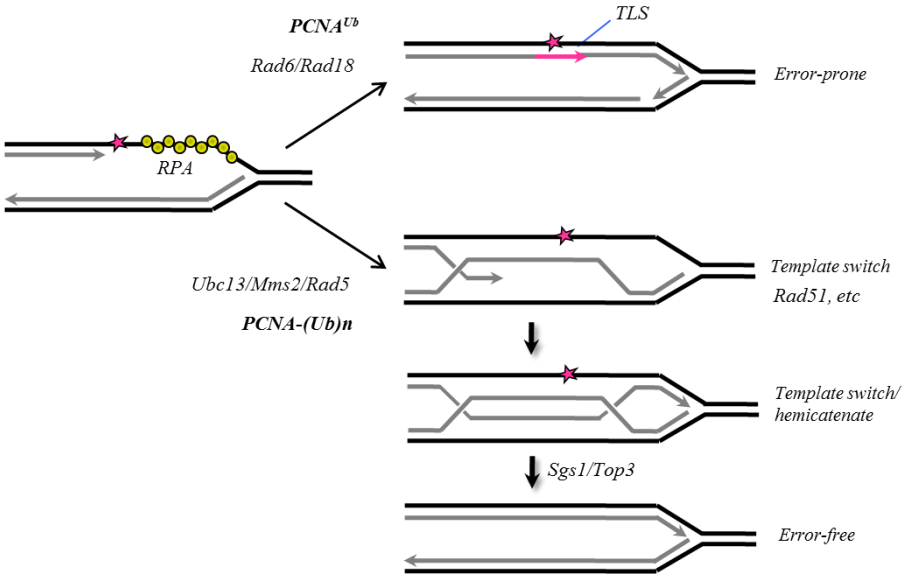

Figure 3. DNA damage tolerance (DDT) mechanisms. When replication forks encounter DNA lesions, the DNA polymerase stalls but the helicase continues to unwind the parental DNA, generating stretches of ssDNA that are rapidly covered by RPA. Before the lesion is repaired, two main alternatives exist to promote DNA replication through the lesion: mutagenic TLS, favoured by PCNA-Ub (top branch) or error-free TS, favoured by PCNA-$(Ub)_n$ (bottom branch). The names of the proteins playing key roles in these pathways are indicated.

1.2.1. Template switching (TS)

When PCNA is polyubiquitinated by Rad18, Rad5, and Ubc13-Mms2 and sumoylated by Ubc9 and Siz1 this mode of DDT is preferred (Hoege *et al.*, 2002; Branzei *et al.*, 2008). In TS, lesions are bypassed by temporally replacing the damaged template with the intact template provided by the newly synthesized daughter strand of the sister chromatid (reviewed in Chand and Cimprich, 2009). The X-shaped structures formed after the stand invasion can be processed by the resolvosome without generating crossovers (Raynard *et al.*, 2006). However, new evidence in yeast suggests that in some cases TS may also produce complex chromosomal rearrengements (reviewed in Heyer *et al.*, 2010; Branzei *et al.*, 2011). Interestingly, Polα/Prim1 complex promotes TS in yeast, suggesting that a priming event could be needed during TS (Fumasoni *et al.*, 2015).

1.2.2. Translesion synthesis (TLS)

PCNA monoubiquitylation at Lys164 by Rad6 and Rad18 favors TLS over TS (Hoege *et al.*, 2002). To date, the list of known TLS polymerases includes all members of the Y-family (Polη, Polι, Polκ and Rev1), members of the B-family polymerases (Pol ζ and Polδ), the A-family (Polθ and Polν) and the X-family (Polβ, Polμ and Polλ) (reviewed

in Knobel and Marti, 2011). Each polymerase has evolved to bypass specific lesions and can perform a set of distinct functions during DDT. The precise physiological role for each TLS polymerases has not been established but they can deal with lesion that include UV photoproducts, 8-oxo-G, deoxyuracil, bulky adducts, abasic sites, intra and inter strand-crosslinks, benzo(α)pyrene-guanine and thymine glycol (reviewed in Loeb and Monnat 2008).

The current model for the TLS mechanism implicates two steps. First, the replicative polymerase is substituted by a TLS-polymerase that incorporates nucleotide/s opposite the lesion. Then, the same or a different TLS polymerase elongates the newly synthesized strand with several nucleotides to allow the replicative polymerase to be engaged again (Shachar *et al.*, 2009). Polη, Polι and Polκ are polymerases that can perform the insertions, directly opposite of the lesion, while the extension mainly relies on Pol ζ and in some cases Polκ (Livneh *et al.*, 2010). Other polymerases can act as "inserter" or "extender" depending on the lesion. For instance, Polθ can insert adenine opposite an AP site, but it can also carry out the extension step from mismatches after error-prone dNTP incorporation by Polι (Seki *et al.*, 2004; 2008). In specific cases, the insertion and the extension is performed by the same TLS polymerase such as Polν opposite to thymine glycol or Polλ against AP sites (reviewed in Knobel and Marti, 2011).

It should be noted that TLS can occur at stalled forks or post-replicatively. In the latter case, replication must be re-initiated downstream of the damaged DNA. Rev1 has the particularity to bind to PCNA and Polη, Polι, Polκ, Polδ or Pol ζ. Hence, Rev1 could provide an "exchange platform" for TLS polymerases at stalled forks to reinitiate the DNA synthesis (Murakumo *et al.*, 2001; Ohashi *et al.*, 2004; Guo *et al.*, 2003; Guo *et al.*, 2006; Acharya *et al.*, 2009; Yoon *et al.*, 2015). Interestingly, Rev1-PCNA interaction is independent of PCNA ubiquitylation and suggests a new model for the regulation of TLS polymerases: their recruitment to stalled forks during S-phase could be mediated by Rev1, while Ub-PCNA would be a signal to recruit them during postreplicative gap filling (Edmunds *et al.*, 2008; reviewed in Sale, 2012).

1.3. DNA polymerases in DNA repair

There are several DNA repair pathways in the nucleus; the choice of the appropriate pathway depends on the type of DNA damage. Thereby, the DNA substrates generated in each type of damage are different. Almost every DNA polymerase participates in DNA repair; some are specialized in one pathway; others can used by multiple DDR pathways (Figure 4; reviewed in Lange *et al.*, 2011). The main mechanisms of repair and the polymerases involved in each one of them are described briefly in this section.

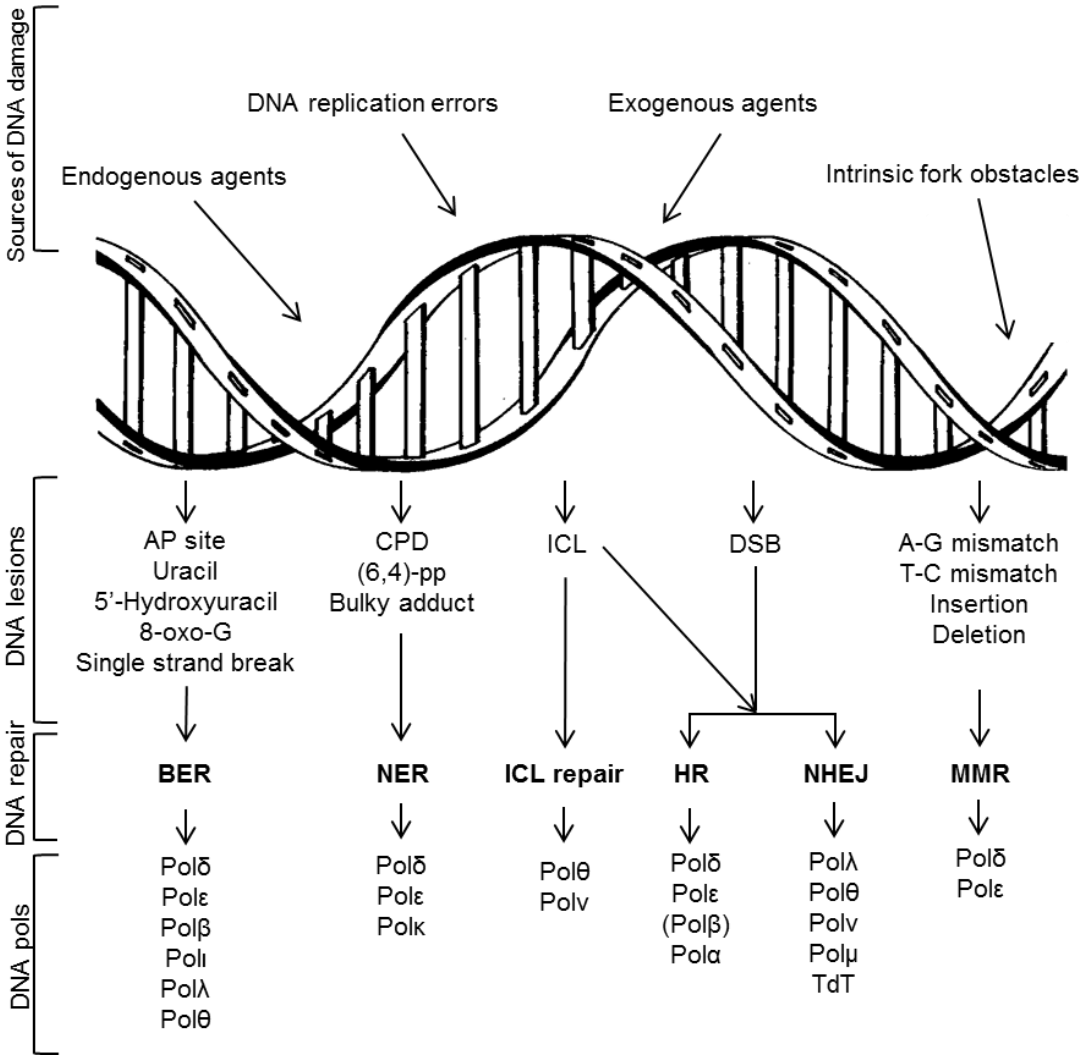

Figure 4. A panoply of DNA polymerases participates in DNA repair to maintain genomic stability. DNA is continually exposed to damaging agents, both exogenous and endogenous. The choice of repair mechanism is largely defined by the type of lesion and the phase of the cell cycle. The DNA polymerases involved in each repair mechanism are shown. AP: apurinic/apyrimidinic site; 8-oxo-G: 8-oxo-2'-deoxyguanosine; CPD: cyclobutane pyrimidine dimer; (6,4)-pp: 6-4 photoproduct; ICL: Inter-strand crosslink; DSB: Double-strand break; BER/NER: Base/Nucleotide Excision Repair; HR: Homologous Recombination; NHEJ: Non-Homologous End-Joining; MMR: Mismatch Repair.

1.3.1. Nucleotide Excision Repair (NER)

This process comprises global genome repair (GG-NER) and transcription-coupled repair (TC-NER). This pathway removes a variety of bulky, DNA-distorting lesions, including UV-induced damage and chemical adducts. This process comprises global genome repair and transcription-coupled repair. The initial recognition of damaged DNA by the NER proteins is followed by dual incision to excise a short oligomer (30nt) including the lesion; the subsequent gap is filled and ligated by Polδ, Polε and/or Polκ (reviewed in Gillet and Scharer, 2006; Hanawalt and Spivak, 2008; Ogi *et al.*, 2010).

1.3.2. Base Excision Repair (BER)

This repair process removes damaged bases such as oxidation (8-oxo-G), alkylation or abasic sites. BER has been classified according to the length of the repair patch as either "short-patch BER" (one nucleotide) or "long-patch BER" (more than one nucleotide). First, a DNA glycosylase recognizes the damage and eliminates it leaving an abasic site (AP: apurinic/apirimidinic site). Then an AP endonuclease cleaves the AP site to yield a 3'OH group adjacent to a 5'deoxyribosephosphate (dRP). Combined the action of a DNA glycosylase and an AP lyase may leave a one nucleotide gap between the 3'OH and the 5' phosphate. In higher eukaryotes, Polβ is the main polymerase that fills the short-patch BER (reviewed in Almeida and Sobol, 2007), but in its absence, the reaction can be carried out by Polλ or Polθ (Braithwate *et al.*, 2005; Prasad *et al.*, 2009). These polymerases typically insert a single dNTP and remove the 5'dRP left through its dRP lyase activity. In long-patch BER (2-10 new dNTPs), DNA synthesis is probably performed by Polδ and Polε along with processivity factor PCNA. These two polymerases perform strand displacement meaning that the downstream 5'DNA end is "displaced" to form a flap (Stuki *et al.*, 1998). Polβ has been also described to perform long-patch displacing synthesis, so it can participate in both BER pathways (reviewed in Almeida and Sobol, 2007). The low fidelity Polι binds to XRCC1 (an important BER factor) and is the only Y-family polymerase with dRP-lyase activity (Petta *et al.*, 2008; Bebenek *et al.*, 2001). Other DNA polymerases like Polλ and Polθ have been proposed as backup enzyme for BER (Braithwaite *et al.*, 2005; Prasad *et al.*, 2009).

1.3.3. Mismatch-repair (MMR)

This pathway recognizes the mismatch, additions or deletions generated by replicate DNA polymerases. Their repair implies the excision of a region in the newly synthesized strand that contents the error, followed by a correct DNA synthesis (reviewed in Hanawalt and Spivak, 2008). Polε and Polδ have been implicated in the excision through their exonuclease activities (Longley *et al.*, 1997; reviewed in Kunkel and Erie, 2015).

1.3.4. DSB repair

DSB are particularly dangerous as they are a leading cause of chromosomal rearrangements (Jackson *et al.*, 2009). DSB may occur during physiological process such as DNA replication, meiosis or V(D)J recombination, or as a consequence of external DNA damaging agents such as UV-light or ionizing radiation. These lesions can be repaired through two different pathways: Homologous recombination (HR) and non-homologous end-joining (NHEJ).

1.3.4.1. Homologous Recombination (HR)

This repair pathway is used after S-phase when a homologous DNA molecule is available and requires the processing of the DSB 5' end by an exonuclease 5'-3' which generates 3' overhangs that are covered by RPA. The union allows the recruitment of Rad51 forming a nucleoproteic filament. Rad51 directs the single strand invasion to the sister chromatid, followed by faithful DNA synthesis using the replicative polymerases (Bärtsch *et al.*, 2000; reviewed in Renkawitz *et al.*, 2014). In postsynapsis three subpathways of HR are distinguished (BIR, SDSA and dHJ), each with specific enzymatic requirements that have been only partially defined (reviewed in Heyer *et al.*, 2010). Polβ is also required in the repair of the DSB through HR during early meiotic processes (Kidane *et al.*, 2010). Notably, this mechanism is also used to repair ICL and ssDNA gaps (reviewed in Heyer *et al.*, 2010).

1.3.4.2. Non-Homologous End-Joining (NHEJ)

NHEJ is used to repair DSB when the sister chromatid is not available. The first step consists of DSB recognition by the heterodimer Ku70/Ku80 that covers DNA and prevents the degradation of either end. Then, DNA-PK favors the linkage of both sides

through protein-protein interaction. In most cases, the ends are processed, leaving small gaps that must be filled. Polλ and Polν participate in this process. Both polymerases interact with the NHEJ machinery through its BRCT domain. Apart from Polλ and Polν, Terminal deoxynucleotydil Transferase (TdT) has been implicated in the natural NHEJ that occur in immunoglobulin V(D)J gene recombination in B-cells. Polθ participates in the class switch recombination in B-cells (Yousefzadeh *et al.*, 2014) and also in an alternative NHEJ (alt-NHEJ) which is independent of Ku70/Ku80 (reviewed by Wood and Doublié, 2016).

1.3.5. Inter-strand crosslink (ICL) repair

ICL lesions can be caused by nitrous gas, psoralen, aldehydes, cisplatin and ionizing radiation. These lesions are highly cytotoxic and their repair mechanism is under active investigation. Polθ and Polν, both belonging to the A-family, are known to participate in ICL repair. Both possess a helicase linked to polymerase domain and have high processivity (Seki *et al.*, 2003; Marini *et al.*, 2003). ICL repair implies the use of TLS polymerases (Rev1, Polν and Polζ) to allow the replication progress in HR events (reviewed in Deans and West, 2011).

1.3.6. DNA repair in the mitochondria

Mitochondria also possess effective DNA repair mechanisms which remains less understood. Both BER (short-patch and long-patch) mechanisms are important for the repair of mtDNA, as mitochondria suffer from ROS generated during oxidative phosphorylation (Akbari *et al.*, 2008). MMR has also been described to occur (de Souza-Pinto *et al.*, 2009). Polγ is the only polymerase described in these two pathways (Copeland *et al.*, 2010). It is still not known if other mechanisms are involved in the repair of other specific lesions in mtDNA, such as bulky adducts or UV-photoproducts. For instance, it was found that UV photoproducts are persistent in the mitochondrial genomes. In addition to Polγ, Polζ and the newly discovered PrimPol have been found in the mitochondria and the lack of any of them perturbs mtDNA replication (García-Gómez *et al.*, 2013; Singh *et al.*, 2015).

2. DDR against UV-induced DNA damage

UV-irradiation is known to induce deleterious effects on nucleic acids and proteins, which have been linked to malignant melanoma and other skin cancer types (Narayanan

et al., 2010; Rastogi *et al.*, 2010). The UV spectrum of sunlight is divided into three regions: UVA (320-400nm), UVB (290-320nm) and UVC (320-400nm). While UV-C light is almost completely absorbed by the stratospheric ozone layer, UVA and UVB reach the earth's surface. UVB is considered to be more carcinogenic than UVA, as it directly causes two types of DNA lesions that compromise the conformation of the DNA helix: cyclobutane pyrimidine dimers (CPD) formed between adjacent thymidine (T) or cytosine (C) residues, and 6-pyrimidine-4-pyrimidone photoproducts ((6,4)-pp). The most abundant photoproduct is the CPD, which constitutes 80% of the total lesions. Despite the fact that (6,4)-pp is less abundant (20% of the lesions), this adduct is of high biological importance and known to be much more mutagenic than CPDs. Besides this in mice, CPDs and (6,4)-pp lesions are repaired with different kinetics in the epidermis and dermis (Qin *et al.*, 1995). Most (6,4)-pps are removed from the skin within 3 days. In contrast, the removal of CPDs is gradual. More than 80% if CPDs are removed from epidermal cells within 5 days, but less than 50% are removed from dermal fibroblasts in the same time frame. These characteristics are consistent with the repair of UV-lesions observed in mouse and human cultured epidermal keratinocytes and dermal fibroblasts (Courdavault *et al.*, 2005; Mitchell *et al.*, 1990). In addition, UVA and UVB damage DNA indirectly by the generation of reactive oxygen species (ROS), which in contact with DNA lead to the formation of 8-oxo-G and deoxyuracil lesions. These lesions do not distort the DNA helix and they are therefore less harmful than the photodimers (reviewed in Lommel and Hanawalt, 1993; Zaidi *et al.*, 2012).

As described before, these lesions can be bypassed during DNA replication to be repaired postreplicately. *In vitro*, CPD lesions can be bypassed by Polη, Polι, Polκ, Polμ, Polθ and Polζ; (6,4)-pp can be bypassed by Polη, Polι, Polθ and Polζ and 8-oxo-G by Polι, Polκ, Polμ, Polβ, Polλ and Polη (reviewed in Knobel and Marti, 2011). In human cells and mouse fibroblasts it has been shown that in opposite to UV lesions Rev1 is indispensable for TLS mediated by Polη, Polι and Polκ but is not required for TLS by Polζ. Therefore the current model for TLS synthesis against CPDs and (6,4)-pps is thought to occur either by Rev1 (Polη, Polι and Polκ) or Polζ (Yoon *et al.*, 2015). This insertion performed by TLS polymerases is normally mutagenic, although it is worth saying that Polη catalyzes error-free synthesis opposite to CPD lesions (Johnson *et al.*, 2000). Indeed, mice deficient in Polη or/and Polι are sensitive to UV-induced tumorigenesis (Lin *et al.*, 2006; Ohkumo *et al.*, 2006) and mice deficient in Polζ present

an extreme sensitive to UV irradiation developing skin ulcers with low dose of UV-B (Lange *et al.*, 2013). Moreover, Xeroderma Pigmentosum variant syndrome (XP-V) is a human disorder where severe truncations of the protein Polη results in a strong susceptibility to sunlight-induced skin cancers (Kannouche and Stary, 2003).

Cells have evolved with specific mechanisms to repair these lesions. CPD lesions can be removed by GG-NER or TC-NER mechanisms. In transcriptionally active genes, CPD clearance is faster due to the TC-NER mechanism. In contrast, (6,4)-pp are preferentially removed by GG-NER (Vreeswijk *et al.*, 1994; Balajee *et al.*, 1999). Mice deficient in XPC (GG-NER) or Ercc6 (TC-NER) displayed extreme UV susceptibility (Berg *et al.*, 2000; Doig *et al.*, 2006). As explained before, 8-oxo-G lesions are also produced after UV irradiation. This type of lesion is rapidly repaired by BER pathway. Again, mice deficient in proteins involved in this pathway such as Ogg1 developed SCC and mesenchymal tumors after chronic exposure to UV-radiation (Kunisada *et al.*, 2005).

3. DNA primases

The function of DNA primases is to initiate DNA replication by synthesizing short RNA oligonucleotides *de novo*, which then serve as primers for replicative polymerases. Due to the semi-discontinuous nature of DNA replication, primases are essential not only at the replication origins, but also during the synthesis of the lagging strand where they initiate the synthesis of each Okazaki fragments (Ogawa *et al.*, 1985; van der Ende *et al.*, 1985; reviewed in Frick and Richardson, 2001). Unlike in the nucleus, no primases have been described to operate in mtDNA. Instead, primer synthesis relies on mitochondrial RNA polymeras (Wanrooij *et al.*, 2008; Fuste *et al.*, 2010).

In eukarya, the canonical primase is comprised of two subunits (Prim1/Prim2), and it forms a complex with Polymerase α, itself a heteromider formed by PolA1-PolA2 (Foiani *et al.*, 1991; reviewed in Frick and Richardson, 2001; Muzi-Falconi *et al.*, 2003). Prim1 is the catalytic subunit and belongs to the large superfamily of Archeo-Eukaryotics primase (AEP), compared with other DNA and RNA polymerases, exhibits the lowest fidelity. Nonetheless, replication accuracy is not compromised since the RNA primers are eliminated by nucleases during Okazaki fragment maturation and replaced with DNA, synthesized by the replicative polymerases (Sheaff and Kuchta, 1994). The Polα-Primase complex can interact with a broad network of proteins,

including Cdc45, RPA and PARP (Weisshart *et al.*, 2000). The recruitment of Polα-primase complex onto replication is believed to occur through the interaction with Cdc45-MCM2-7 (Kukimoto *et al.*, 1999; Labib *et al.*, 2002). The role of the interactions with PARP is still not clear, although it may be involved in recruiting the primase to damaged sites (Dantzer *et al.*, 1998). In *Xenopus laevis* the activation of the checkpoint requires the recruitment of the Polα-Prim-Cdc45 onto chromatin (Michael *et al.*, 2000).

The AEP superfamily includes primases in archaea, virus and eukaryotes, whereas all the bacterial primases belong to the DnaG-like superfamily (Kuchta and Stengel, 2010). AEP superfamily comprises 13 major families, 12 of which can be also organized into three higher-order clades; the AEP-proper clade, the nucleocytoplasmic large DNA viruses (NCLDV)-herpesvirus clade and the PrimPol clade (Iyer *et al.*, 2005; reviewed in Guilliam *et al.*, 2015).

Most AEP members are heterodimeric, containing a small catalytic subunit and a large accessory subunit. The AEP superfamily is distinguished by a characteristic catalytic core composed by three conserved motifs (A, B and C). Motif A or hhhDhD/E motif (where h is an hydrophobic residue), motif B or sxH motif (where s is a small residue) and motif C or an hD/E motif (Figure 5; Iyer *et al.*, 2005). Motif A and C are involved in divalent metal ion coordination for catalysis, whereas motif B is required in nucleotide binding (Augustin *et al.*, 2001; Lao-Sirieix *et al.*, 2005; Lipps *et al.*, 2004). This mechanism is supported by structural information extracted from the preternary complex of a mycobacterial AEP bound to dsDNA and the incoming nucleotide (UTP; Brissett *et al.*, 2011). Mutagenesis studies have shown that these three motifs are crucial to maintain the catalytic activity (Figure 5; Copeland *et al.*, 1995; Augustin *et al.*, 2001; Lipps *et al.*, 2003; Della *et al.*, 2004; Galal *et al.*, 2012). In addition, some AEPs also possess a Zn binding motifs and helicase domains (Iyer *et al.*, 2005).

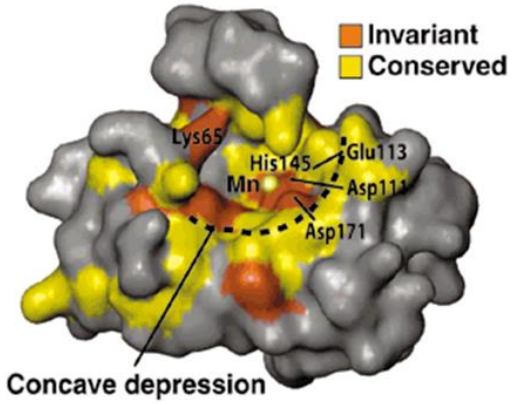

Figure 5. A common fold structure for the PrimPol proteins from the AEP family. Modeling of the pRN1 ORF904 protein, the first AEP primase defined in the Prim-Pol clade. The solvent-accessible surface is colored. Yellow and orange colors correspond to invariant and conserved residues in the AEP family, respectively. Essential residues for DNA polymerase/primase activity are indicated (taken from Lipps *et al.*, 2004).

Besides their fundamental role in DNA replication, AEP proteins have been also identified in DSB repair through NHEJ in prokaryotes (reviewed in Guilliam *et al.*, 2015). In addition, a member of the AEP superfamily, PrimPol, has been recently involved in a new DDT mechanism (Mourón *et al.*, 2013).

4. PrimPol a novel primase and polymerase enzyme in eukaryotes

Human PrimPol gene (CCDC111), located in chromosome 4q35.1, was predicted to be a member of the AEP family, specifically to the PrimPol clade (Iyer *et al.*, 2005). PrimPol contains the active-site A, B and C motifs and a putative Zn ribbon similar to that of herpesvirus UL52 primase and other AEP-like enzymes. Evolutionary, PrimPol an archaic enzyme present in the majority eukaryotic species, with the notable exception of fungi (Figure 6; García-Gómez *et al.*, 2013; Bianchi *et al.*, 2013; Wan *et al.*, 2013).

Members of the PrimPol family have the motif A variant DxE instead of the DxD motif present in most other AEP members. These are two of the three amino acids (D114, E116 and D280) in charge of metal coordination at the active site (Figure 6; García-Gómez *et al.*, 2013; Bia nchi *et al.*, 2013; Wan *et al.*, 2013).

A

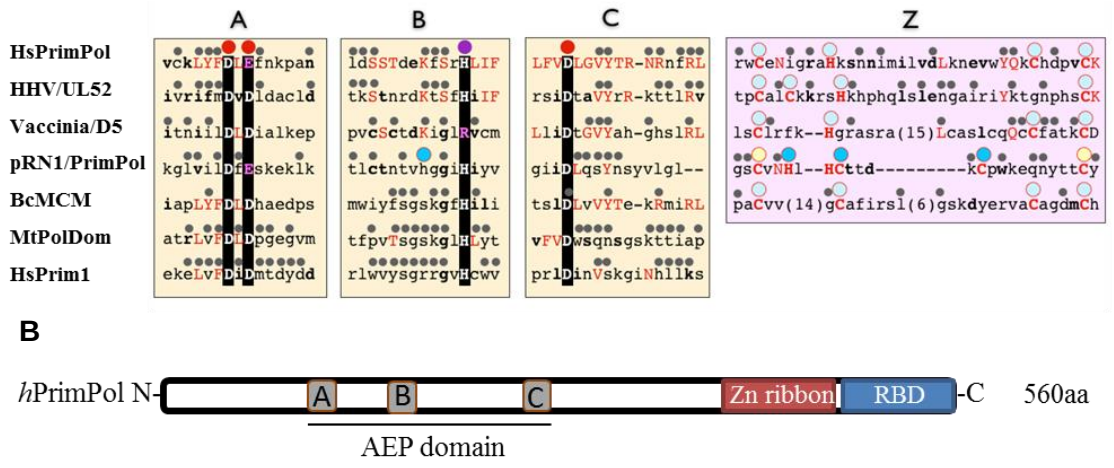

Figure 6. Conserved motifs in human PrimPol protein. A. Main conserved regions of representative proteins from different clades in the AEP family. Large dots indicate metal ligands (in red), nucleotide ligands (purple), and demonstrated (cyan) or potential (light blue) cysteine residues forming a Zn finger. Small dots indicate invariance within each group of AEP-related enzymes. Sequence alignment provided by Dr. Luis Blanco (García-Gómez *et al.*, 2013). **B.** Primary structure of human PrimPol indicating the positions of the conserved A, B and C motifs in the AEP domain, a Zn finger domain and an RPA-binding domain. (RBD).

In vitro, PrimPol possesses both primase and polymerase activity; which it is able to synthesize short oligonucleotides *de novo*, and it can also elongate prexisting primers. Strikingly, PrimPol primase activity can use either dNTPs and NTPs or a combination of both. PrimPol can elongate primers, again, using either dNTPs or NTPs, albeit with a much higher efficiency with dNTPs. The nature of the pre-existing primer (DNA or RNA) does not affect the polymerase activity of PrimPol. When D114 and E116 (DxE) were converted into alanines (AxA mutant) by site-directed mutagenesis, both primase and polymerase activities were abolished. Hence, primase and polymerase activities share a common site (García-Gómez *et al.*, 2013; Bianchi *et al.*, 2013; Wan *et al.*, 2013).

PrimPol is a low-processivity, error-prone polymerase and it lacks proofreading activity. The base substitution rate of PrimPol ($51x10^{-5}$) is in the range of the X-polymerases family and the single nucleotide insertion/deletion (indel) rate ($310x10^{-5}$) is as high as the Y-polymerases family (Martínez-Jiménez *et al.*, 2015). Interestingly, PrimPol can perform TLS-synthesis *in vitro* in front of a several type of DNA lesions including common oxidative DNA lesions (8-oxo-G and deoxyuracil) and UV-induced CPDs (García-Gómez *et al.*, 2013; Bianchi *et al.*, 2013; Mourón *et al.*, 2013; Zafar *et al.*, 2014). What is more, it can bypass one of the most complex lesions, (6,4)-pp and apurinic sites (AP). In these cases, PrimPol is capable of realigning the primer end to a

downstream position, looping out the lesion without copying it (García-Gómez *et al.*, 2013; Mourón *et al.*, 2013).

4.1. Repriming downstream of a DNA lesion

In the DDT response, lesions can be bypassed by the initiation of a new DNA strand downstream of the damaged template, leaving behind an unreplicated ssDNA gap to be repaired post-replicatevely. This mechanism was originally, reported in bacteria, yeasts and mammalian cells particularly after UV irradiation (Heller and Marians, 2006; Lopes *et al.*, 2006; Langston and O'donnell, 2006; Callegari and Kelly, 2006; Callegari *et al.*, 2010; Elyers *et al.*, 2011). Reinitiation of DNA synthesis ahead of the lesion strictly requires a primase activity. Whereas in the lagging strand this repriming event could be readily performed by Polα/Prim1 complex, it is not clear which enzyme acts in the leading strand. Recent work in murine and human cells has proposed that PrimPol catalyzes these priming events to facilitate fork progression after UV challenge or dNTP attrition (Figure 7; Mourón *et al.*, 2013).

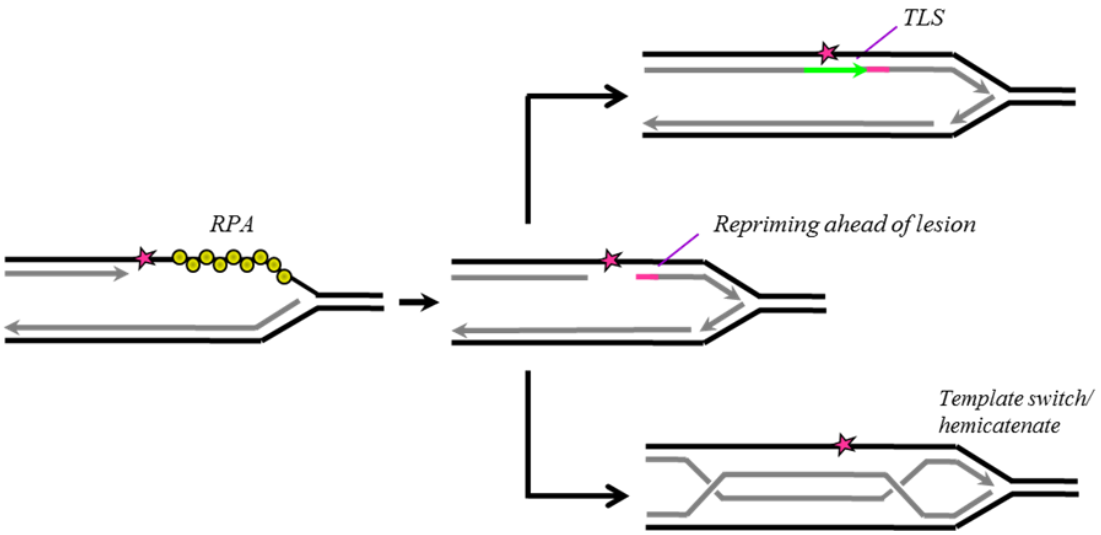

Figure 7. A repriming event downstream of the DNA lesion facilitates DDT. In a situation of replication stress such as the one described in Figure 3, a repriming event may occur, facilitating the restart of DNA synthesis downstream of the lesion. The short unreplicated gap can then be fixed post-replicatively by either TLS, HR or other DNA repair pathways.

4.2. PrimPol subcellular distribution suggests nuclear and mitochondrial functions

A biochemical fractionation of cells revealed that PrimPol is distributed in the cytosol, mitochondria and nucleus. It has been postulated that it may be involved in DDT in both cellular compartments with DNA. Indeed, PrimPol gene silencing or ablation affects mitochondrial and nuclear DNA replication (García-Gómez *et al.*, 2013; Mourón *et al.*, 2013).

PrimPol associates with nuclear chromatin during G1 and S phase, and influences the rate of fork progression, even in the absence of exogenous challenges. PrimPol deficiency induces RS in otherwise unchallenged conditions. Therefore, PrimPol is proposed to have a role during normal DNA replication, probably monitoring fork progression through slow replication zones or other natural impediments. Indeed, PrimPol is required to restart forks stalled by HU, which reduces dNTP levels. Additionally, PrimPol is recruited onto chromatin after UV irradiation, independently of the checkpoint response (Figure 8). It has been reported that PrimPol C-terminal domain interacts with RPA1 (RPA70; Figure 6B; Wan *et al.*, 2013; Guilliam *et al.*, 2014). Therefore the RPA binding domain (RBD) of PrimPol, together with the Zn finger domain, may act as a chromatin-recruitment mechanism. Interestingly, PrimPol also interacts with mitochondirla single strand binding protein (mtSSB) suggesting the same mode of recruitment to mtDNA.

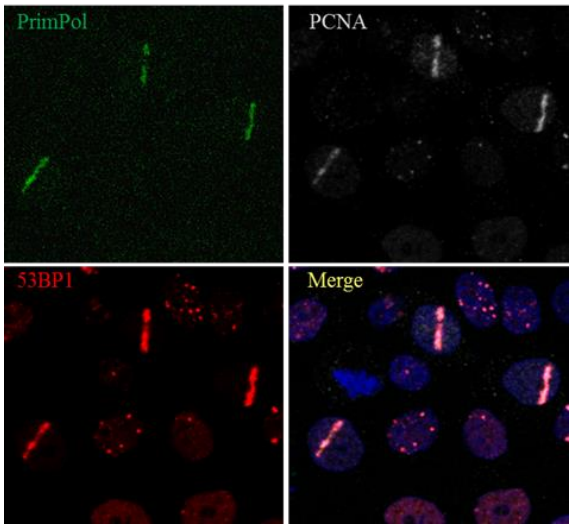

Figure 8. PrimPol is recruited onto DNA damaged by UV irradiation in HeLa cells. In cells treated with a UV-laser as described (Mouron *et al.*, 2013), GFP-tagged PrimPol can be seen rapidly recruited onto the UV-damaged site. PCNA and 53BP1 are also shown as positive controls.

The primase activity of PrimPol is required to bypass UV-induced lesions *in vivo*, as primase-null PrimPol versions with intact TLS polymerase activity failed to promote fork restart (Figure 9; Mourón *et al.*, 2013). PrimPol and Polη, both known to efficiently

bypass CPD lesions *in vitro*, act independently to promote fork progression through UV-induced damage suggesting that PrimPol would initially reprime ahead of the DNA lesion leaving an unreplicated gap to be repaired post-replicatively by Polη (or other TLS polymerases) or HR (Mouron *et al.*, 2013). Recent studies also support that PrimPol acts preferentially through its primase activity for replicative tolerance of G quadruplexes in DT40 cells (Schiavone *et al.*, 2016). In avian cells, PrimPol has shown to reprime DNA synthesis also after chain-terminating nucleosides (CTNAs), such as azidothymidine or cytarabine (important antivirals) (Kobayashi *et al.*, 2016).

Whether PrimPol's TLS activity is important for other specific lesions remains to be elucidated. The lack of PrimPol also prevents the recovery of mtDNA copy number after transient drug-induced mtDNA depletion. The fact that PrimPol efficiently bypasses 8-oxo-G lesions suggests that PrimPol could act as TLS in the mitochondria (García-Gómez *et al.*, 2013). PrimPol interacts with Twinkle, the mitochondrial helicase, and *in vitro* data has shown that Twinkle enhances PrimPol DNA synthesis on both undamaged and damaged templates. In contrast, Polγ is unable to enhance PrimPol DNA synthesis upon oxidative stress (Stojkovic *et al.*, 2016).

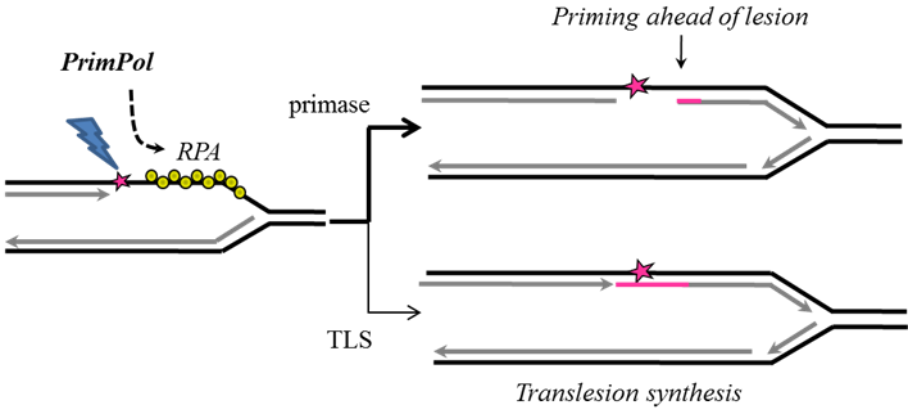

Figure 9. Two possible mechanisms for PrimPol function. The RPA-covered stretch of ssDNA generated by a stall fork is likely to recruit PrimPol. Our previous data (Mourón *et al.*, 2013) indicates that PrimPol uses its primase activity to reinitiate a new DNA strand ahead of the lesion. Taking into account its activities in vitro, PrimPol could also operate as a TLS polymerase and bypass the lesion directly.

4.3. Regulation of PrimPol activity by other factors

Unlike canonical TLS polymerases, hPrimPol does not interact, nor is it stimulated by, unmodified or monoubiquitinated PCNA (Guilliam *et al.*, 2013). As explained before,

RPA and mtSSB interact with PrimPol. Both proteins have been shown to suppress *de novo* primer synthesis and impede primer extension by PrimPol *in vitro* (Wan *et al.*, 2013; Guilliam *et al.*, 2013). This suggests that *in vivo*, PrimPol may prime at regions where RPA/mtSSB has been displaced by other replication factor, or where RPA/mtSSB DNA binding is prevented, for instance, in G4 quadruplex structures.

Polymerase δ-interacting protein 2 (PolDIP2) was also identified in a pull-down screen as a partner of PrimPol (Guilliam *et al.*, 2016). As PrimPol, PolDIP2 is also localized in mitochondria and nucleus (Lui *et al.*, 2003; Cheng *et al.*, 2005). This protein stimulates the *in vitro* activity of Polδ and the processivity and fidelity of lesion bypass by Polλ and Polη (Xie *et al.*, 2005; Tissier *et al.*, 2013; Maga *et al.*, 2013). Furthermore, PolDIP2 interacts also with Polζ and Rev1, although the relevance of this interaction remains unknown (Tissier *et al.*, 2013). PolDIP2 enhances PrimPol DNA binding and polymerase activity, with a minimal effect on its priming function. Moreover, PolDIP2 increases the efficiency and fidelity of 8-oxo-G bypass by PrimPol *in vitro* (Guilliam *et al.*, 2016).

Despite the evident importance of PrimPol in DDT mechanisms, the implications of PrimPol in human disease and the consequences of PrimPol ablation in mammals remain still under investigated. Therefore, in this thesis we performed (1) structure-function analyses of PrimPol conserved amino acid that could be implicated in human disease and (2) a study of the effects of PrimPol ablation using a PrimPol knock-out mouse model.

OBJECTIVES

OBJECTIVES

1. Structure-function analyses in human PrimPol: functional relevance of amino acids W87, F88, Y89, Y90, belonging to the evolutionary conserved "WFYY" motif. This objective also included a functional validation of the importance of conserved Y100 residue.

2. Characterization of the effects of PrimPol ablation in cells and in a mammalian organism:

2.1. Determine the dynamics of DNA replication and UV-susceptibility in PrimPol-deficient mouse embryonic fibroblasts.

2.2. Study the physiological impact of PrimPol ablation in the mouse, including its sensitivity to UV-induced DNA damage.

MATERIALS AND METHODS

MATERIAL AND METHODS

1. Mice procedures

1.1. Ethical statement

Mice were kept in the Animal Facility at CNIO in accordance with institutional policies and the "Federation for Laboratory Animal Science Associations" (FELASA) guidelines. All animal procedures were approved by the Animal Experimental Ethics Committee of the Instituto Carlos III (Madrid, Spain).

1.2. Treatment of mice with TPA

TPA (Sigma-Aldrich) was dissolved in acetone at a concentration of 3.4 nmol/200 μL. The dorsal hair of the mice was shaved, 48 h before TPA treatment. 200 μL of TPA were applied to the dorsal skin twice per week for 2 weeks. 30 min before euthanasia, an i.p. injection of BrdU (100 μg/g body weight) was administered. The back skin was subject to histological examination. The degree of hyperplasia was estimated using Panoramic Viewer software on images of H&E-stained sections.

1.3. Treatment of mice with UV radiation

In the acute irradiation regime, the dorsal hair of mice was shaved 48h before administration of a single dose of 3000J/m^2 UVB in a device using Philips UVB TL 20W/12 RS lights. Mice were sacrificed at 1, 2, 3, 4 or 5 days post-irradiation. 30 min before euthanasia, an i.p. injection of BrdU (100 μg/g body weight) was administered. The degree of hyperplasia and cellular density in the dorsal skin were estimated using Panoramic Viewer software on images of H&E-stained sections.

In the chronic UV irradiation regime, the dorsal hair of mice was shaved 48 h before the initial UV radiation and once a week thereafter. Mice were irradiated three times per week using the same device as for the acute irradiation, but the dose was lowered to 1800 J/m^2 UVB. The overall health and external aspect of irradiated mice were monitored weekly. Mice were sacrificed at the end of the experiment (or before, if the humane endpoint criteria were met), and different tissues (ear, dorsal and tail skin, eyes)

were selected for histopathological analyses. The spleen was removed in the necropsies and weighed.

Finally, in the melanoma-inducing protocol, neonates were irradiated in a 6 well-plate placed 20 cm beneath the bank of sunlamps (Philips F40 UV lamps). The total radiation was 6240 J/m^2 UVB and 3310 J/m^2 UVA. After exposure, newborn mice were returned to their cages with their mothers. Signs of tumor development or other UV-associated morbidity symptoms were monitored weekly.

1.4. Body temperature and blood analyses

Body temperature was measured using a Cibertec RTC-1 Thermo Controller rectal probe. For blood analysis, mice were anesthetized with isoflurane for the duration of the procedure (1-2 min). Blood samples were collected in EDTA-containing tubes (BD Microtrainer), and blood cell populations were measured in an Abbacus cell counter.

1.5. X-ray densitometry

Body fat percentage was assessed using DEXA scan (PIXImus2; Lunar, Madison, WI). Mice were anesthetized with isoflurane for the duration of the procedure (10 min). Each mouse was scanned with the limbs and tail stretched away from the body, and the head was excluded from the analyses.

2. Mice genotyping

Genotyping was performed by PCR analyses of genomic DNA isolated from tail clips following a standard protocol (Malumbres *et al.*, 1997). Tails were lysed in PCR-K buffer (50 mM KCl, 1.5 mM Tris-HCl pH 8.5, 0.01% gelatin, 0.45% NP-40, 0.45% Tween-20, 100 µg/mL proteinase K (Roche)) for 2 h at 55ºC in agitation. Proteinase K was inactivated at 95ºC for 15 min. Each PCR reaction was done with 2 µL of Taq polymerase (Ecogen), 2.5 µL of 10X Taq reaction buffer (Ecogen), 1.5 µL of 50 mM $MgCl_2$ (Ecogen), 1 µL of each primer from a 10 µM dilution in H_2O, 1 µL of 10 mM dNTPs (Fermentas), and H_2O to a final volume of 25 µL. The different primers used for mice genotyping are listed in Table 2.

Primer name	Sequence (5'→ 3')
OST FW	CCTACATCTGCAAGAAGACTTAGC
OST RV	ACACTGGGTCCCTTTACAGATGG
LTR RV	ATAAACCCTCTTGCAGTTGCATC

Table 2. Primers for mice genotyping.

3. Cell culture experiments

3.1. Cell lines and manipulations

The stable cell line shPrimPol-HeLa was generated in the laboratory as part of a previous study (Mourón *et al.*, 2013). Expression of PrimPol shRNA was induced with 1μg/mL doxycycline (dox) for 3 days. DNA sequences encoding wild-type (WT) PrimPol, or PrimPol versions AxA (Mourón *et al.*, 2013), W87G, F88L, Y89D, Y90D and Y100H were cloned into Gateway expression vectors introducing an N-terminal V5 tag (Invitrogen). Transient transfections were performed using Lipofectamine 2000 (Invitrogen).

PrimPol$^{+/+}$, PrimPol$^{+/-}$ and PrimPol$^{-/-}$ MEFs were specifically obtained for this study. All cells were grown in complete DMEM (Lonza) supplemented with 10% FBS plus 10% penicillin-streptomycin. Cell lines were tested monthly for mycoplasma contamination.

3.2. Primary Mouse Embryonic Fibroblasts (MEFs) isolation

Mouse embryos were obtained at E12.5 days. Pregnant females were sacrificed by cervical dislocation and uterine horns containing the embryos were transferred to a sterile PBS solution in a laminar flow hood. Embryos were collected from the uterus, fetal liver was excised and a fragment of tissue was taken for molecular genotyping. The rest of embryonic tissue was minced and treated with 0.25% trypsin-EDTA (Sigma-Aldrich) for 20 min at 37ºC. Cells were further disaggregated by pipetting, transferred to 9mL medium (DMEM complete (Lonza), 15% FBS, 10% penicillin/streptomycin solution (Invitrogen)), seeded in tissue culture plates and grown at 37ºC and 5% CO_2. Cells were expanded and frozen at passage 1 in 90% FBS, 10% dimethyl sulfoxide

(DMSO, Sigma-Aldrich). All experiment with primary MEFs were performed at low passage number (≤ 4).

3.3. Proliferation curves with MEFs

Aliquots of 90,000 cells were seeded in 6-well plates in duplicate. After 3 days in culture a 1:2 split was performed to avoid confluency. Proliferation rate was estimated by counting cells at each time point using a Neubauer hemocytometer.

3.4. Sister Chromatid Exchange (SCE) analyses

Exponentially growing cells were labeled for 38h with 10 μM BrdU. Colchicine (0.1 μg/mL) was added for the last 2h prior to harvesting the cultures. For metaphase spread preparation, cells were subjected to an osmotic shock (75 mM KCl for 20 min at 37ºC), centrifuged for 10 min at 200g and fixed by drop-wise addition of Carnoy's fixative solution (ice-cold 3:1 methanol:acetic acid). Cells were subjected to 3 cycles of centrifugation and Carnoy's solution addition before storing them at -20ºC. For chromosome spreading, microscope slides were soaked in 45% acetic acid and drops of the cell suspension were spread on the slide. Slides were then incubated in 0.1M phosphate buffer (pH 6.8) containing Hoechst 33258 (Sigma) (0.11 mg/mL) for 20 min in darkness. After the exposure of slides to fluorescent light for an hour, the slides were digested with disodic phosphate (1M, pH 8) at 88ºC for 5 min and then washed with distilled water. After air-drying, chromosomes were stained with 5% Giemsa (Sigma). SCE events were scored and normalized to the total number of analyzed chromosomes.

3.5. Oncogenic transformation assay

pBabe (empty), pBabe-H-RasV12 and pBabe-H-RasV12/E1A retroviral supernatants were produced by calcium phosphate transfection of 293T cells following a standard protocol (Wigler *et al.*, 1977). MEFs were grown until near confluency before infecting them with the retroviral supernatants. 24h later the medium was changed and 10 days post-infection plates were fixed with 1% glutaraldehyde, stained with 0.1% cristal violet in 10% ethanol and scored for number of colonies.

3.6. Single-molecule analysis of DNA replication in stretched fibers

DNA fiber spreads were prepared using a published protocol (Terret el al, 2009) with slight modifications that are described below. To evaluate the rate of fork progression, exponentially growing cells were sequentially pulse-labeled for 20 min with 50 μM chlorodeoxyuridine (CldU) and 250 μM iododeoxyuridine (IdU). To evaluate fork restart, cells were first pulsed with CldU for 20 min and then irradiated with UVC (30 J/m^2) or treated with 6 mM HU (Sigma-Aldrich) for 5h. 30 min after exposure to UV light, or immediately after the HU incubation, cells were pulsed with IdU for 20 min in fresh medium. Cells were harvested and resuspended in cold PBS at $0.25 \cdot 10^6$ cells/mL. 2 μL of cell suspension were placed on a microscope slide and lysed for 6 min in 10 μL of pre-warmed (30ºC) spreading buffer (0.5% SDS, 200mM Tris-HCl pH 7.4, 50 mM EDTA). Slides were tilted at a 15º angle to allow DNA suspension to run slowly down the slide, and the resulting DNA spreads were air-dried, fixed in cold 3:1 methanol: acetic acid for 2 min and kept overnight at 4ºC.

Slides were treated with 2.5 N HCl for 30 min, washed three times in PBS and blocked in 1% BSA, 0.1% Triton X-100 in PBS for 1h before incubation with CldU, IdU and ssDNA primary antibodies (Table 4) diluted in blocking solution (1/100) for 1h. Fluorophore-conjugated secondary antibodies were added for 30 min. ProLong Gold antifade reagent (Invitrogen) was used as mounting media for IF.

Microscopy analysis was carried out using a Leica DFC350 FX microscope. DNA staining was used to confirm fiber integrity. Fork progression rate was monitored in second-labeled (IdU) tracks. The length of more than 300 tracks was measured per condition using ImageJ software and conversion factor 1μm = 2.59kb (Jackson and Pombo 1998). To evaluate fork restart, 500 structures (restarted forks and non-restarted forks) were counted per condition. The result is shown as the percentage of bicolor tracks divided by all the counted structures.

3.7. Immunofluorescence

Cells grown on polylysine-treated coverslips were fixed with 4% paraformaldehyde (PFA) in PBS for 15 min, permeabilized with 0.5% Triton X-100 in PBS for 5 min and treated with blocking solution (3% BSA, 5% normal donkey serum (Jackson

ImmunoResearch) and 0.05% Tween-20 in PBS) for 30 min. Primary and fluorophore conjugated-secondary antibodies were diluted in blocking solution. The primary antibodies used for IF are listed in Table 4. Nuclei were stained with 1 μg/μL DAPI (Sigma) in PBS for 1 min. ProLong Gold antifade reagent was used as mounting media for IF. For CPD and (6,4)-pp immunodetection, cells were subjected to a pre-extraction step with 0.3% Triton X-100 in CSK buffer (10mM PIPES pH 7.0, 0.1M NaCl, 0.3M sacarose and 3mM $MgCl_2$ 0.5mM PMSF) for 5 min at 4ºC.

Images were acquired in a Leica DFC350 FX confocal microscope. Image analysis was performed at the Confocal Microscopy Unit at CNIO, using pre-designed routines for nuclei detection and intensity measurement in the Definiens software (Definiens, Germany).

3.8. Flow cytometry analysis

For BrdU incorporation analysis, cells were pulse-labeled with 10 μM BrdU for 30 min. Cells were trypsinized, washed with PBS and fixed overnight at 4ºC in 70% ethanol. DNA denaturation and cell permeabilization was carried out with 2N HCl for 20 min at 37ºC. Cells were washed twice in PBS for HCl neutralization and incubated for 1 h with FITC-BrdU antibody (BD Biosciences Pharmigen) in 1% BSA PBS- 0.05% Tween-20. For DNA content analysis, cells were incubated overnight in DNA staining solution (25 μg/mL propidium iodide (Sigma-Aldrich)), 10 μg/mL RNase A (Qiagen)).

Data acquisition was carried out in a FACS Canto II cytometer (Becton-Dickinson) and data were analyzed using Flow Jo software (Tree Star).

4. RNA expression analyses

4.1. RNA isolation, retrotranscription and quantitative PCR (RT-qPCR)

Tissues were disrupted and homogenized in Trizol (Invitrogen) using a bead-beating system (Precellys). Total RNA was isolated according to Trizol manufacturer's instructions. Potential contaminant genomic DNA was removed by DNaseI digestion (Roche). 1μg of RNA was converted to cDNA with Maxima First Strand cDNA kit (Themo). cDNAs were diluted 1/10 and qPCR was performed in triplicates using SYBR green-Real Time PCR master mix (Applied Biosystems). Primers used for RT-qPCR

analysis are shown in Table 3. The $2\Delta\Delta^{Ct}$ method was used to quantify amplified fragments. Expression levels were normalized to GAPDH housekeeping gene. RT-qPCR analysis were done using a 7900HT Fast Real Time PCR System equipment and analyzed with SDS 2.2.2 Software (Applied Biosystems).

Gene	Primer	Sequence (5'→ 3')
PRIMPOL	*PRIMPOL-FW*	TAACAAATTGGCCAACCCAGGAG
	PRIMPOL-RV	ACCTTAGCTTCATCATCCTCGGC
GAPDH	*GAPDH*-FW	GCACAGTCAAGGCCGAGAAT
	GAPDH-RV	GCCTTCTCCATGGTGGTGAA

Table 3. Primer sequences for gene expression analyses by RT-qPCR.

5. Protein analyses

5.1. Whole tissue and cell extracts

Mouse tissues were lysed in RIPA lysis buffer (1% NP-40, 0.1% SDS, 50mM Tris-HCl pH 7.4, 150mM NaCl, 0.5% sodium deoxycholate, 1mM EDTA, 1mM $NaVO_4$, 0.5 mM NaF, 0.1mM PMSF, protease inhibitors (Roche)) for 20 min on ice and sonicated (Branson sonicator 102C) for 30 s at 20% amplitude. Extracts were clarified by high-speed centrifugation (15min/16000g/4ºC). Protein was quantified using BCA kit (Pierce) according to manufacturer's protocol.

For whole cell extracts intended for immunoblot analysis, cells were trypsinized, collected by centrifugation (1200 rpm, 5 min), washed with PBS and lysed in Laemmli Sample Buffer (50 mM Tris-HCl pH 6.8, 10% glycerol, 3% SDS, 0.006% w/v bromophenol blue and 5% 2-mercaptoetanol) at 5000 cells/µL and subsequently sonicated for 30 seconds at 15% amplitude.

5.2. Chromatin fractionation protocol

Biochemical fractionations to separate soluble and chromatin-enriched fractions were performed as described (Méndez and Stillman, 2000). Briefly, cells were resuspended at $2 \cdot 10^7$ cells/mL in buffer A (10mM HEPES pH 7.9, 10mM KCl, 1.5mM $MgCl_2$, 0.34M sucrose, 10% glycerol, 1mM DTT, 1mM $NaVO_4$, 0.5mM NaF, 5mM β-

glycerophosphate, 0.1mM PMSF, protease inhibitors cocktail (Roche)), and incubated on ice for 5 min in the presence of 0.05% Triton X-100. Low-speed centrifugation (4min/600g/4ºC) allowed the separation of the cytosolic fraction (supernatant) and nuclei (pellet). The cytosolic fraction was clarified by high-speed centrifugation (15min/16000g/4ºC). Nuclei were washed with buffer A and subsequently subjected to hypotonic lysis in buffer B (3mM EDTA, 0.2mM EGTA, 1mM DTT, 1mM $NaVO_4$, 0.5mM NaF, 5mM β-glycerophosphate, 0.1mM PMSF, protease inhibitors cocktail (Roche)) for 30 min on ice. Nucleoplasmic and chromatin-enriched fractions were separated after centrifugation (4min/600g/4ºC). Chromatin was resuspended in Laemmli sample buffer and sonicated twice for 30 seconds at 15% amplitude.

Alternatively, when indicated HeLa cells were lysed and fractionated using a Cell Fractionation Kit (MitoSciences ab109719), which allowed the isolation of mitochondrial, cytoplasmic and nuclear fractions.

5.4. Immunoblots

SDS-polyacrylamide gels and immunoblotting were performed following standard protocols (Harlow and Lane, 1999). The primary antibodies used are listed in Table 4. Horseradish peroxidase (HRP)-conjugated secondary antibodies (Amersham Biosciences) and ECL developing reagent (Amersham Biosciences) were used.

6. Histological analyses

Histopathological analysis was performed at the Compared Pathology Unit, CNIO. Briefly, tissues were fixed overnight in 10% buffered formaline, embedded in paraffine and sectioned (5 μm). Samples were deparaffinized, re-hydrated and stained with hematoxylin-eosin (H&E). For immunohistochemistry (IHC) stainings, tissues were subjet to antigen retrieval and blocking of endogenous enzymatic activities. Tissue slides were digitalized using a Mirax scanner (Carl Zeiss) and equivalent areas per tissue and group were analyzed using the AxioVision digital image processing software (Carl Zeiss), if necessary. Tumor identification and classification was performed by Dr. Alba de Martino (Compared Pathology Unit, CNIO).

Antibody	Use	Supplier	Ref/Catalogue #
(6,4)-pp (64M-2 clone)	IF	Cosmo Bio Co.	NMDND002
α-fetoprotein	IHC	R&D Systems	AF5369
α-tubuline	WB	Sigma	T9026
ATP-synthase	WB	Abcam	AB43176
BrdU	IHC	GE Healthcare	RPN202
BrdU-FITC	FACS	BD-Biosciences	BD 556028
CD3	IHC	Santa Cruz	Sc-1127
CD31	IHC	Abcam	AB28364
CldU (BrdU-clone BUI/75)	IF	Abcam	AB6326
CPD (TDM-2 clone)	IF	Cosmo Bio Co.	NMDND001
CTCF	WB	Millipore	07-729
F4/80	IHC	ABD Serotec	MCA497
H3	WB	Abcam	AB1791
IdU (BrdU-clone B44)	IF	BD-Biosciences	BD 347580
Mek2	WB	BD Transduction	610235
p53	WB	Cell Signaling	9282
PAX5	IHC	Santa Cruz	Sc-1974
hPrimPol	WB	R. Freire's lab	Mourón *et al.*, 2013
mPrimPol	WB	R. Freire's lab	-
PPARγ	WB	Cell Signaling	2435
pS139-H2AX (γH2AX)	WB, IHC	Millipore	07-164
pS15-p53	WB	Cell Signaling	9284S
p(S4/S8)-RPA	WB	Bethyl laboratories	A300-245A
RPA	WB	Cell Signaling	2208
SREBP1	WB	Abcam	AB3259
ssDNA	IF	Millipore	MAB3034
V5 epitope tag	WB	Invitrogen	R960-25

Vimentin	IHC	Cell Signaling	5741

Table 4. Antibodies used in this study

7. Biochemical assays (Dr. Luis Blanco's laboratory data)

7.1. DNA primase assay

DNA primase assay of the PrimPol mutants was evaluated using a 29-mer oligonucleotide (5'-T_{15}CCTGT_{10}-3') as template, which contains a putative herpes virus priming imitation site (GTCC), as described (García-Gómez *et al.*, 2013). The reaction mixture (20μL) contained buffer R (50 mM Tris pH 7.5, 5% Gly, 75 mM NaCl, 1mM $MgCl_2$, 1 mM DTT and 0.1 μg/μL BSA), [γ-^{32}P]ATP (16 nM; 3000 C_i/mmol), 10 μM dGTP and various concentrations of the different mutants (50, 100, 200 and 400nM). The reaction was incubated during 60 min at 30ºC. Reactions were stopped by addition of formamide loading buffer (10 mM EDTA, 95% v/v formamide and 0.3% w/v xylene-cyanol) and loaded in 8 M urea-containing 20% polyacrylamide sequencing gels.

7.2. DNA polymerase activity

A 15-mer oligonucleotide primer (5'-GATCACAGTGAGTAC-3') was labeled using T4 PNK (New England Biolabs) and [γ-^{32}P]ATP (3000 C_i/mmol), and hybridized to a 28-mer oligonucleotide template (5'-AGAAGTGTATCTCGTACTCACTGTGATC-3') in 20 mM Tris, 0.5 M NaCl, heated up to 80ºC and cooled down to RT. The resulting hybrid had a 5' protrusion of 13 templating nucleotides. The reaction mixture (20μL) contained buffer R (50 mM Tris pH 7.5, 5% Gly, 75 mM NaCl, 1mM $MgCl_2$, 1 mM DTT and 0.1 μg/μL BSA) contained 5 nM [γ-^{32}P]ATP-labeled template-primer, 100 μM dNTP and different concentration of the different mutants (50, 100 and 200 nM). The reaction was incubated during 60 min at 30ºC. Reactions were stopped and analyzed as in the DNA primase assay.

RESULTS

RESULTS

Chapter 1: Structure-function analysis of hPrimPol

1. Analysis of the WFYY motif

1.1. WxxY is a conserved motif in PrimPol proteins

Despite the importance of PrimPol in damage tolerance during DNA replication (Bianchi *et al.*, 2013; García-Gómez *et al.*, 2013; Wan *et al.*, 2013; Mourón *et al.*, 2013) its association with human disease remains largely unknown. Interestingly, a variation in the human PrimPol gene (CCDC111) had been identified in a set of patients with high myopia (Zhao *et al.*, 2013). Specifically, exome sequencing at candidate patients identified a missense mutation (Y89D) in PrimPol protein. Amino acid sequence alignment reveals that Tyr89 is part of a conserved motif (WFYY) in higher eukaryotes. Nevertheless, extending the sequence alignment to more primitive organisms reveals that Tyr89 and Phe88 of the WFYY motif are not conserved in other eukaryotes and archaea. In contrast, their neighbor amino acids Trp87 and Tyr90 are highly conserved suggesting that this motif may be important for PrimPol function (Figure 10A and B).Phe88 and Tyr89 are frequently exchanged for other residues. For this reason, this PrimPol motif could be more strictly defined as WxxY.

The active site of PrimPol includes three negatively charged residues (D114, E116 and D280) that are presumably in charge of coordinating the metal activation (Bianchi *et al.*, 2013; García-Gómez *et al.*, 2013). The WFYY motif is in close proximity to the active site. In order to evaluate the importance of this conserved domain, four different PrimPol mutants (W87G, F88L, Y89D and Y90D) were generated, including the presumed "pathological mutation" in Tyr89. To determine their activity in human cells, we have worked with a HeLa-shPrimPol cell line (Mourón *et al.*, 2013) in which a shRNA molecule targeting PrimPol mRNA can be induced with doxycycline (dox). As shown in Figure 11, addition of dox efficiently downregulated the endogenous PrimPol, while exogenous PrimPol (either WT or mutant) was introduced from expression plasmid. The expression levels of all PrimPol variants were monitored with PrimPol and V5 antibodies, and they were comparable in all cases.

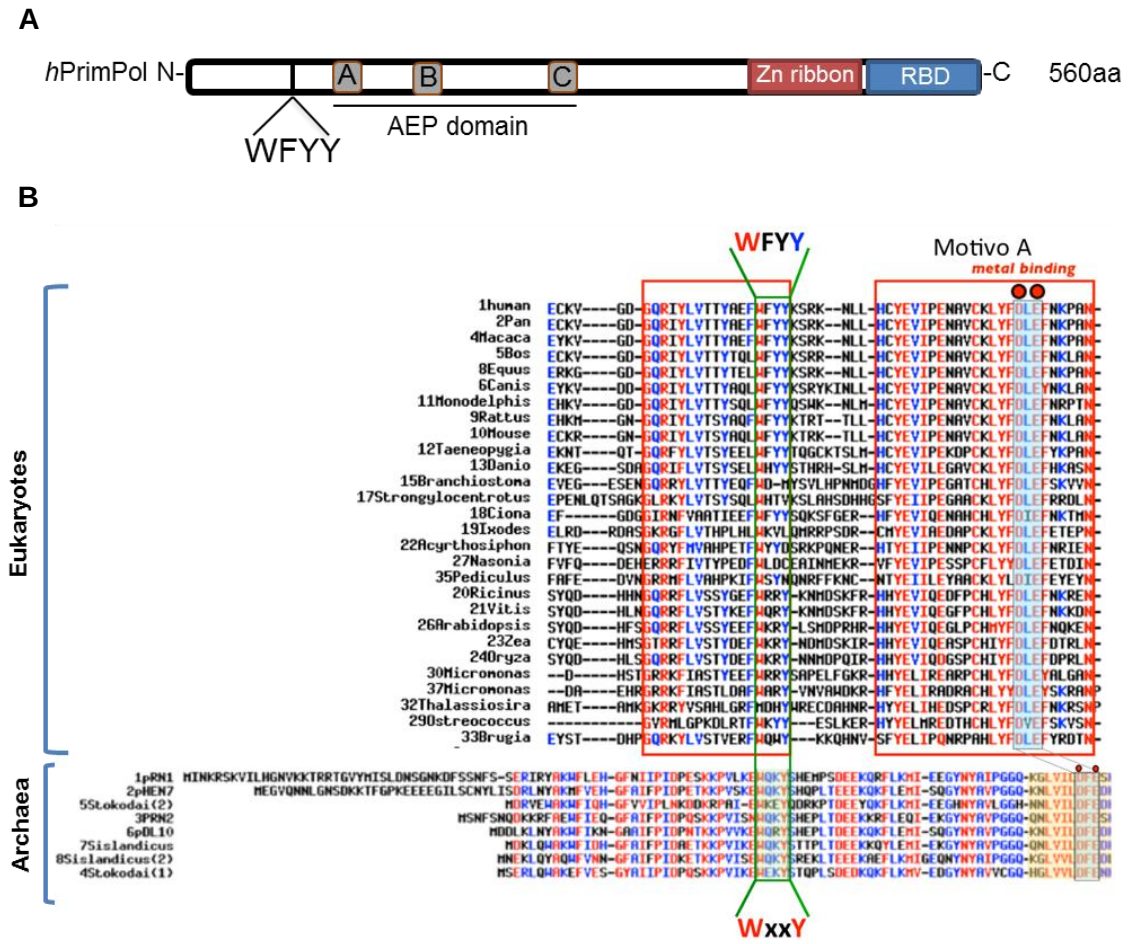

Figure 10. The conserved WFYY domain in PrimPol protein. A. Schematics of hPrimPol showing the positions of conserved active site motifs A, B and C, shared by members of the AEP superfamily, and a Zn-finger domain similar to that of herpesvirus UL52 primase; the WFYY motif described in this chapter is located next to the motif A. **B.** Amino acid sequence alignment of the segment that contains WFYY motif in different eukaryotic and archaeal PrimPol proteins. The motif could be strictly defined as WxxY, the tryptophan (W) is strictly invariant and the tyrosine (Y) is highly conserved in PrimPol proteins. Sequence alignment provided by Dr. L. Blanco (CBMSO, Madrid).

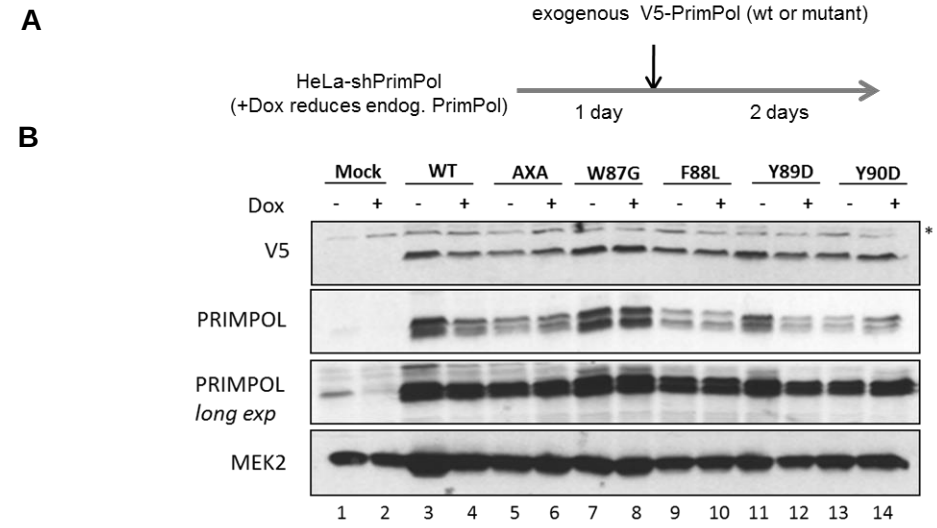

Figure 11. PrimPol replacement assay. A. Schematics of the experimental design. **B.** Immunoblot showing expression levels of WT, AxA, W87G, F88L and Y90D PrimPol variants. Downregulation of endogenous upon dox treatment is shown in lines 1-2. MEK2 levels are shown as loading control.

1.2. Trp87 and Tyr90 are required for PrimPol function in S-phase

First, the activity of the PrimPol mutant versions was evaluated in unperturbed S-phase using stretched DNA fibers. This approach allows the visualization of newly synthesized DNA tracks at the single molecule level. To perform this experiment, living cells were sequentially pulse-labeled with halogenated nucleosides 5-cloro-deoxyuridine (CldU) and 5-iodo-deoxyuridine (IdU). After this, genomic DNA was extracted and stretched onto glass slides, stained with IdU and CldU-specific antibodies, and visualized by immunofluorescence (IF) microscopy. The configuration of replication tracks on single DNA molecules allows the identification of origins, ongoing forks, stalled forks, termination and even re-replication events (Figure 12A and B) (Dorn *et al.*, 2009; Técher *et al.*, 2007). As previously reported (Mourón *et al.*, 2013), PrimPol downregulation led to a decrease in fork rate. This reduction was caused by the absence of PrimPol since it could be reverted by reintroduction of exogenous WT-PrimPol. In contrast, reintroduction of a catalytically inactive PrimPol in which the two carboxylate residues Asp114 and Glu116 have been mutated to alanine (AxA-PrimPol; García-Gómez *et al.*, 2013) did not rescue the phenotype. This "PrimPol replacement" method was used to assess the activity *in vivo* of W87G, F88L, Y89D and Y90D PrimPol variants. W87G and Y90D mutants did not rescue the loss of endogenous PrimPol, whereas F88L and Y89D restored the fork rate to the same extent as WT-PrimPol (Figure 13). This initial result suggests an important role for residues W87 and Y90 in PrimPol activity.

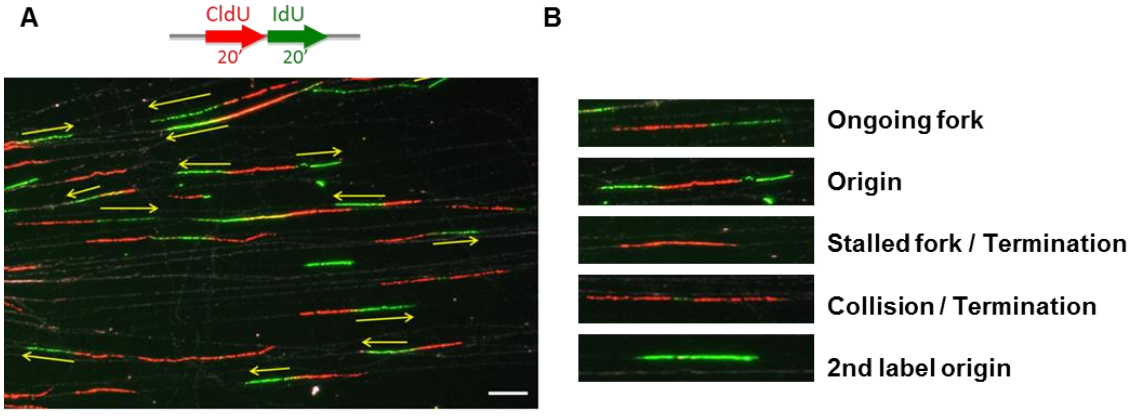

Figure 12. Replication structures detected by DNA fiber spreading. A. Microscopy image of stretched DNA fibers derived from cells sequentially labeled with CldU (red) and IdU (green). Yellow arrows indicate IdU tracks from ongoing forks, normally used to measure FR values. A ssDNA antibody (grey) was used to monitor the integrity of the DNA fibers. Scale bar, 10 μm. **B.** Representative pictures of the types of structures that can be identified with this technique.

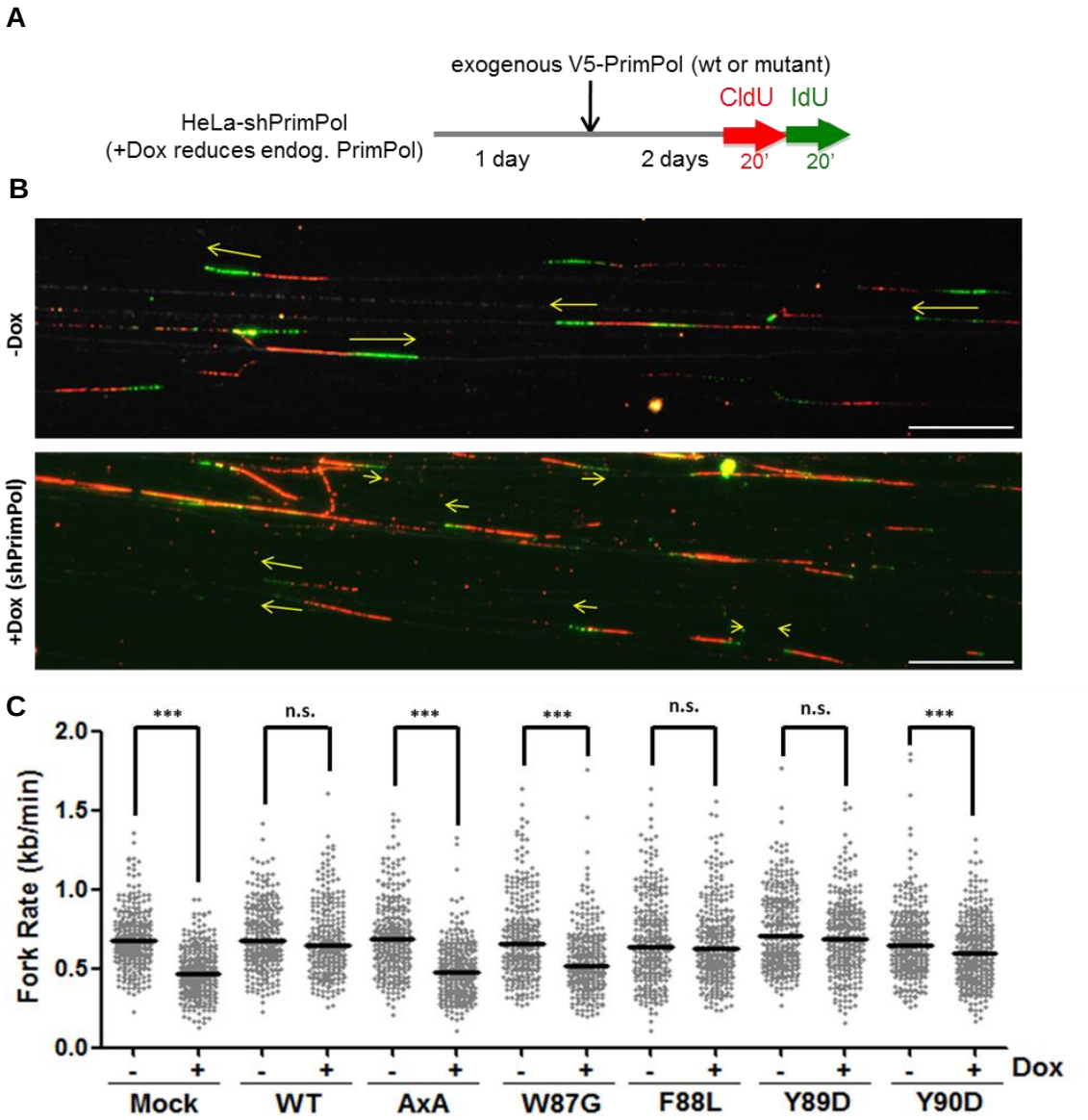

Figure 13. PrimPol Trp87 and Tyr90 are required to maintain the replication fork rate in S-phase. **A.** Workflow of the experiment. After the introduction of exogenous PrimPol (48h), cells were incubated with CldU (red) and IdU (green) and stretched DNA fibers were obtained. **B.** Representative pictures of the DNA fibers before and after dox treatment. Scale bar, 10 μm. **C.** FR values calculated from stretched DNA fibers. Reduction of endogenous PrimPol causes significant drop in FR. The capacity of V5-tagged WT, AxA or different PrimPol mutants to complement the absence of endogenous PrimPol was estimated. N forks >300; n.s.: non-significant; ***p<0.001 (Mann-Whitney test).

1.3. Trp87, Phe88 and Tyr90 are necessary for PrimPol function in response to UV-induced DNA damage

Next, we used a variation of the DNA fiber assay to monitor the progression of replication forks through specific challenges. HeLa-shPrimPol cells were pulse-labeled with CldU (20') and irradiated with UV light (30J/m^2) before pulse-labeling with IdU (20'). In this setting, forks arrested by UV irradiation should have incorporated only the

first analog, whereas those that continued DNA synthesis should be labeled with both analogs (Figure 14A and B). As previously reported (Mourón *et al.*, 2013), loss of PrimPol markedly reduced the percentage of forks displaying continuous synthesis. This phenotype was fully reversed by cotransfection of a plasmid encoding WT PrimPol, but not the AxA catalytic variant. When the new mutants were tested in this assay, we found that Y89D variant restored the loss of endogenous PrimPol to the same extent of the WT version, whereas W87G, F88L and Y90D PrimPol mutants did not (Figure 14C). Therefore, amino acids W87 and Y90 (as seen before), but also F88, play a role in the function of PrimPol in response to UV radiation.

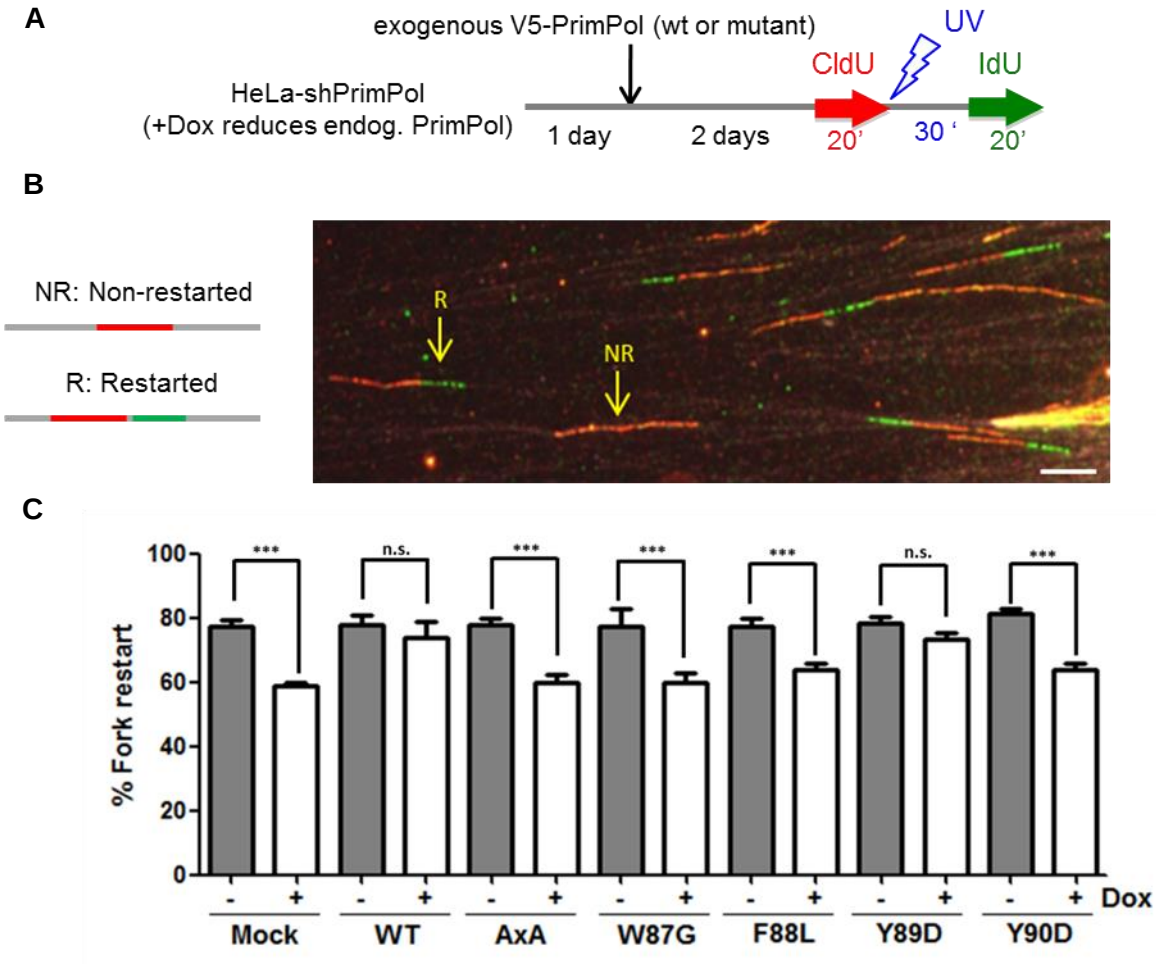

Figure 14. Trp87, Phe88 and Tyr90 residues are necessary to reprime UV-stalled forks. A. Workflow of the experiment. After the introduction of exogenous PrimPol (48h), cells were incubated with CldU (red) before a single irradiation with UV (30 J/m^2). After 30 min, cells were incubated with IdU (green) and stretched DNA fibers were obtained. **B.** Representative picture of DNA fibers. A restarted (R) fork and a non-restarted fork (NR) are marked with yellow arrows. Scale bar, 10 μm..**C.** Quantification of the percentage of fork restart upon UV-irradiation in HeLa-shPrimPol cells with or without dox treatment. N structures= 500. One-way ANOVA, Bonferroni Post-test were applied, ***p<0.0001, n.s: non-significant. Reduction of endogenous PrimPol reduces the fraction of rescued forks. The capacity of V5-tagged WT, AxA or the indicated PrimPol versions to rescue the phenotype was assessed.

Because PrimPol contributes to restart DNA synthesis also after exposure to HU, an ribonucleotide reductase inhibitor that reduces cellular dNTP levels (Mourón *et al.*, 2013), we next tested the WFYY mutants in a dork rescue assay after HU treatment (Figure 15A). As it happened with UV radiation, mutants W87G, F88L and Y90D failed to rescue the loss of WT PrimPol whereas Y89D did not, validating that Trp87, Phe88 and Tyr90 are critical for PrimPol function in fork restart (Figure 15B).

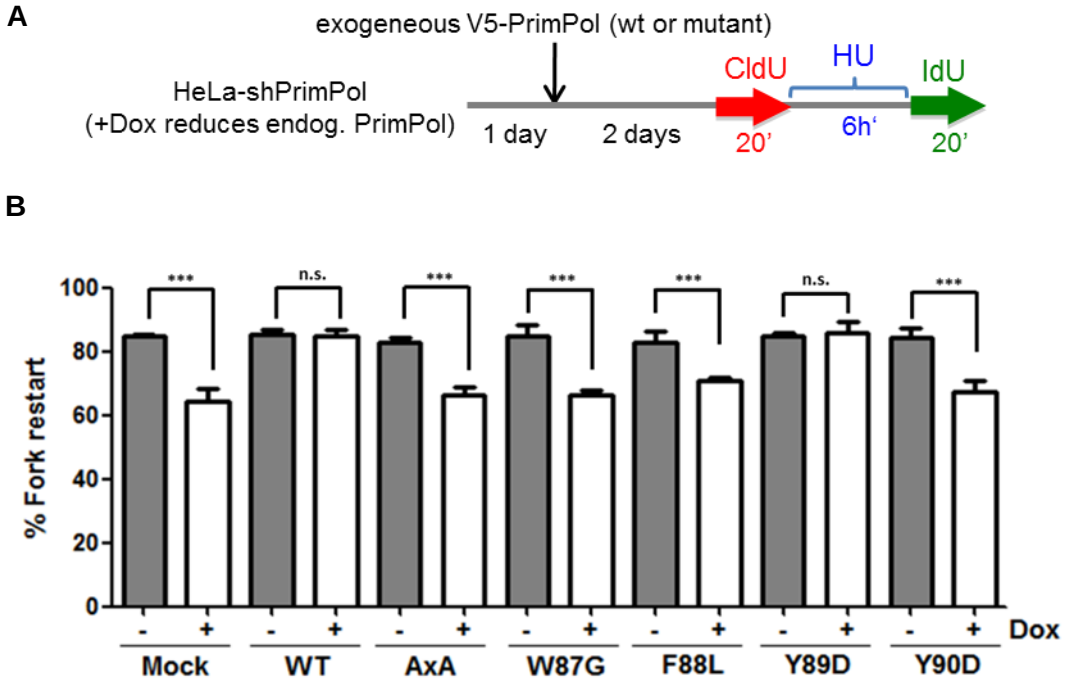

Figure 15. Trp87, Phe88 and Tyr90 residues are necessary to reprime HU-stalled forks. A. Workflow of the experiment. After the introduction of exogenous PrimPol (48h), cells were incubated with CldU (red) before a single irradiation with HU (5 mM) during 6 hours. Then, cells were incubated with IdU (green) and stretched DNA fibers were obtained. **B.** Histograms show the quantification of the percentage of fork restart upon HU treatment in HeLa-shPrimPol cells with or without dox treatment. N structures= 500. One-way ANOVA, Bonferroni Post-test were applied, ***p<0.0001, n.s: non-significant. Reduction of endogenous PrimPol reduces the fraction of rescued forks. The capacity of V5-tagged WT, AxA or the indicated PrimPol versions to rescue the phenotype was assessed.

1.4. Mutations in WFYY motif does not alter PrimPol subcellular distribution

In HeLa cells, PrimPol protein is distributed in nucleus, mitochondria and cytoplasm (García-Gómez *et al.*, 2013). To rule out the possibility that the inactive mutants could display an inappropriate *in vivo* distribution, the levels of PrimPol were tested in each subcellular compartment after biochemical fractionation (Figure 16). WT V5-tagged PrimPol was also used to evaluate any possible effect of the tag in the subcellular distribution. Importantly, none of the mutants showed an abnormal distribution.

Therefore, the effects observed in the stretched DNA fibers experiments are the consequence of defects in protein activity rather than a deficient subcellular distribution.

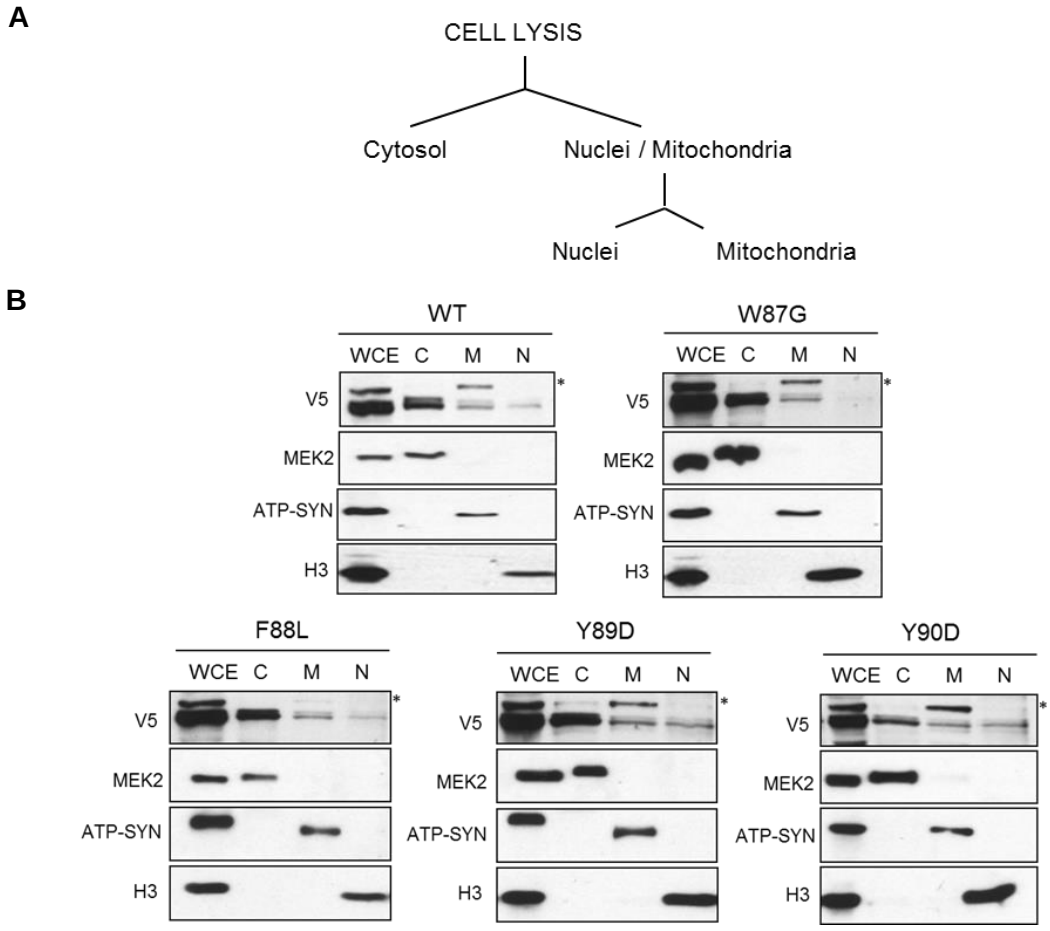

Figure 16. Mutations in the WFYY motif do not alter the subellular localization of PrimPol. A. Schematic of the biochemical fractionation (See Methods). **B**. Immunoblots showing the levels of the indicated proteins in whole cell extract (WCE), cytosol (C), mitochondria (M) and nuclear (N) fractions. MEK2, ATP-SYNTHASE (ATP-SYNT) and H3 were used as controls of the biochemical fractionation.

1.5. Trp87 and Tyr90 are essential for the primase and polymerase activities of PrimPol

The *in* vivo data described previously indicates that Trp87 and Tyr90 are important for all PrimPol activities tested, and Phe88 also required for fork restart after UV or HU challenge. In collaboration with Dr. Luis Blanco's laboratory (CBMSO, Madrid) the biochemical activity of the same PrimPol variants were assessed *in vitro*. In perfect concordance with the *in vivo* data W87G and Y90D PrimPol point mutants were completely inactive for their primase activity. F88L PrimPol variant shows a modest primase activity, while the "pathological mutant" Y89D was active (Figure 17A). Similar results were obtained when the DNA polymerase activity was tested *in vitro*.

W87G and Y90D were inactive, F88L was active but less functional than the WT version and Y89D mutant was fully active in this primer elongation assay (Figure 17B).

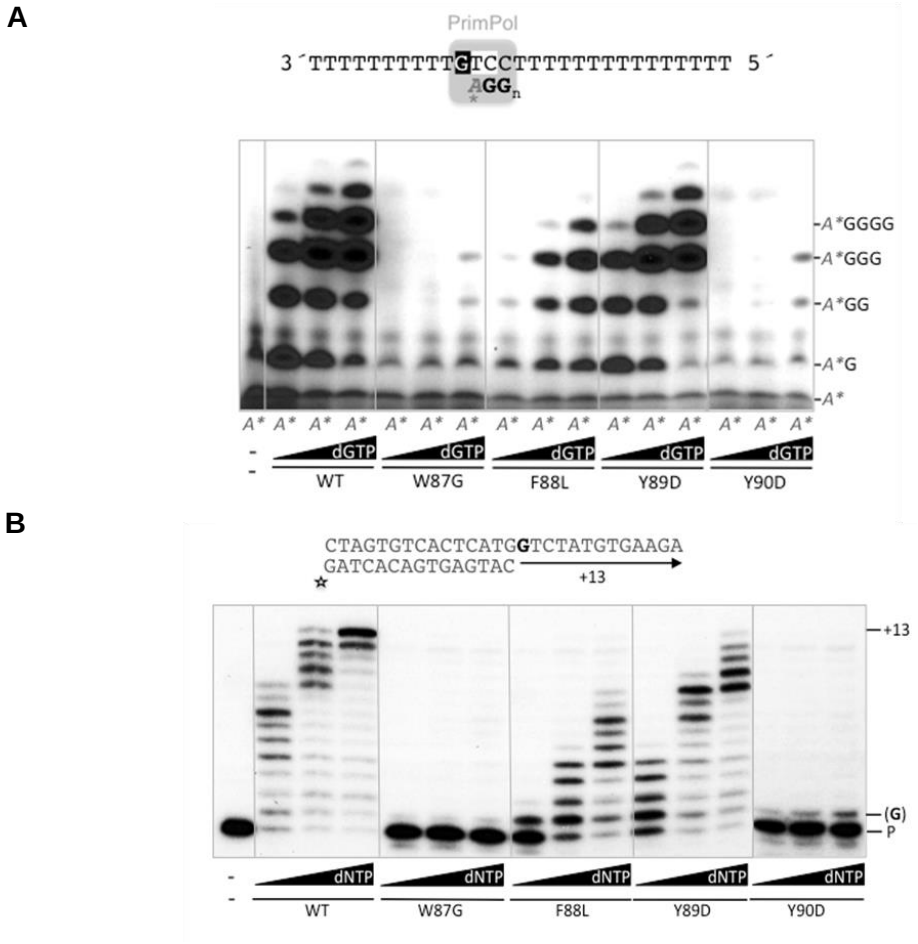

Figure 17. Trp87 and Tyr90 are essential for hPrimPol primase and polymerase activities. A. Primase assay using an oligonucleotide containing a primase-preferred sequence (GTCC). Labeled (γ-32P)-ATP was provided as the 5' nucleotide and dGTP as the 3' nucleotide. hPrimPol forms the expected A*G product which is subsequently expanded by reiterative insertion of dG. **B.** Running star DNA polymerization by hPrimPol. Primer elongation is measured by changes in the labeled primers mobility (Biochemical data obtained from Dr. Luis Blanco laboratory (CBMSO, Madrid).

1.6. WFYY motif is necessary for DNA-enzyme-dNTP preternary complex formation

The formation of stable complexes between PrimPol and its substrates (DNA and dNTPs) can be assessed by Electrophoretic Mobility Assay (EMA). PrimPol is able to form a complex with ssDNA and an incoming nucleotide (Figure 18A). Preternary complex (enzyme-DNA-dNTP) formation was affected by mutations in the WFYY motif. F88L and Y89D could perform the formation of the preternary complex, although less efficiently than WT PrimPol. W87G and Y90D were defective in the

formation of the complex because they cannot bind the incoming 3' nucleotide (Figure 18B). All the mutants were able to bind DNA to the same extend ruling out the possibility of unappropriated preternary complex formation due to DNA binding alterations (Figure 19).

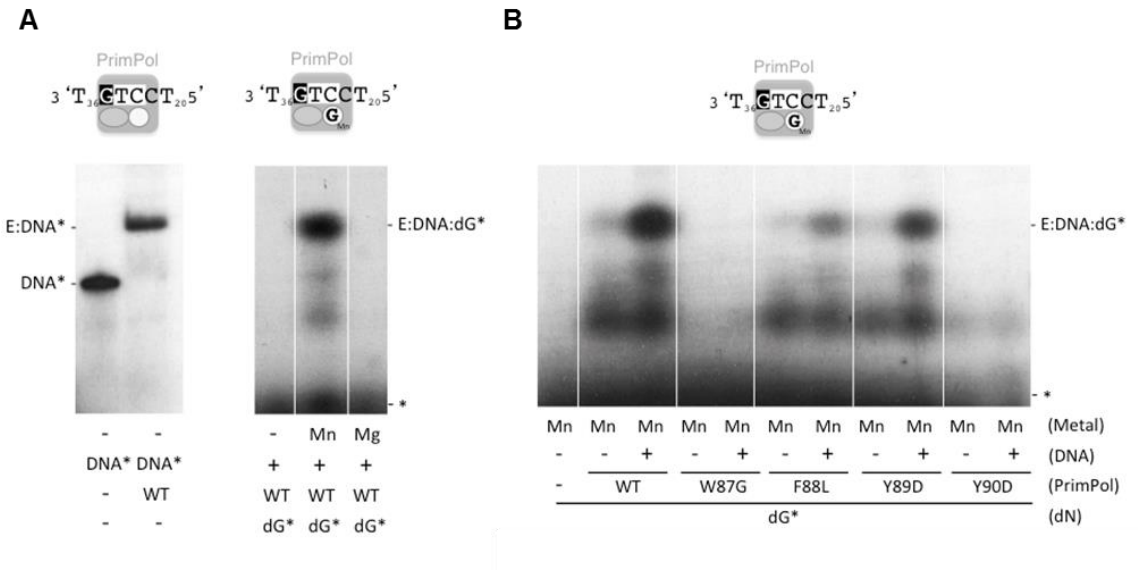

Figure 18. Role of the WFYY motif in the interaction of hPrimPol with DNA and nucleotides. A. hPrimPol forms a stable preternary complex with ssDNA and an incoming 3' nucleotide. left panel: binary complex of hPrimPol with labeled ssDNA (E:DNA*); both 5' nucleotide (primer) and 3' nucleotide (incoming) binding sites are empty. Right panel: Mn^{+2}-dependent detection of a preternary complex (E: DNA:dG*); the 3'nucleotide now occupies its position. **B.** Preternary complex formation by WT or mutant hPrimPol was determined by EMSA (Biochemical data obtained from Dr. Luis Blanco laboratory (CBMSO, Madrid).

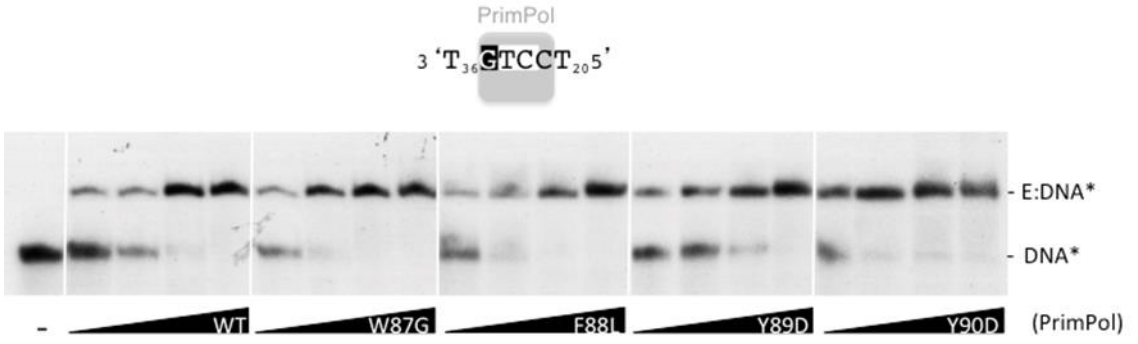

Figure 19. Alterations in the WFYY motif did not impair DNA binding. Electrophoretic mobility shift assay (EMSA) showing a stable interaction of hPrimPol with labeled ssDNA, which is not affected by any of the investigated mutations at the WFYY motif. The positions of the free DNA and the DNA-PrimPol complex (E-DNA*) are indicated. (Biochemical data obtained from Dr. Luis Blanco laboratory (CBMSO, Madrid).

In summary, conserved WFYY motif is necessary for the formation of the preternary complex (E:DNA:dNTP) in the active site entrance channel and therefore for the

primase and polymerase acitvities of PrimPol. Remarkably, Y89D seems to be a fully active PrimPol variant. Therefore, its participation in the etiology of myopia needs to be revised (see Discussion).

2. Tyr100 in hPrimPol

Alterations in PrimPol found in human cancers are normally mutations or homozygous deletions. The most common PrimPol mutations in cancer (L79R, L96I, R417L/W and H426N) produce the loss of PrimPol catalytical activity (Calvo and Blanco, unpublished results). We have paid special attention to one particular mutation in cancer (Y100H) because Tyr100 is a highly conserved residue in eukaryotic PrimPol (Figure 20A). This amino acid is located next to the A motif of PrimPol. Besides this, alignment with other AEP primases shows that primases that insert only NTPs, such as Prim1, have a His in the steric gate, whereas those capable of inserting dNTPs possess a Tyr in this position (Figure 20B). Therefore, we decided to analyze whether this change detected in a cancer cell might influence affinity for the sugar moiety. Indeed, the *in vitro* biochemical characterization of the Y100H mutant performed by Dr. Luis Blanco laboratory (CMBSO, Madrid) indicates that the primase and polymerase activities are preserved but with a change in sugar discrimination, as it preferentially insert NTP over dNTPs (Figure 21).

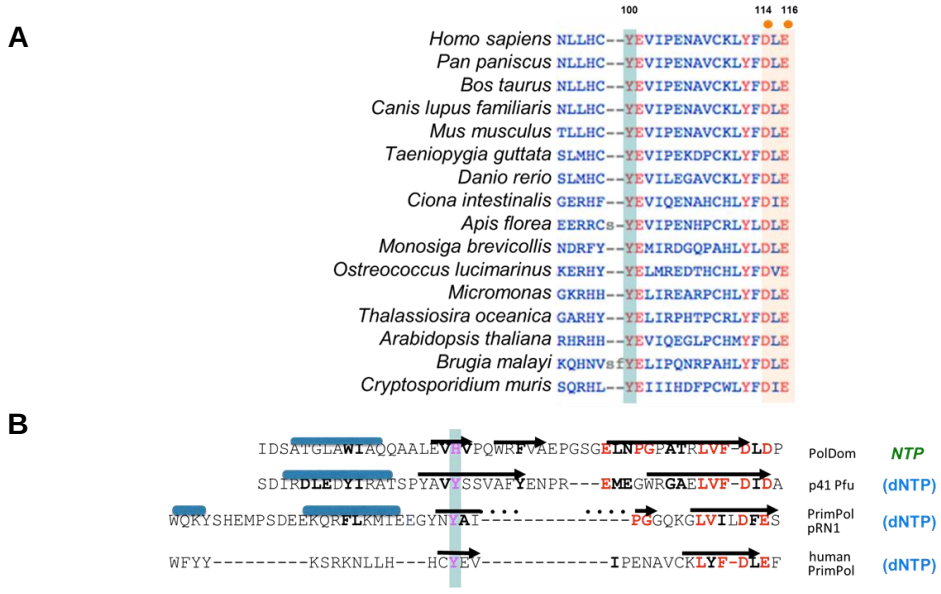

Figure 20. Tyrosine 100 of hPrimPol protein is a highly conserved residue in eukaryotic PrimPol. A. Tyr100 that appears to be mutated in a cancer cell line is located next to the active site in the A motif. This Tyr100 is highly conserved in high eukaryotes. **B.** Tyrosine is conserved in proteins which insert preferentially dNTPs and histidine is preserved in PolDom which inserts mainly rNTPs.

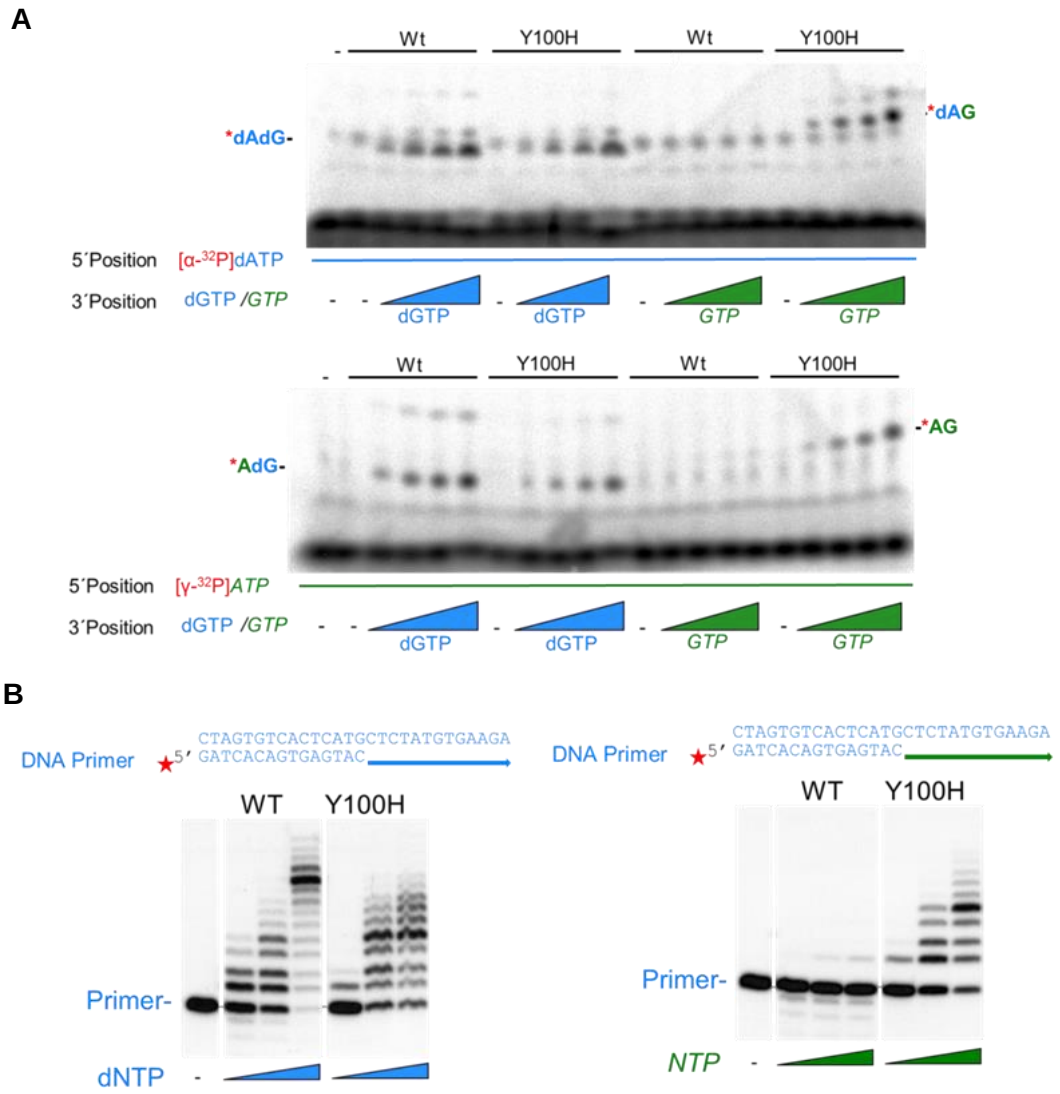

Figure 21. Y100H PrimPol point mutations is fully active but changes the sugar discrimination from dNTPs to NTPs. A. Primase assay using an oligonucleotide containing a primase-preferred sequence (GTCC). Labeled (γ-32P)-ATP was provided as the 5' nucleotide and dGTP as the 3' nucleotide (dGTP or GTP as indicated). hPrimPol forms the expected A*G product which is subsequently expanded by reiterative insertion of dG. **B.** Running star DNA polymerization by hPrimPol. Primer elongation is measured by changes in the labeled primers mobility. In left panel the 3' nucleotide was dNTP whereas in the right panel was NTP. (Biochemical data obtained from Dr. Luis Blanco laboratory (CBMSO, Madrid).

We have assessed the capacity of Y100H PrimPol to ensure proper fork progression in unperturbed S-phase using stretched DNA fibers. As shown in Figure 22, addition of dox efficiently downregulated the endogenous PrimPol, while exogenous PrimPol (either WT or mutant) was introduced from expression plasmid. The expression levels of all PrimPol variants were monitored with PrimPol and V5 antibodies, and they were comparable in all cases. Expression of V5-Y100H after ablation of endogenous PrimPol in HeLa-shPrimPol cells can restore the FR values to the same extent than the wild-type version (Figure 23).

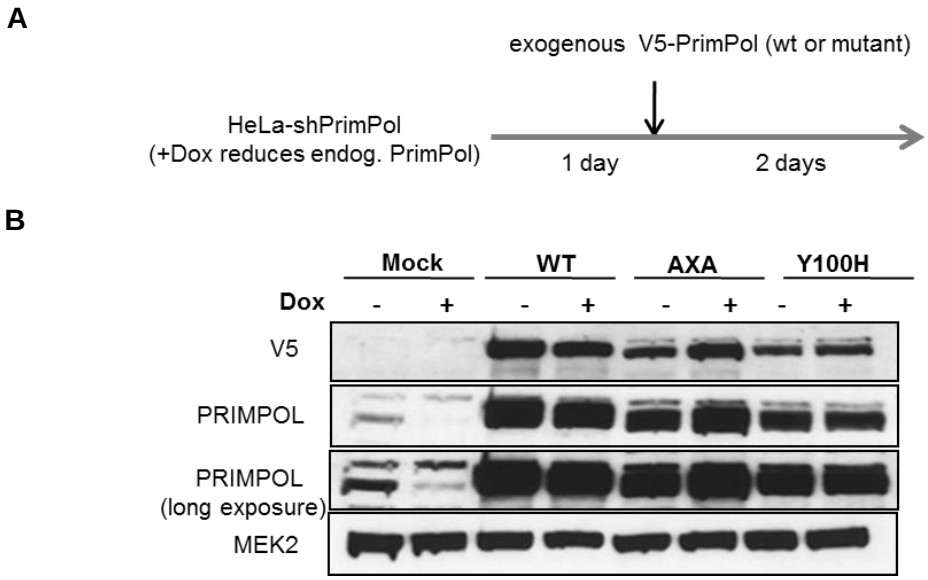

Figure 22. PrimPol replacement assay. A. Schematics of the experimental design. **B.** Immunoblot showing expression levels of WT, AxA, W87G, F88L and Y90D PrimPol variants. Downregulation of endogenous upon dox treatment is shown in lines 1-2. MEK2 levels are shown as loading control.

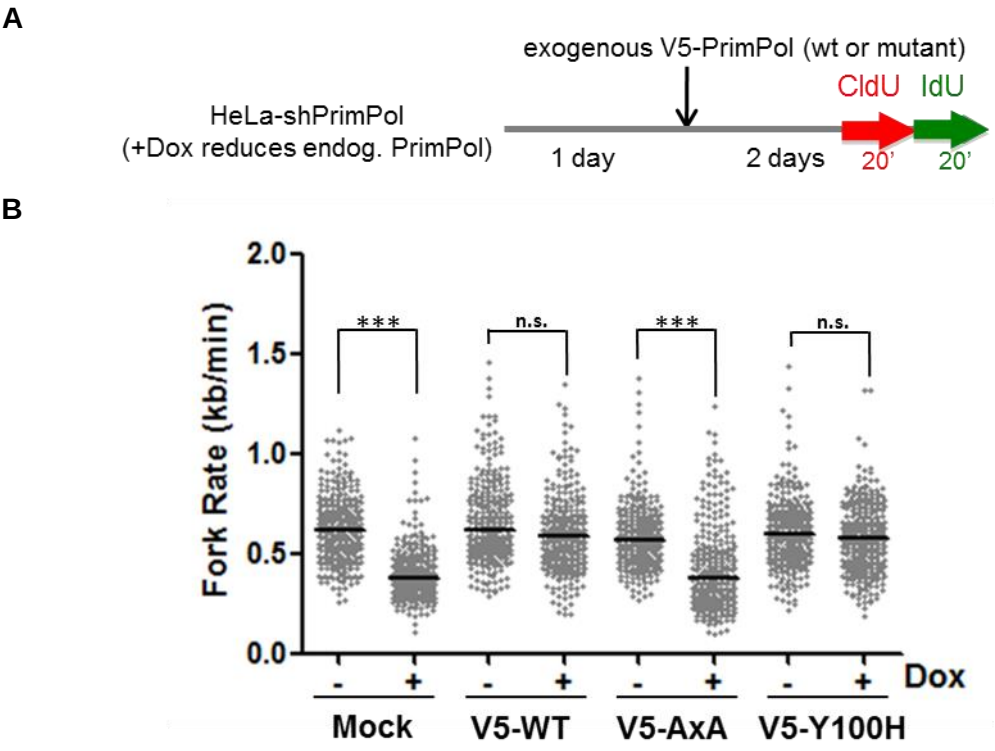

Figure 23. Y100H PrimPol mutant can maintain the replication fork rate in S-phase. A. Workflow of the experiment. After the introduction of exogenous PrimPol (48h), cells were incubated with CldU (red) and IdU (green) and stretched DNA fibers were obtained. **B.** FR values calculated from stretched DNA fibers. Reduction of endogenous PrimPol causes significant drop in FR. The capacity of V5-tagged WT, AxA or Y100H PrimPol mutant to complement the absence of endogenous PrimPol was estimated. N forks >300; n.s.: non-significant; ***p<0.001 (Mann-Whitney test).

Y100H-PrimPol variant also displayed the ability to restart forks arrested with HU to the same extend as WT-PrimPol variant suggesting (Figure 24), that this specific point mutation does not compromise the *in vivo* function of hPrimPol. However, whether the change in dNTP/NTP preference introduces any problem related to genomic instability remains to be evaluated.

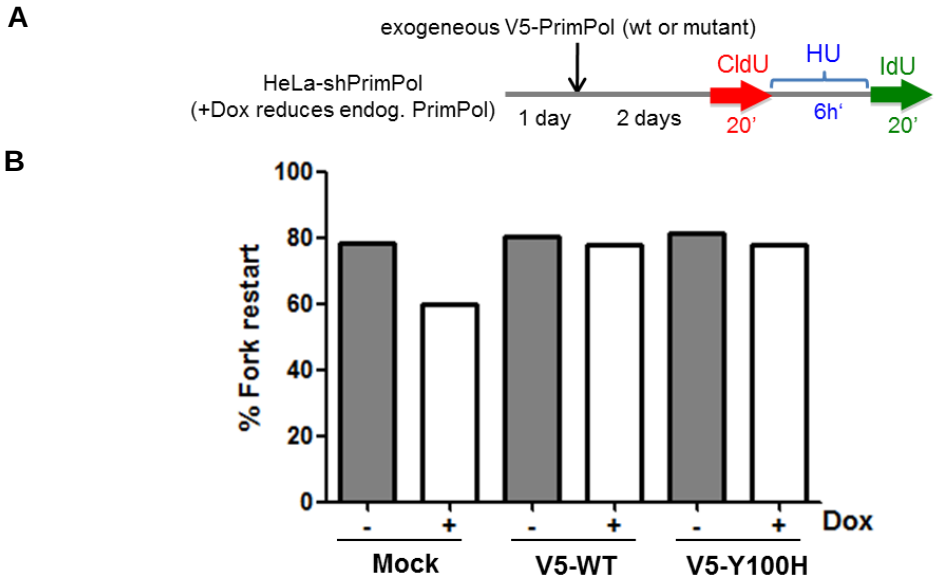

Figure 24. Y100H PrimPol variant can reprime HU-stalled forks. A. Workflow of the experiment. Workflow of the experiment. After the introduction of exogenous PrimPol (48h), cells were incubated with CldU (red) before a single irradiation with HU (5 mM) during 6 hours. Then, cells were incubated with IdU (green) and stretched DNA fibers were obtained. **B.** Histograms show the quantification of the percentage of fork restart upon HU treatment in HeLa-shPrimPol cells with or without dox treatment. N structures= 500. Reduction of endogenous PrimPol reduces the fraction of rescued forks. The capacity of V5-tagged WT or Y100H PrimPol versions to rescue the phenotype was assessed.

Altogether, Tyr100 of PrimPol is an important residue for sugar discrimination. The change of this amino acid for a His favors the introduction of NTPs instead of dNTPs. This residue change seems not to affect the activity *in vivo* observed at the single molecule level.

Chapter 2: A PrimPol KO mouse model

1. PrimPol is ubiquitously expressed in mouse tissues

To obtain information about PrimPol expression in the mouse, we quantitatively assessed PrimPol mRNA levels by RT-qPCR in different organs extracted from 12-week-old wild-type mice. PrimPol mRNA levels were normalized to the expression levels of housekeeping gene GAPDH. We observed that PrimPol was expressed in all tested organs (Figure 25). The highest expression levels were detected in the skin, bone marrow, spleen and gastrointestinal tissues. Notably, expression levels were lower in muscle and liver, despite their abundance in mitochondria. We conclude from this analysis that PrimPol is ubiquitously expressed in the tissues of healthy young mice.

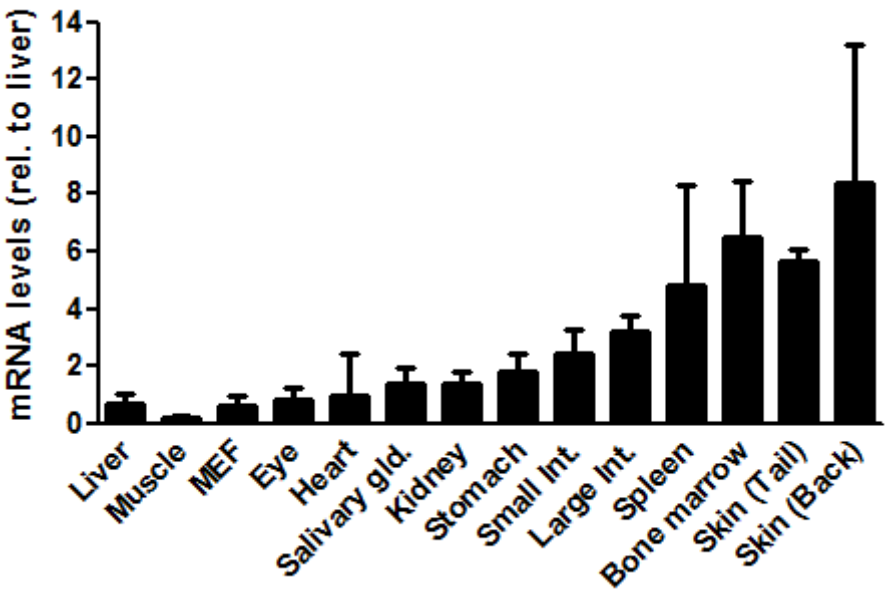

Figure 25. Ubiquitous expression of PrimPol in young mice. PrimPol expression levels were quantified by RT-qPCR on total RNA isolated from the indicated organs. PrimPol mRNA levels were normalized to GAPDH gene expression. Histogram represents expression as fold change, calculated on the average PrimPol levels in four mice relative to expression in the liver (n=4, 2 male and 2 female; 12 weeks old).

2. PrimPol$^{-/-}$ mouse model

In order to study the role of PrimPol *in vivo*, we obtained a KO PrimPol mouse model generated by "gene-trap" (Texas A&M Health Science Center Institute of Biosciences and Technology). In this model, the insertion of a gene trap cassette in the 5'-UTR of

murine PrimPol gene disrupts gene expression (Figure 26A). The gene-trap allele is subsequently referred as PrimPol^{-}. After the original mouse line was introduced by embryo rederivation into the CNIO Animal Facility, the genetic background was enriched in C57BL/6 by continued intercrosses with pure C57BL/6 mice. Genotype was routinely confirmed by genomic PCR (Figure 26B).

Both PrimPol$^{+/-}$ and PrimPol$^{-/-}$ mice were viable and born at Mendelian rates, viable and fertile (Figure 26C). Neither PrimPol$^{+/-}$ nor PrimPol$^{-/-}$ male or female mice displayed any indication of reduced fertility (Figure 26D).

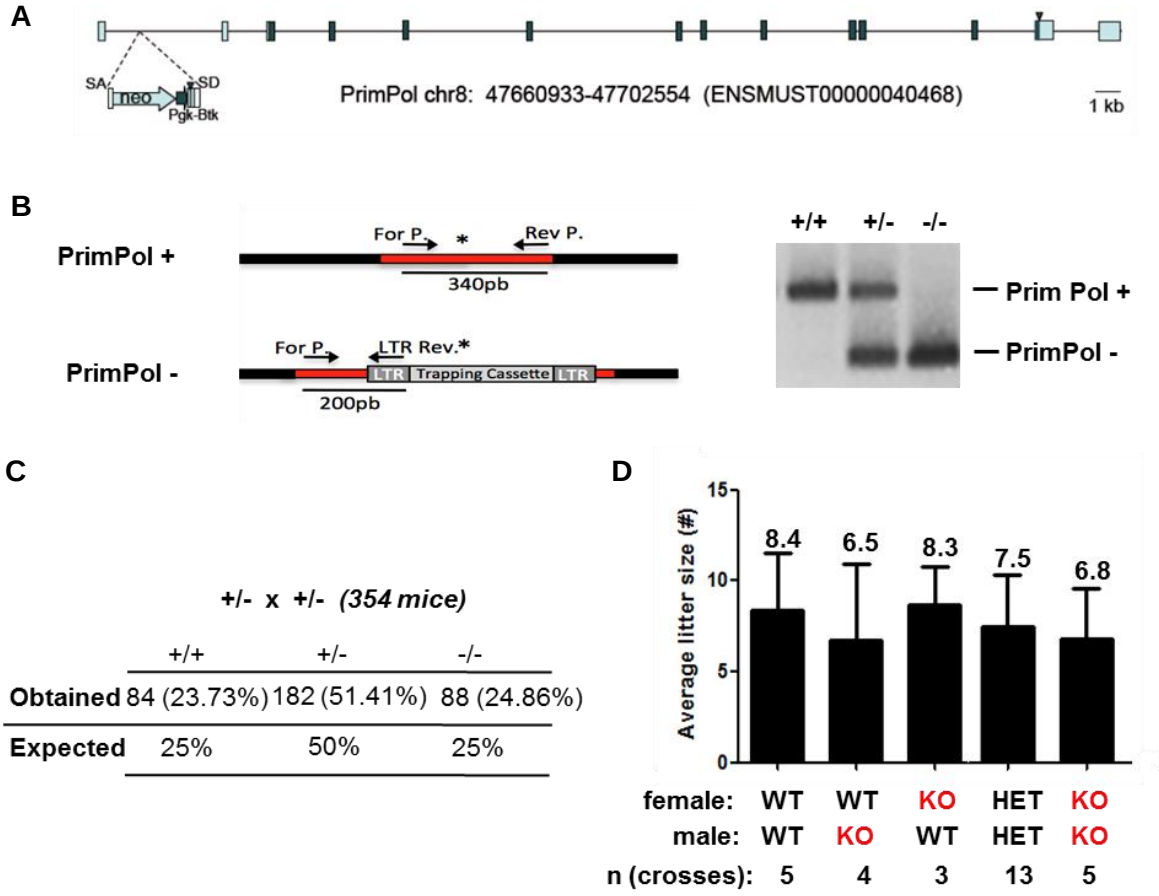

Figure 26. A viable strain of PrimPol-deficient mice. A. Gene-trap insertion in the 5'-UTR generates a knock-out allele in the murine PrimPol gene. **B.** Left. Three-primer genotyping strategy from genomic DNA yields a 340 bp product in the wt PrimPol allele and a 200 bp product in the null allele. Right, genotyping of one mice of each genotype (PrimPol$^{+/+}$, PrimPol$^{+/-}$ and PrimPol$^{-/-}$). **C.** Expected and obtained percentages of PrimPol$^{+/+}$, PrimPol$^{+/-}$ and PrimPol$^{-/-}$ newborn after PrimPol$^{+/-}$ x PrimPol$^{+/-}$ breeding showing that PrimPol$^{-/-}$ mice are born at Mendelian rates. **D.** PrimPol$^{-/-}$ mice are fertile. Histogram shows the average litter size and standard deviation of the indicated crosses. The genotypes of the paretns (WT, HET and KO) and the number of litters scored of each type of cross are indicated (n).

The complete ablation of PrimPol expression was confirmed by protein immunoblots in mouse embryonic fibroblasts (MEFs) and bone marrow derived from PrimPol$^{-/-}$ mice (Figure 27). We also noticed a downregulation in the endogenous PrimPol levels in the heterozygous mice (Figure 27A and B). PrimPol levels were downregulated in PrimPol$^{+/-}$ and undetectable in PrimPol$^{-/-}$ cell extracts. Notably, the antibody used for the murine extracts seems to be more specific in bone marrow than in MEFs.

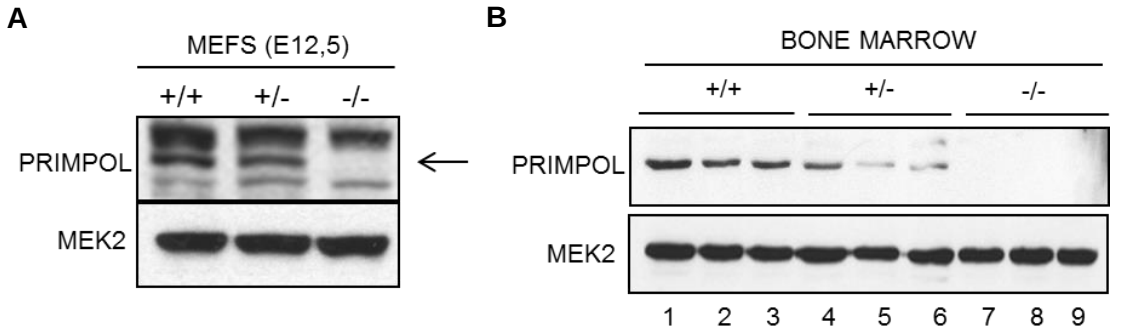

Figure 27. PrimPol levels in MEFs and bone marrow. A. PrimPol protein levels in PrimPol+/+, PrimPol+/- and PrimPol-/ MEFs as determined by immunoblots. Arrow marks the specific band corresponding to murine PrimPol. MEK2 was used as a loading control. **B.** PrimPol protein levels in PrimPol+/+, PrimPol+/- and PrimPol-/- bone marrow from three mice of each genotype as determined by immunoblots. MEK2 was used as a loading control.

2.1. DNA replication and cell proliferation in PrimPol$^{-/-}$ primary cells

In human tumoral cell lines and in avian cells loss of PrimPol slows down proliferation rate and induces replicative stress and genomic instability (Mourón *et al.*, 2013; Wan *et al.*, 2013; Bianchi *et al.*, 2013). In contrast, the effects of PrimPol ablation had not been established in primary mammalian cells. PrimPol$^{+/-}$ were not affected in their proliferation rate, but PrimPol$^{-/-}$ MEFs proliferated at a slower rate in culture (Figure 28A). The global efficiency of DNA synthesis, assessed by BrdU incorporation was not affected, but PrimPol deficient cells presented a slight accumulation in G2/M population (Figure 28B). To monitor the presence of replicative stress, we evaluated the levels of γH2AX and p-(S4/S8)RPA proteins by immunoblot. No differences were found in these RS markers. However, we observed that PrimPol$^{-/-}$ MEFs displayed higher levels of endogenous p53 (Figure 28C) which may contribute to the accumulation of cells in G2/M and the reduction in proliferation rate. Moreover, PrimPol$^{-/-}$ MEFs displayed lower FR values (Figure 28D; Mourón *et al.*, 2013) suggesting that the lack of PrimPol compromises the normal DNA replication.

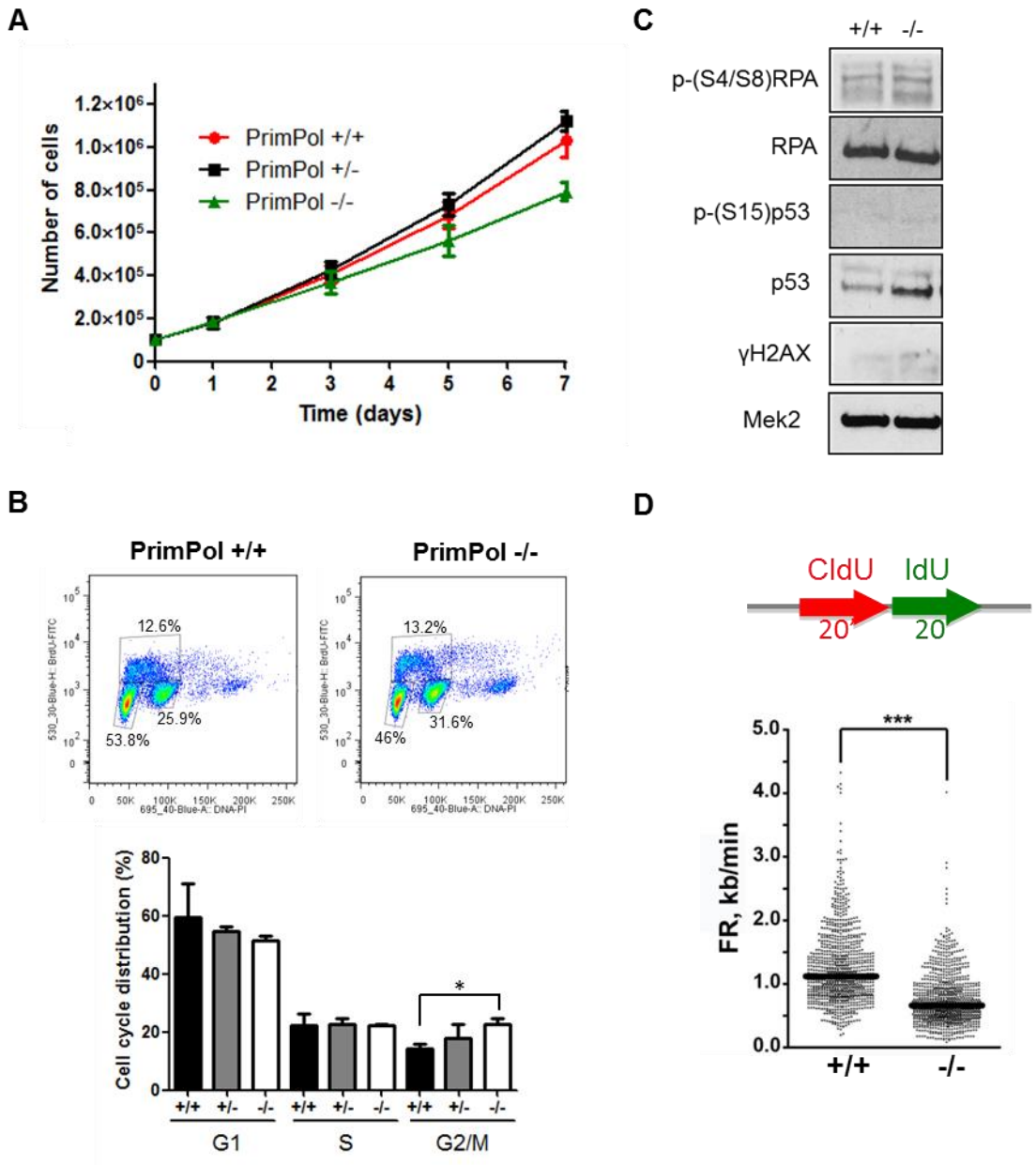

Figure 28. Mild effects in cell proliferation in PrimPol-deficient MEFs. A. Proliferation curves of PrimPol$^{+/+}$, PrimPol$^{+/-}$ and PrimPol$^{-/-}$ MEFs (n = 3 experiments, error bars present to SD). **B.** Immunoblot for p-RPA, RPA (total), p-p53, p53 (total) and γH2AX. MEK2 was used as loading control. **C.** BrdU incorporation profiles in PrimPol$^{+/+}$ and PrimPol$^{-/-}$ MEFs analyzed by flow cytometry (upper part). Cells were pulse-labeled with BrdU for 30 min and stained with PI for DNA content. (lower part) Quantification of the cell cycle distribution of 4 different clones of PrimPol$^{+/+}$, PrimPol$^{+/-}$ and PrimPol$^{-/-}$ MEFs. Error bars present SD. *p<0.05. **D.** FR values calculated from stretched DNA fibers. PrimPol ablation causes significant drop in FR. Black line indicates the median. N forks >300; n.s.: non-significant; ***p<0.001 (Mann-Whitney test; Part D extracted from Mourón *et al.*, 2013).

2.2. PrimPol deficiency affects the homologous recombination rate in MEFs

Upon fork collapse, replication can be rescued by a priming event downstream of the lesion, in the absence of PrimPol this pathway is compromised (Mourón *et al.*, 2013; Wan *et al.*, 2013; Bianchi *et al.*, 2013). In single-molecule analysis of DNA replication, PrimPol deficient MEFs displayed short labeled-tracks (Mourón *et al.*, 2013). However, flow cytometry analysis of cell cycle and proliferation curves do not reflect an extensive problem, which could indicate that stalled forks are rescued by template switching (TS) mechanisms (reviewed in Pertmann and Helleday, 2010; Branzei, 2011). If this was the case, crossover events should be visualized as sister chromatid exchanges (SCE) on metaphase chromosomes (Sonoda *et al.*, 1999). Cells were labeled for 38hwith BrdU and BrdU incorporation was visualized on metaphase chromosomes by light microscopy (Figure 29A). The frequency of SCE events was found to be higher in PrimPol$^{-/-}$ MEFs (Figure 29B). This result has implications in the role of PrimPol in the choice between mechanisms of damage tolerance (see Discussion).

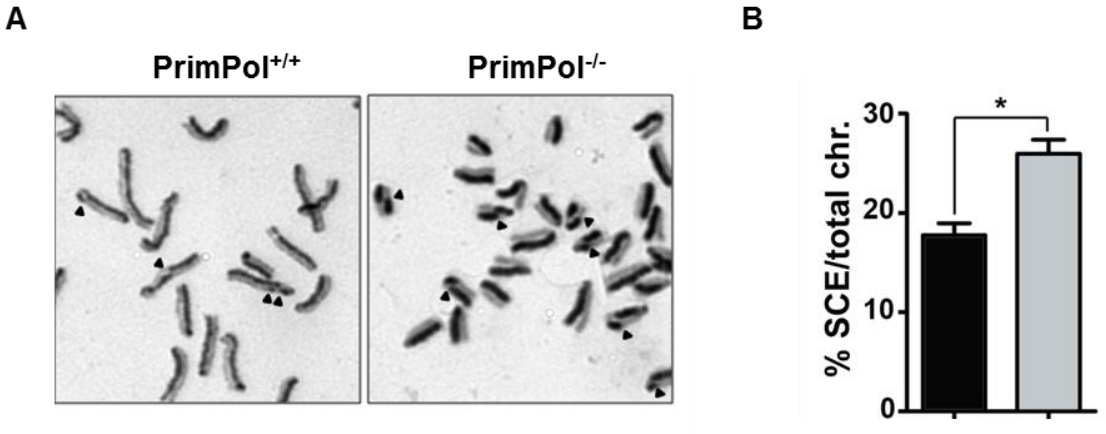

Figure 29. PrimPol deficiency increases SCE. A. Representative pictures of metaphase spreads in PrimPol$^{+/+}$ and PrimPol$^{-/-}$ MEFs. **B.** Quantification of SCE events in PrimPol$^{+/+}$ and PrimPol$^{-/-}$ MEFs (n=3 experiments) *p<0.05.

2.3. Primpol loss sensitizes cells to UV-radiation

In human tumor cell lines challenged with UV radiation, PrimPol is facilitating the start of stalled forks via its interaction with RPA (Mourón *et al.*, 2013; Wan *et al.*, 2013). Therefore, we decided to characterize in more detail the possible protective role of PrimPol to UV radiation.

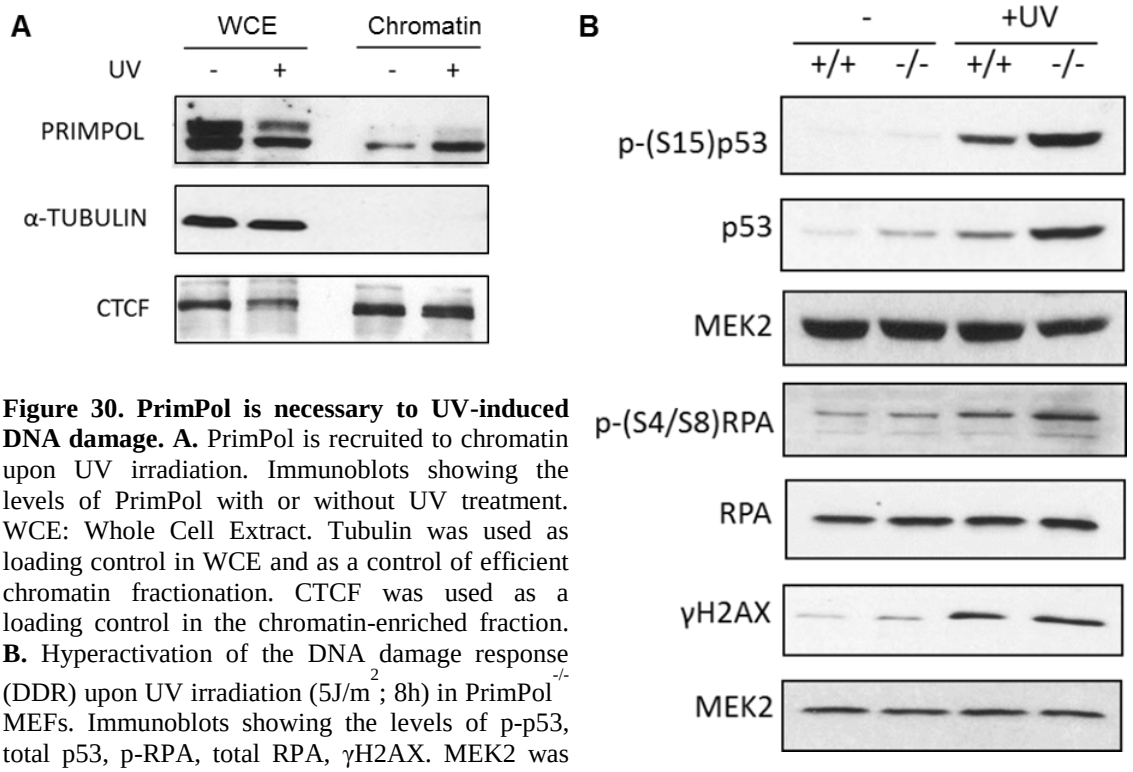

Figure 30. PrimPol is necessary to UV-induced DNA damage. A. PrimPol is recruited to chromatin upon UV irradiation. Immunoblots showing the levels of PrimPol with or without UV treatment. WCE: Whole Cell Extract. Tubulin was used as loading control in WCE and as a control of efficient chromatin fractionation. CTCF was used as a loading control in the chromatin-enriched fraction. **B.** Hyperactivation of the DNA damage response (DDR) upon UV irradiation ($5J/m^2$; 8h) in PrimPol$^{-/-}$ MEFs. Immunoblots showing the levels of p-p53, total p53, p-RPA, total RPA, γH2AX. MEK2 was used as a loading control.

We first confirmed that PrimPol is recruited onto chromatin in UV-challenged MEFs. Indeed, 3h after irradiating cells with UV ($30J/m^2$), the fraction of PrimPol protein with the chromatin increased in comparison to untreated cells (Figure 30A). Next, we monitored the presence of γH2AX, p-(S4/S8)RPA and p-(S15)p53 and the total levels of these proteins by Western-Blot 8h after challenging the cells with UV. In untreated conditions there was a slight increase in total p53 in PrimPol$^{-/-}$ MEFs which could reflect the mild proliferative problem (Figure 30B). This increase was more prominent after UV irradiation and was accompanied by the detection of p-(S15)p53 (Figure 30B). In addition, PrimPol$^{-/-}$ MEFs displayed lower BrdU incorporation 8h after UV challenge, although this problem is solved at later time points probably by compensatory mechanisms (Figure 31A and B).

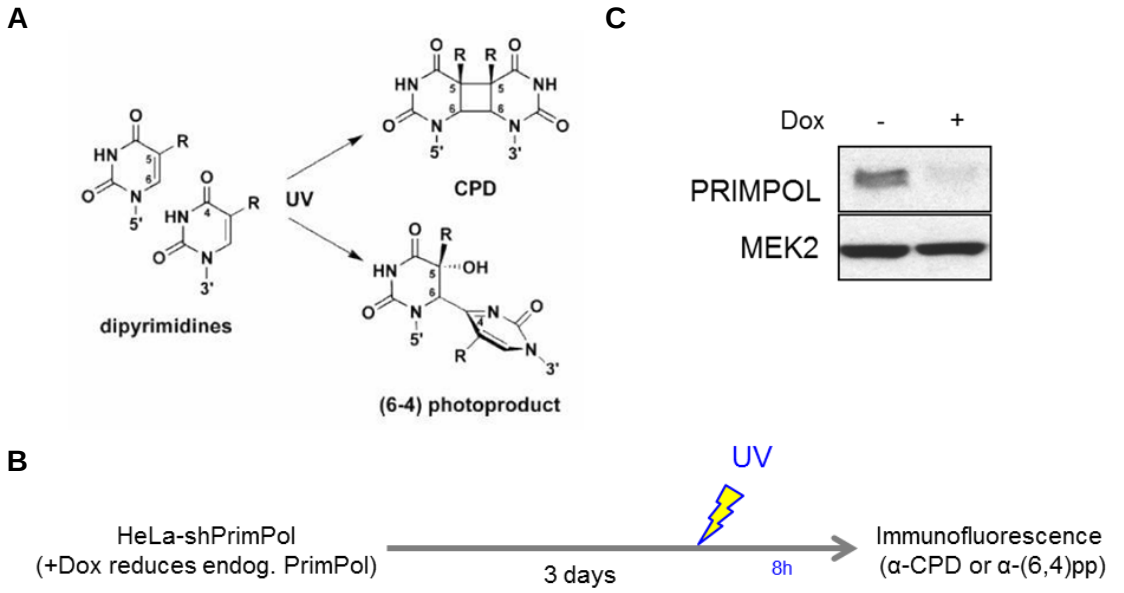

Figure 31. Schematics of the experiment. A. Structures of DNA lesions induced by UV light. **B.** Workflow of the experiment. After UV irradiation (5J/m^2; 8h), cells were fixed and immunostained with α-CPD or α-(6,4)pp (see Methods). **C.** Immunoblot showing hPrimPol levels before and after dox treatment in HeLa-shPrimPol cells. MEK2 was used as loading control.

The most common DNA lesions induced by UV are pyrimidine dimers, CPD and (6,4)-pp, both of which can stall the progression of replication forks (Figure 31A). If these lesions are not properly repaired, forks can collapse leading to double strand breaks formation (reviewed in Muñoz and Méndez, 2016). PrimPol is capable of bypassing these two types of lesions *in vitro* (Mourón *et al.*, 2013), although there is no information about the possibility of bypassing these lesions *in vivo*. Therefore, we have evaluated the persistence of pyrimidine dimers after UV irradiation. For technical reasons related to antibody specificity, these assays were conducted in HeLa-shPrimPol cells (Figure 31B and C). We observed that the absence of PrimPol produces an accumulation of CPDs and (6,4)-pp lesions in good agreement with the *in vitro* data (Figure 32 and 33). Notably, (6,4)-pp staining shows high levels of background as observed in the untreated conditions.

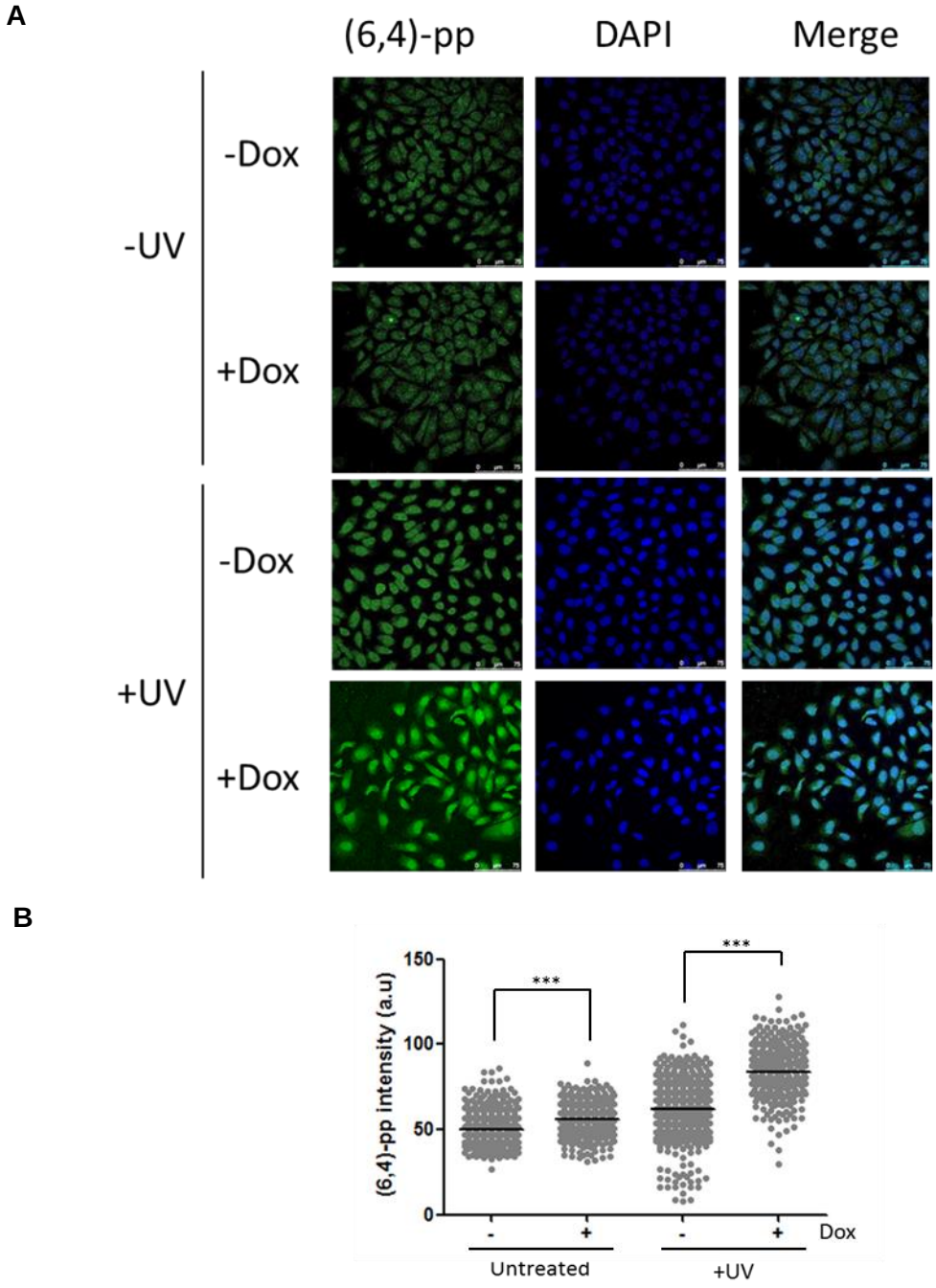

Figure 32. PrimPol-deficient cells accumulate (6,4)-pp lesion after UV irradiation. A. Representative IF images showing (6,4)-pp levels in the cell nuclei after UV irradiation. **B.** Quantification of the intensity of (6,4)-pp nuclear staining (n>273 nuclei in each condition). ***p<0.001 (Mann-Whitney test).

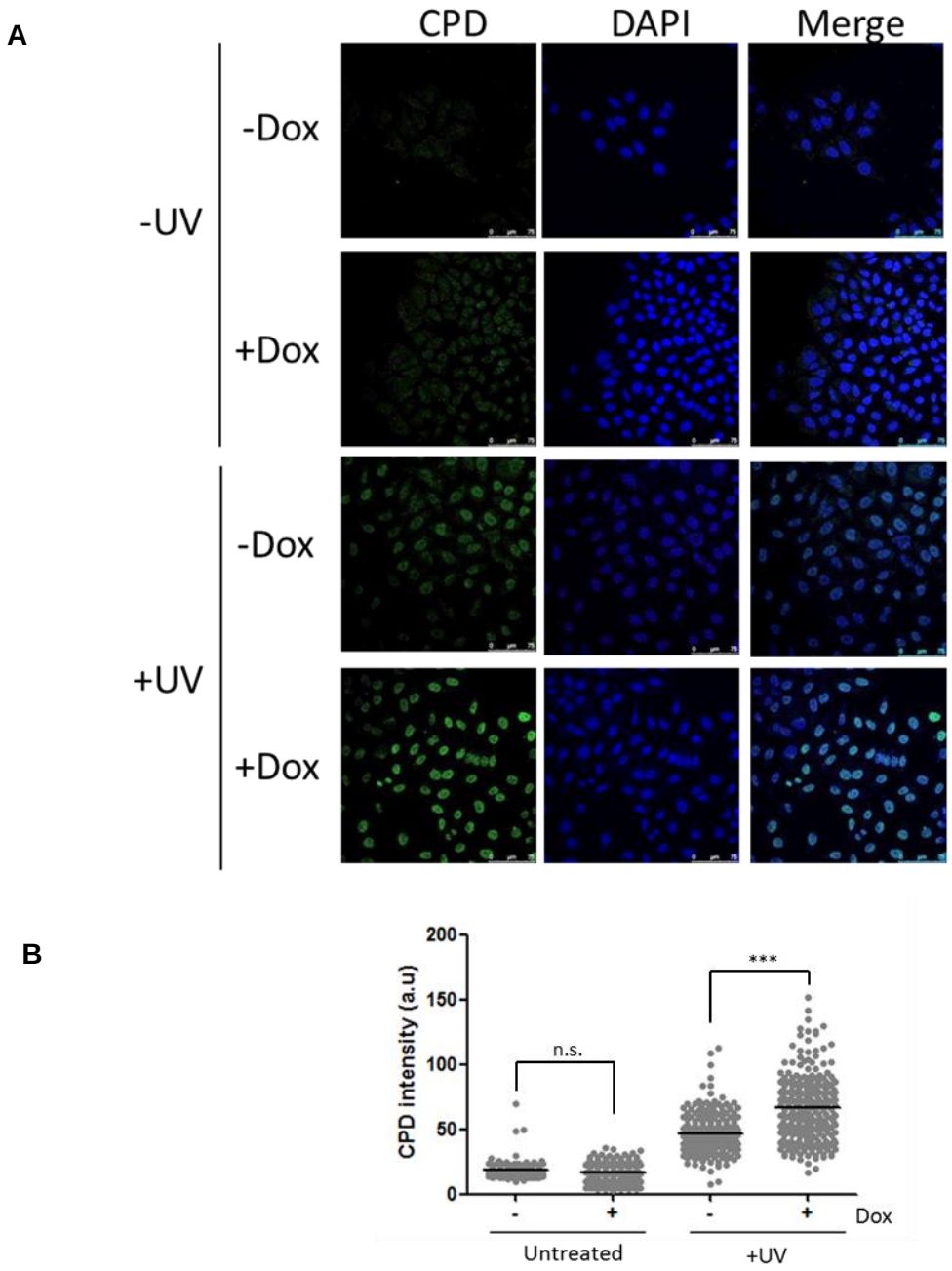

Figure 33. PrimPol-deficient cells accumulate CPD lesion after UV irradiation. A. Representative IF images showing CPD levels in the cell nuclei after UV irradiation. **B.** Quantification of the intensity of CPD nuclear staining (n=262 nuclei in each condition). n.s.: non-significant; ***p<0.001 (Mann-Whitney test).

Altogether, the experiments with cells in culture suggest that PrimPol plays a protective role to UV-induced DNA damage. The lack of PrimPol promotes the hiperactivation of p53, problems with the DNA synthesis and the accumulation of pyrimidine dimers after UV. In chapter 3, the UV-susceptibility of PrimPol mice will be reported in detail.

2.4. PrimPol loss facilitates cell transformation

It is not yet clear whether PrimPol acts as oncogene or a tumor suppressor. We tested how the absence of PrimPol affected cell transformation in primary MEFs transfected with H-RasV12 and E1A. In this classic "colony transformation" assay, PrimPol$^{-/-}$ showed enhanced transformation suggesting that PrimPol may be acting as a tumor suppressor gene (Figure 34A and B).

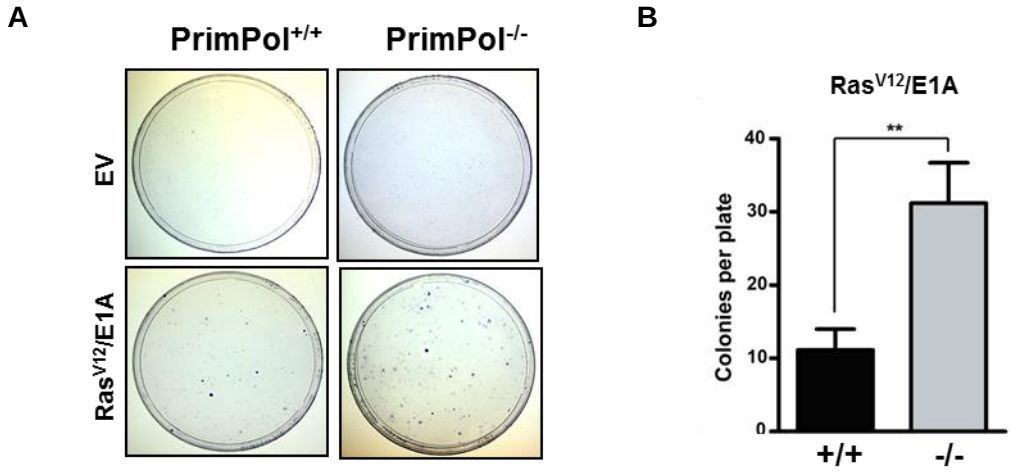

Figure 34. Enhanced oncogenic transformation in PrimPol deficient MEFs. A. Colony formation assay in primary MEFs (PrimPol$^{+/+}$ and PrimPol$^{-/-}$) transfected with H-RasV12/E1A or with empty vector (EV). **B.** Quantification of colonies per plate in PrimPol$^{+/+}$ and PrimPol$^{-/-}$ MEFs. (n= 3 plates) **p<0.01.

2.5. PrimPol deficient mice show mild lymphopenia

As described in Figure 26, PrimPol$^{-/-}$ mice were born at Mendelian rates and were viable. A small set of mice (n=4, 2 males and 2 females) were sacrificed at 12 weeks of age to monitor any possible abnormalities. While the necropsy analysis did not reveal any major phenotype, analysis of blood revealed a mild lymphopenia in PrimPol$^{-/-}$ mice, since they presented lower levels of circulating lymphocytes (Figure 35A). IHC staining of spleen sections showed an increase in DNA damage marker γH2AX, although it did not reach statistically significance (p=0.14) (Figure 35B). Despite these mild effects in young PrimPol-deficient mice, the animals remained healthy and did not show any signs of morbidity in their youth (see below).

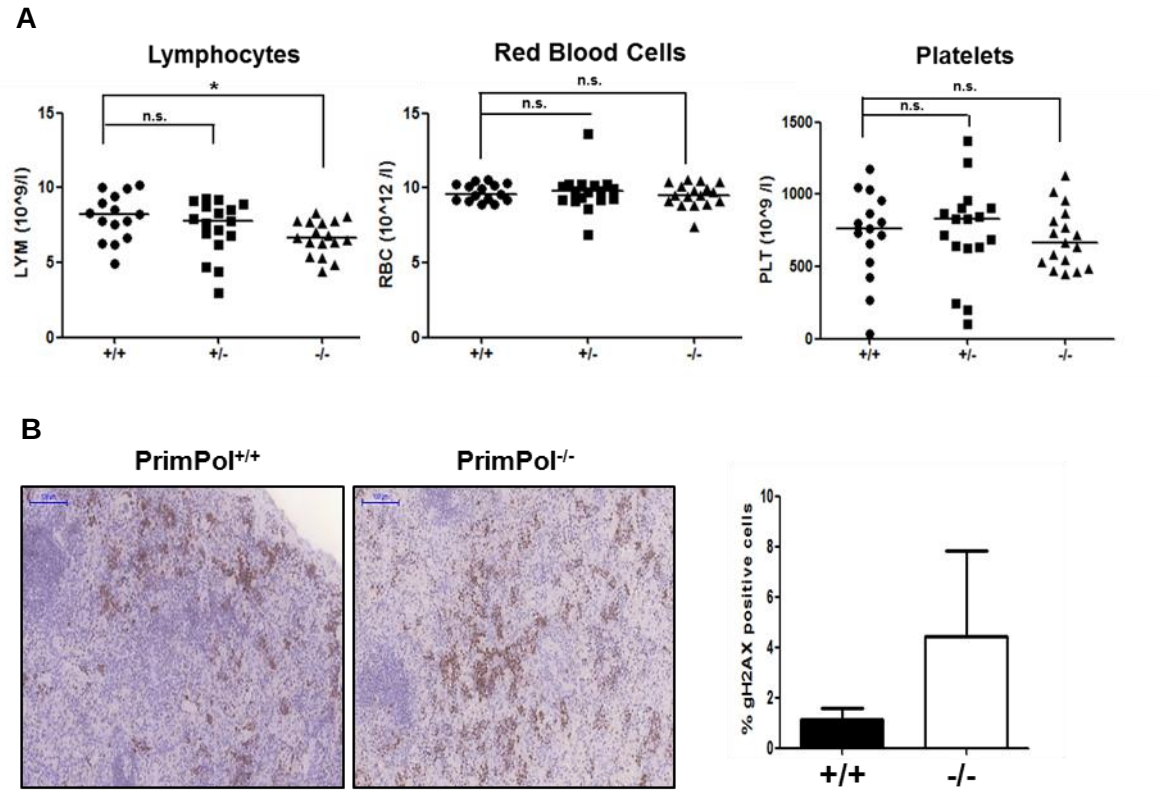

Figure 35. Mild lymphopenia in young PrimPol deficient mice. A. Quantification of lymphocytes, red blood cells and platelets in circulating blood of mice of the indicated genotypes (n = 15 PrimPol$^{+/+}$, 18 PrimPol$^{+/-}$ and 17 PrimPol$^{-/-}$ mice). *p<0.05, n.s.= non-significant. **B.** Left, spleen sections immunostained with γH2AX. Right, quantification of the percentage of positive cells for γH2AX (n=3).

2.6. PrimPol deficiency in longevity studies

To determine the long-term phenotypic effects of PrimPol ablation *in vivo*, cohorts of PrimPol$^{+/+}$, PrimPol$^{+/-}$ and PrimPol$^{-/-}$ mice were arranged for ageing/longevity studies. Mice were monitored routinely and sacrificed at the human endpoint following regulations established by the Animal Experimental Ethics Committee (Instituto de Salud Carlos III). Kaplan-Meier survival curves indicated that PrimPol$^{-/-}$ animals had a mean overall lifespan of 94 weeks, lower than their wt and PrimPol$^{+/-}$ littermates (110.5 and 110, respectively) (Figure 36). All mice in this study were subject to histopathological examination in collaboration with Dr. Alba de Martino (Head, CNIO compared pathology). In the following sections we summarize the phenotypic findings associated to ageing and the results of the histopathology examinations.

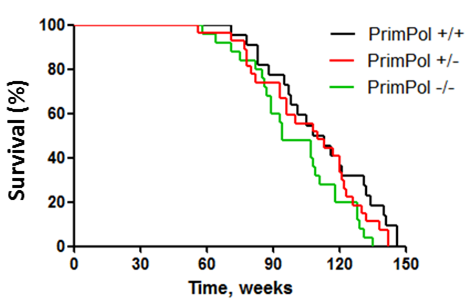

Figure 36. Reduced lifespan after PrimPol ablation *in vivo*. Kaplan-Meier curves for control (black), PrimPol$^{+/-}$ (red) and PrimPol$^{-/-}$ (green) mice. 24 individuals were included in each group. *p<0.05.

2.6.1. PrimPol$^{+/+}$ and PrimPol$^{+/-}$ display signs of alopecia and ocular ulcers

PrimPol$^{+/-}$ and PrimPol$^{-/-}$ mice presented a higher degree of alopecia than PrimPol$^{+/+}$ littermates (Figure 37A). For unknown reasons, this phenotype was more prevalent in females (Figure 37B). Anatomopathological analysis of skin sections revealed the presence of "folded follicles", aberrant structures in which excessive keratinization prevents the release of hair from the follicle. This analysis also revealed the atrophy of sebaceous glands accompanied by a recruitment of mast cells (Figure 37C).

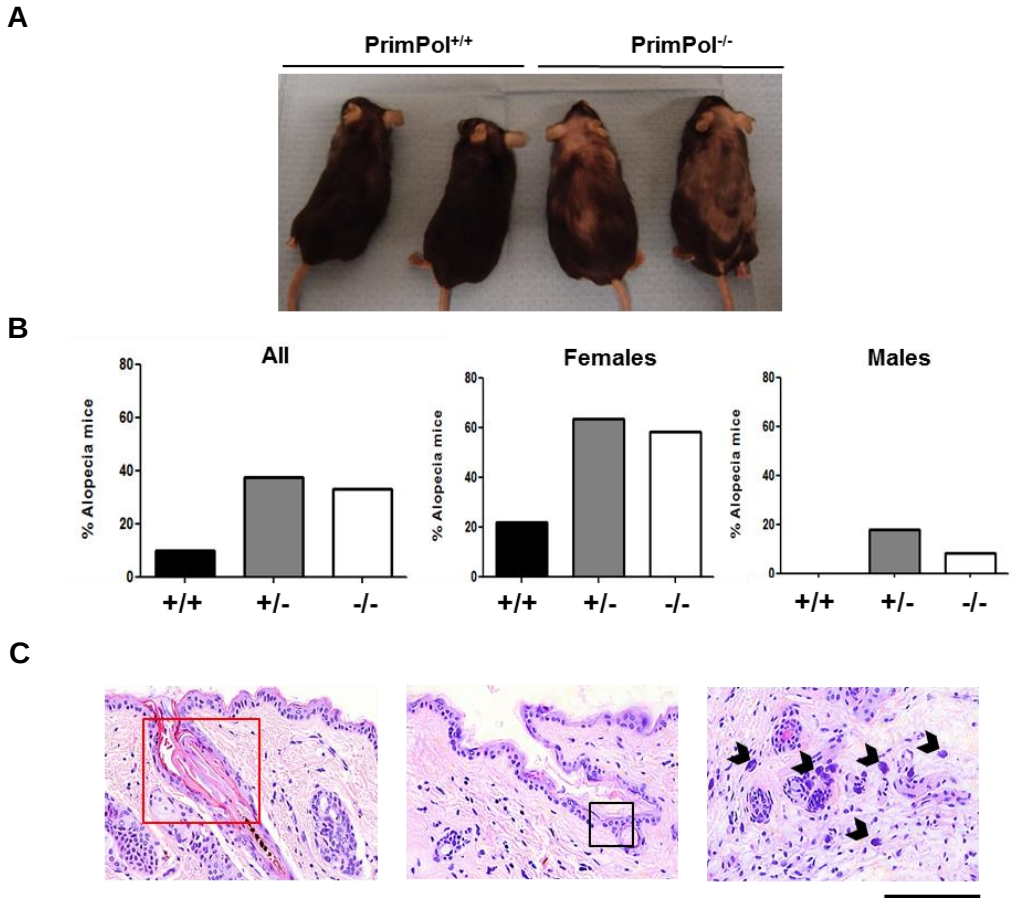

Figure 37. PrimPol deficient mice develop alopecia. A. Representative images of the grade of the hair loss observed in PrimPol$^{-/-}$ mice at 72 weeks old. **B.** Histograms show the percentage of total mice with alopecia in the ageing study. The results are also shown separated by gender. **C.** Representative section of

the skin from PrimPol$^{+/-}$ and PrimPol$^{-/-}$ females mice stained with H&E. Folded follicle (left), atrophic sebaceous gland (middle) and mast cells infiltration indicated with black arrows (right).

Besides the hair loss phenotype, higher frequency of ocular ulcers was observed in PrimPol$^{+/-}$ and PrimPol$^{-/-}$ mice that again, it seemed to be gender-specific being more frequent in females (Figure 38A and B).

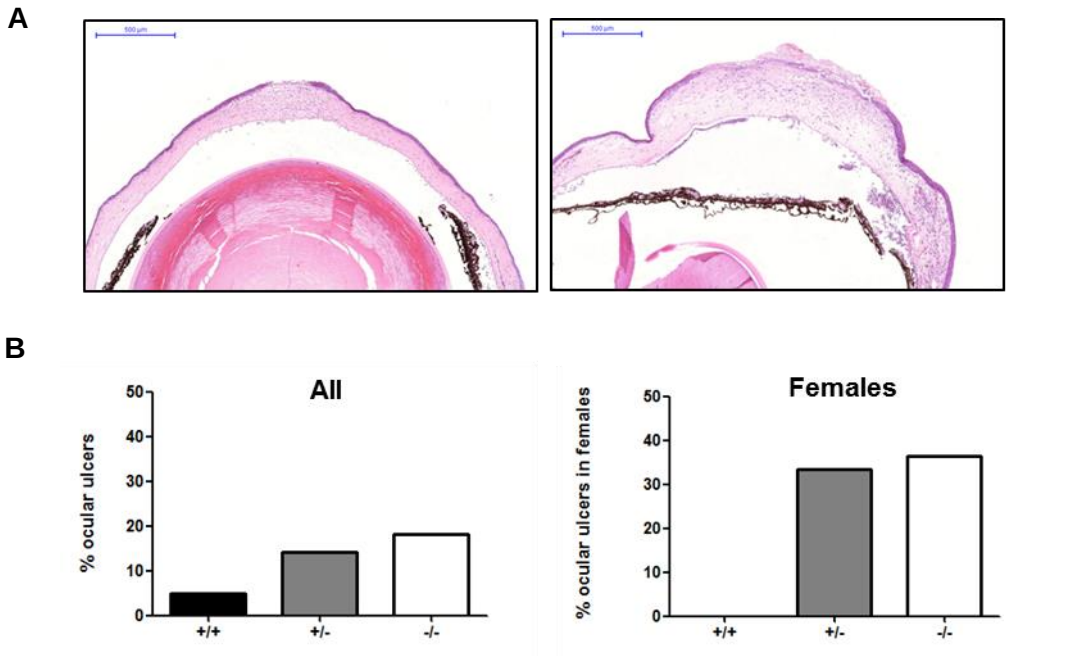

Figure 38. PrimPol deficient mice present higher incidence of ocular ulcers. A. Representative images of two ulcers in PrimPol$^{-/-}$ mice. **B.** Histograms show the percentage of total mice with ocular ulcers in the ageing study (right) and the percentage of females with ocular ulcers.

2.6.2. PrimPol deficient mice are prone to obesity

In addition, during the longevity studies we realized that old PrimPol$^{-/-}$ mice weighted more than their littermates (Figure 39A and B). This obesity became apparent at 90 weeks old and correlated with a higher percentage of body fat as determined by X-ray densitometry (Figure 39C).

Other mouse models defective for DNA repair enzymes have been associated with problems in body weight homeostasis (see Discussion). The specific mechanisms that link genome instability to metabolic syndrome have not been elucidated yet. In this study, we have also evaluated whether any symptom related to defective metabolism could be detected in young PrimPol-deficient mice. First we evaluated the percentage of body fat by X-ray densitometry and did not observe significant differences among the three genotypes (Figure 40A). The expression of the master adipogenic regulator genes

SREBP1 and PPAR-γ was similar in PrimPol$^{+/+}$, PrimPol$^{+/-}$ and PrimPol$^{-/-}$ mice (Figure 40B).

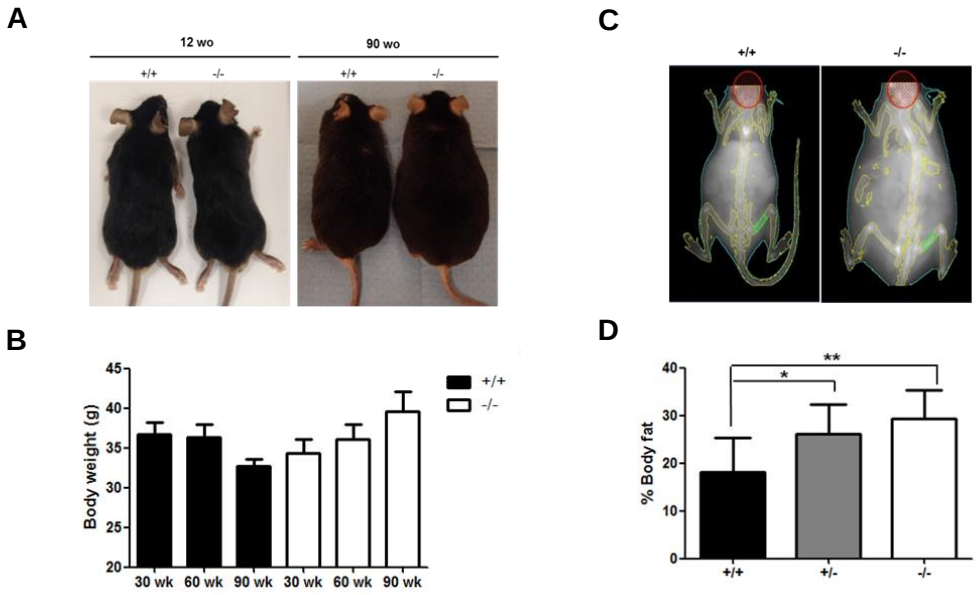

Figure 39. Obesity in old PrimPol deficient mice. A. Representative images of young (12 yo) and old (90 wo) PrimPol$^{+/+}$ and PrimPol$^{-/-}$ mice. **B.** Histogram quantification of body weight at the indicated time points in PrimPol$^{+/+}$ and PrimPol$^{-/-}$ mice. **C**. Representative X-ray densitometry images in PrimPol$^{+/+}$ and PrimPol$^{-/-}$ mice. **D**. Quantification of the percentage of body fat PrimPol$^{+/+}$, PrimPol$^{+/-}$ and PrimPol$^{-/-}$ 90-week-old mice (n= 14 PrimPol$^{+/+}$, 10 PrimPol$^{+/-}$ and 11 PrimPol$^{-/-}$). *p<0.05, **p<0.01.

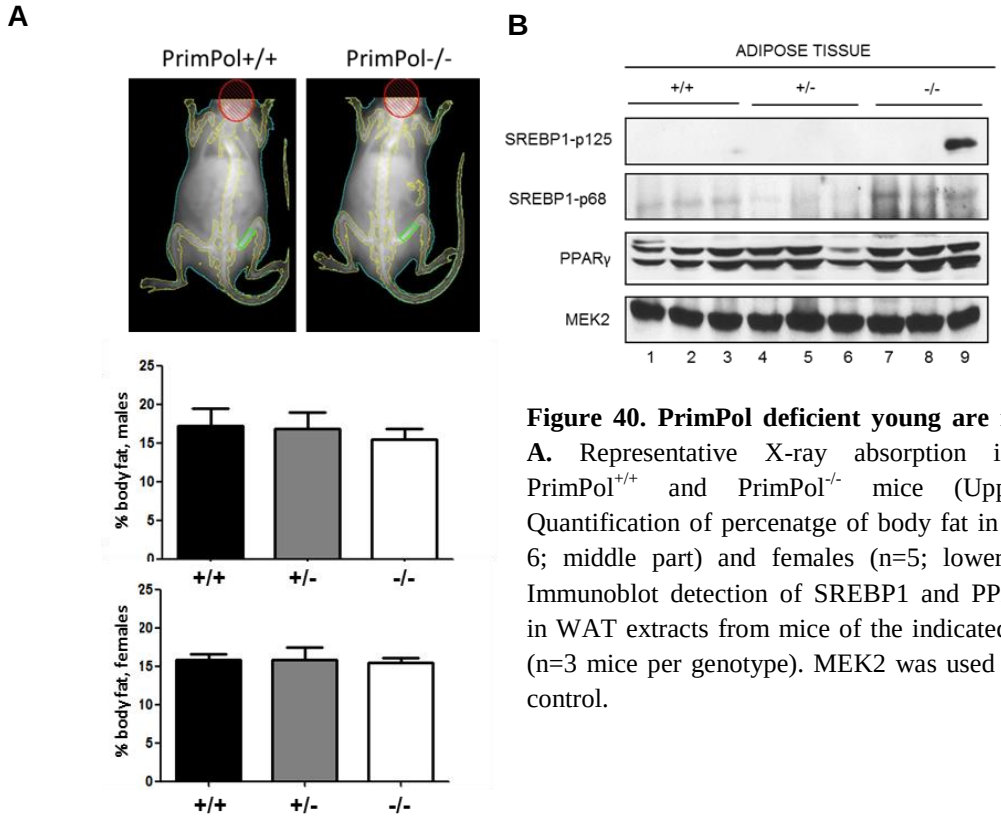

Figure 40. PrimPol deficient young are not obese. A. Representative X-ray absorption images in PrimPol$^{+/+}$ and PrimPol$^{-/-}$ mice (Upper part). Quantification of percenatge of body fat in males (n= 6; middle part) and females (n=5; lower part). **B.** Immunoblot detection of SREBP1 and PPARgamma in WAT extracts from mice of the indicated genotype (n=3 mice per genotype). MEK2 was used as loading control.

Next, we evaluated adipocyte size in white adipose tissue (WAT) and brown adipose tissue (BAT) of 20-week-old mice PrimPol$^{+/+}$, PrimPol$^{+/-}$ and PrimPol$^{-/-}$. While no differences were seen in WAT (Figure 41A, B and C), unexpectedly we observed that PrimPol$^{-/-}$ had smaller BAT adipocytes (Figure 42A, B and C). As BAT is crucial for temperature regulation in rodents, we evaluated the body temperature in these mice. Although the differences did not reach statistically significance, PrimPol$^{-/-}$ mice displayed slightly lower temperature consistent with an atrophic BAT (Figure 43).

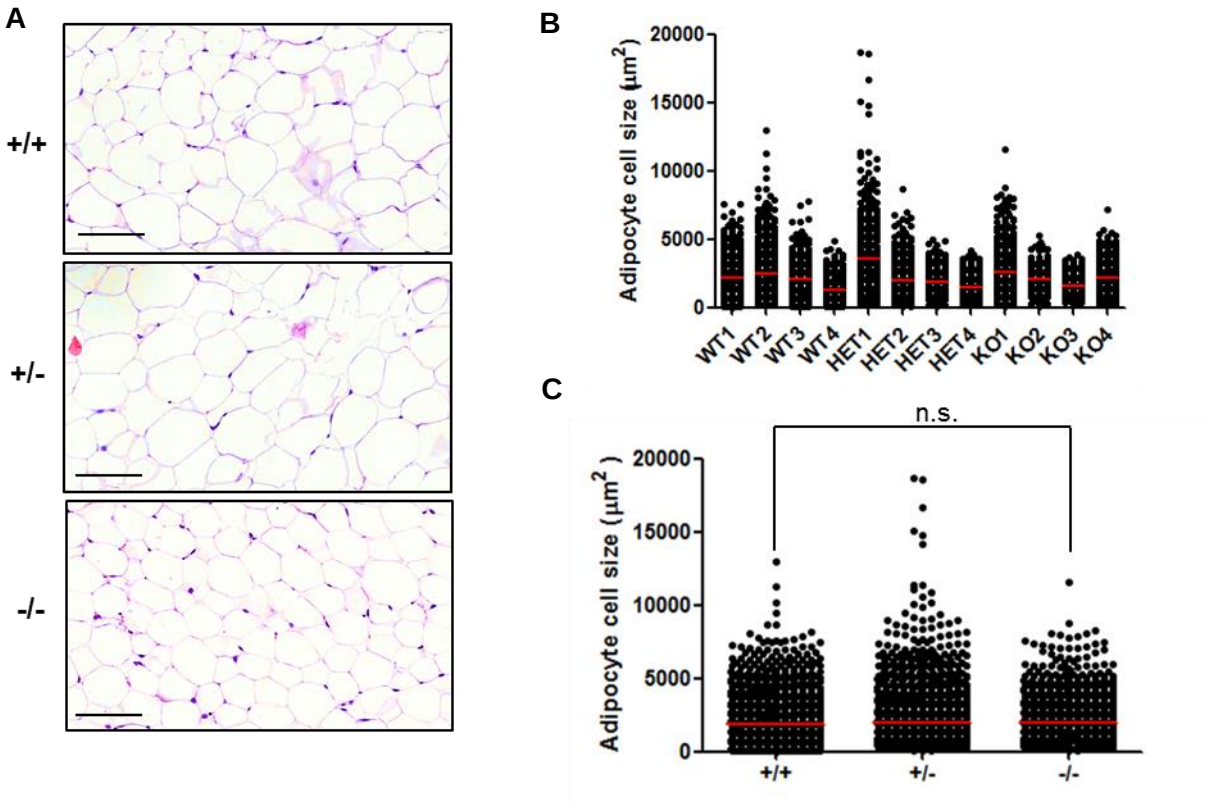

Figure 41. Normal adipocyte size in youn PrimPol-deficient mice. A. Representative WAT sections (H&E) from PrimPol$^{+/+}$, PrimPol$^{+/-}$ and PrimPol$^{-/-}$ mice. Scale bar, 50µm **B.** Adipocyte cell size quantification (n=4 animals per genotype). Red bars indicate the median values. 400 adipocytes were measured per mouse. **C.** Adipocyte cell size quantification. Red bars indicate median values (n=4 mice per genotype). n.s.=non-significant (according to Man-Whitney test).

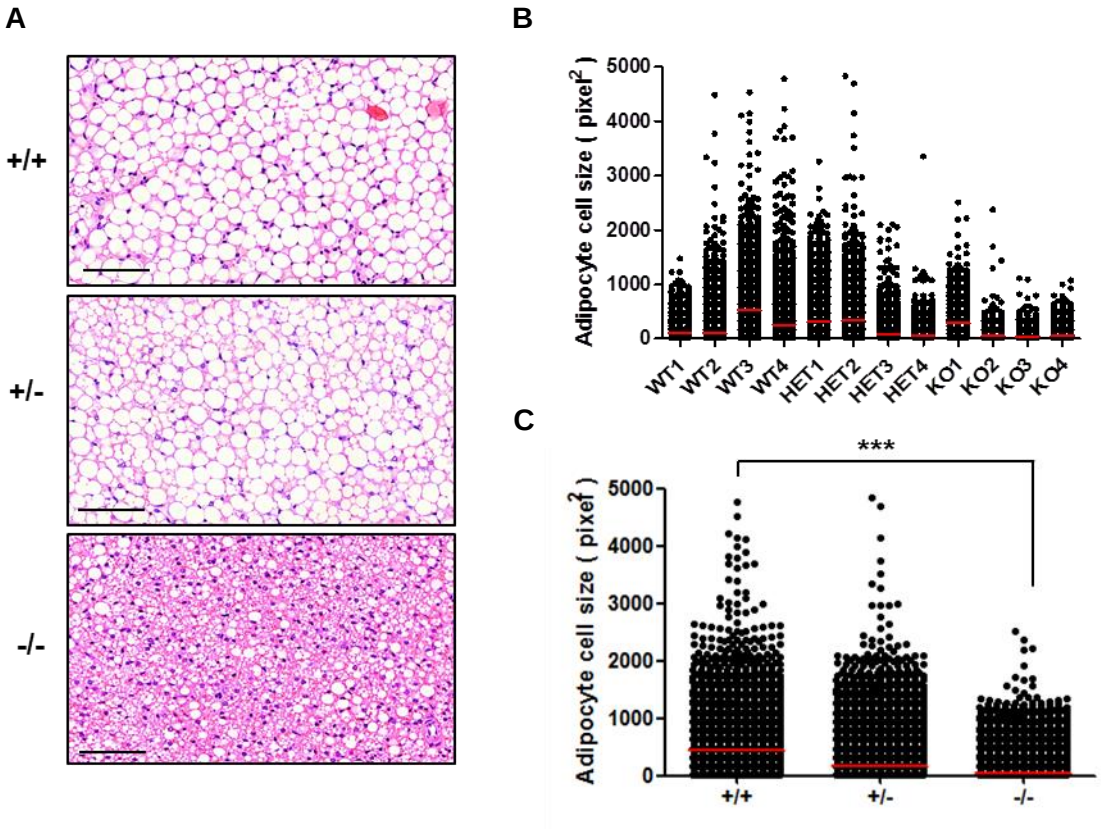

Figure 42. Smaller adipocyte size in youn PrimPol-deficient mice. A. Representative BAT sections (H&E) from PrimPol$^{+/+}$, PrimPol$^{+/-}$ and PrimPol$^{-/-}$ mice. Scale bar, 50µm **B.** Adipocyte cell size quantification (n=4 animals per genotype). Red bars indicate the median values. 400 adipocytes were measured per mouse. **C.** Adipocyte cell size quantification. Bar shows the median value (n=4). $p<0.001$ (according to Mann-Whitney test)

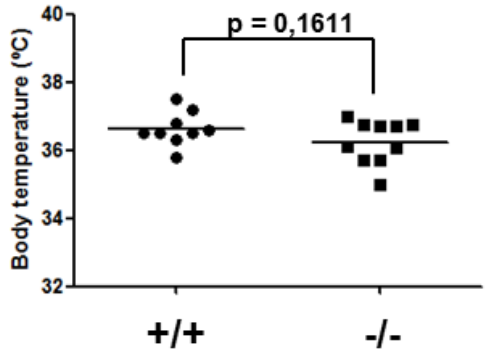

Figure 43. Lower body temperature in young PrimPol deficient mice. Body temperature was measured in 9 PrimPol$^{+/+}$ and 10 PrimPol$^{-/-}$ with an anal probe. Each point indicates an animal. The lines indicate the median.

Additional experiments are required to ascertain the potential metabolic syndrome in PrimPol-deficient mice. At the time of writing this thesis, a pilot experiment with a reduced number of aged mice (2 per genotype) revealed that at 75 weeks old PrimPol$^{-/-}$ females and males exhibited bigger adipocytes in the WAT (Figure 44A and B). Furthermore, histopathological analysis revealed the accumulation of fat in the liver

producing steatosis, again reinforcing the notion that the lack of PrimPol causes a metabolic syndrome (Figure 44C).

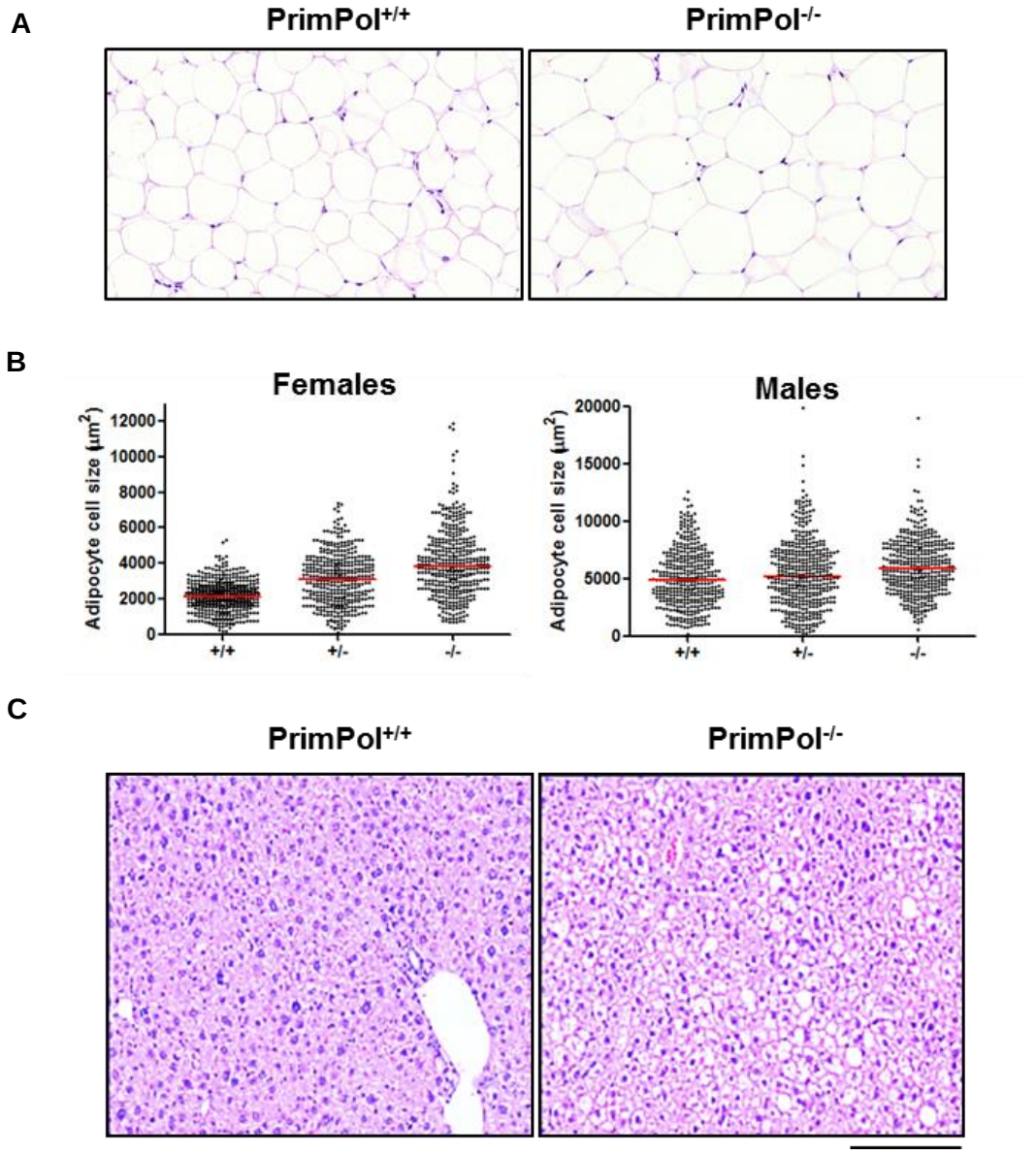

Figure 44. Bigger adipocytes cell size and liver steatosis in old PrimPol$^{-/-}$. A. Representative WAT sections, stained with H&E of PrimPol$^{+/+}$ and PrimPol$^{-/-}$ old mice. **B.** Quantification of adipocyte cell size in old mice (72 weeks old) segregated by gender (n>400 adipocyte measured per condition). **C.** H&E liver sections showing the accumulation of fat.

We conclude from this preliminary analysis that PrimPol seems to be important for fat tissue homeostasis.

2.6.3. PrimPol deficient mice are tumor prone

Most of the mice in the longevity studies suffered from standard age-related health problems, including spontaneous late-onset tumors. The pathological diagnosis of the tumors found and the number of organs infiltrated in each case are shown in Figure 45 and Supplementary table 1-3 (Annex I). As expected in the C57BL/6J genetic background, histiocytic sarcomas and B-cell lymphomas were found at high frequency in all genotypes. However, histopathology analyses revealed that PrimPol$^{-/-}$-derived hematological tumors had an increased capacity of infiltration and expansion. In some cases tumoral cells were found in as many as 18 organs, including some of the typical target organs from metastatic lymphomas like liver, lung and intestine, but also, other tissues in which metastasis are hallmarks of an aggressive pattern such as skin, heart and muscle (Figure 45D).

Apart from hematological tumors, PrimPol$^{-/-}$ mice presented a higher incidence of hepatocarcinomas, which seem to be gender-specific (40% of males; no cases in females). Notably, hepatocarcinomas are linked to metabolic syndrome and obesity so we hypothesized that the appearance of this tumor type was a direct consequence of the obesity in PrimPol$^{-/-}$ mice. Albeit with lower frequency, PrimPol$^{-/-}$ mice also developed lung adenoma, fibrosarcoma and angiosarcoma. Interestingly, 30% of PrimPol$^{-/-}$ mice developed more than one tumor and in few cases displayed a phenomenon known as “tumor collision”, in which two different hematological tumor types compete in the same organ/tissue (Figure 45C).

In summary, these results show that PrimPol loss enhances spontaneous tumorigenesis suggesting again that PrimPol may act as tumor suppressor gene.

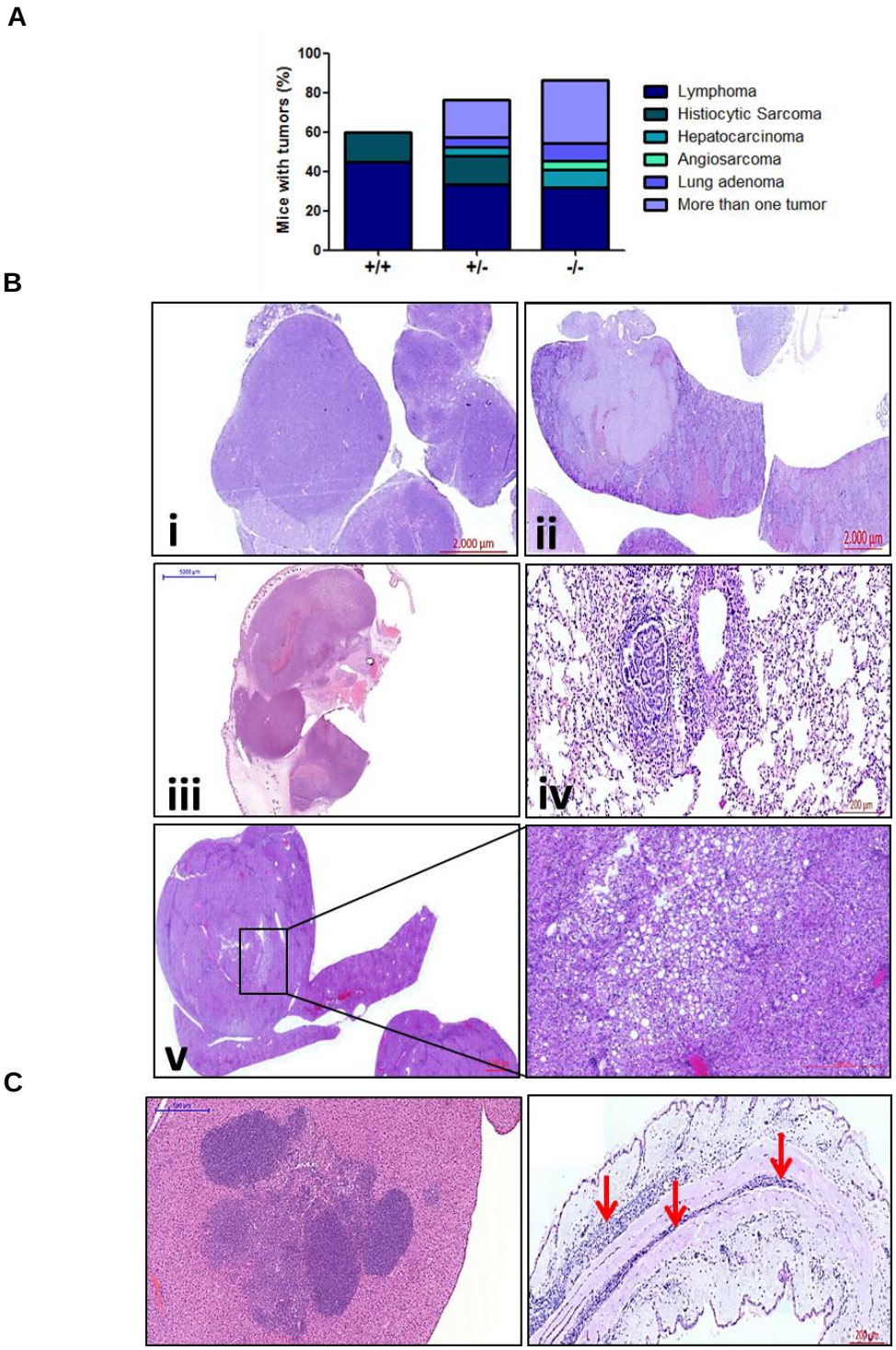

Figure 45. PrimPol deficiency leads to an increase in tumorigenesis. A. Histogram shows tumor incidence in PrimPol$^{+/+}$, PrimPol$^{+/-}$ and PrimPol$^{-/-}$ mice as identified in the necropsy. The group of mice having more than one tumor displayed different combinations (e.g. lymphoma + hepatocarcinoma, lung adenoma + hepatocarcinoma, hemangioma + lymphoma). **B.** Representative H&E stainings of histopathological findings in PrimPol$^{-/-}$ mice. i) B-cell lymphoma; ii) Histiocytic sarcoma; iii) Fibrosarcoma; iv) Lung adenoma; v) Hepatocarcinoma. In the latter, a blow-up section shows an area of massive lipidosis. **C.** Aggressive pattern of hematological neoplasia in PrimPol$^{-/-}$ mice. (left panel) Characteristic H&E staining of a histiocytic sarcoma and B-cell lymphoma in the liver, a feature known as "tumor collision". (right panel) Metastatic B-cell lymphoma infiltrating the dermis and muscle layer in the skin. Red arrows indicate infiltration sites.

Chapter 3: PrimPol deficiency leads to UV-susceptibility

3.1. PrimPol deficient mice are sensitive to acute UV radiation

Due to the relevance of PrimPol function in the response of cultured cells to UV radiation and the observation that PrimPol is highly expressed in the skin, we decided to test whether PrimPol-deficient mice would be sensitive to UV-B radiation.

In the skin of normal mice, UV radiation causes a well-established cascade of responses including a burst in proliferation that causes temporary protective thickening and the replacement of damaged cells (Lu *et al.*, 1999, Lange *et al.*, 2013). To study the sensitivity to acute UV radiation, we irradiated 8-week-old PrimPol$^{+/+}$, PrimPol$^{+/-}$ and PrimPol$^{-/-}$ mice with a single dose of 3000 J/m^2 UV-B and skin sections were examined in cohorts of mice untreated and after 1-5 days (Figure 46A). The hyperplasia induced by UV normally subsides after 4-5 days. In addition, 30 minutes before euthanasia, BrdU was injected intraperitoneally (100μg/mg body weight) to the mice in order to monitor DNA replication in epidermal cells. PrimPol$^{+/+}$ and PrimPol$^{+/-}$ skin sections displayed the expected increase in epidermal thickness that was stabilized by d3-4 and decreased by d5. In contrast, PrimPol$^{-/-}$ mice displayed higher epidermal thickness compared to PrimPol$^{+/+}$ and PrimPol$^{+/-}$ at all time points. In days 4 and 5 this difference in epidermal thickness becomes statistically significant (Figure 46B and C).

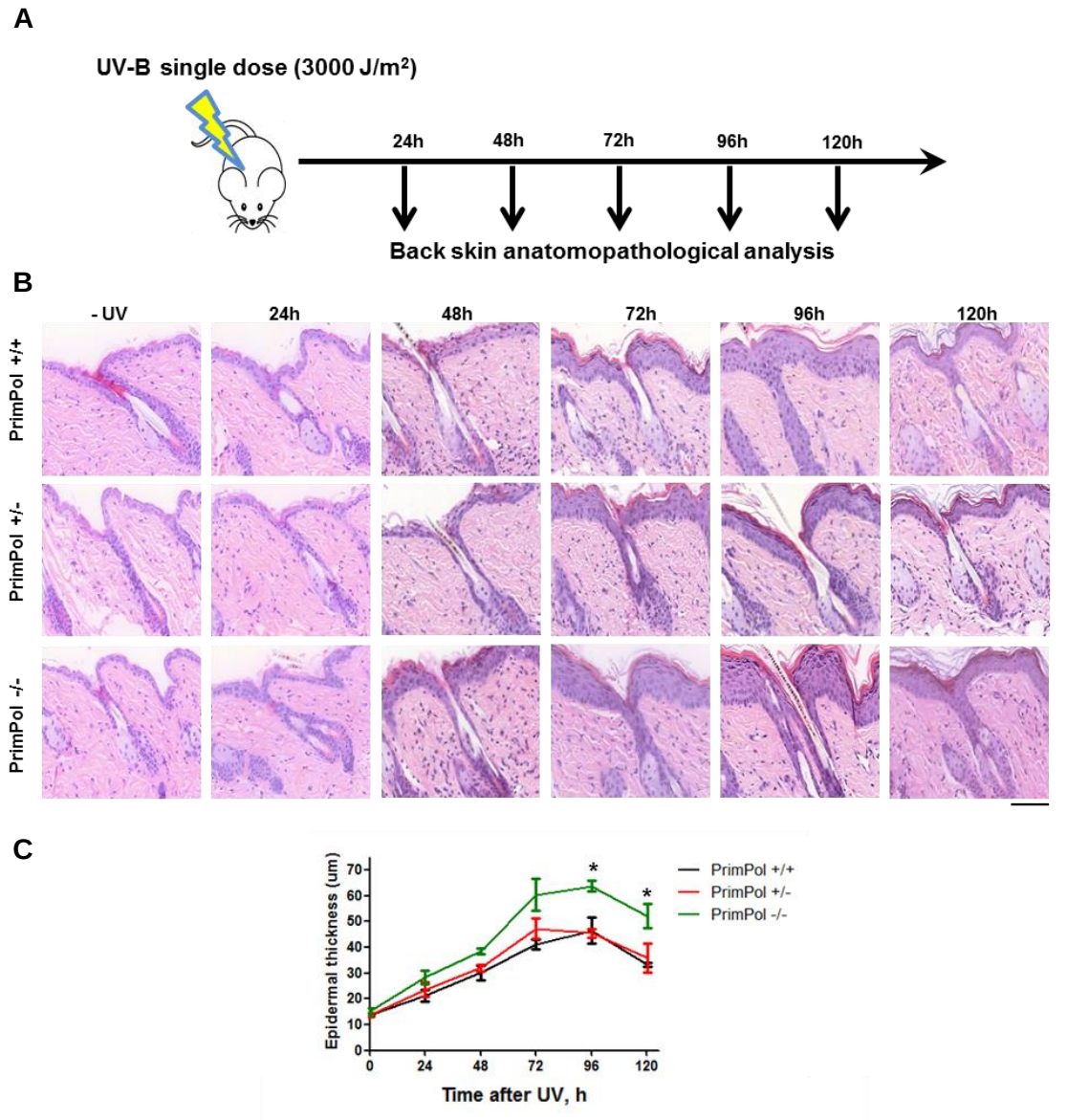

Figure 46. Inefficient repair of UV-damaged skin of PrimPol$^{-/-}$ mice. A. Schematic of the experiment. 4 animals (2 males and 2 females) of PrimPol$^{+/+}$, PrimPol$^{+/-}$ and PrimPol$^{-/-}$ mice per day. BrdU was injected 30 min before euthanasia. **B.** Representative H&E stainings of skin sections of PrimPol$^{+/+}$, PrimPol$^{+/-}$ and PrimPol$^{-/-}$ mice prepared at the indicated time points after UV-B irradiation. Scale bar, 100 μm. **C.** Quantification of epidermal thickness (meand +/- SEM) in PrimPol$^{+/+}$, PrimPol$^{+/-}$ and PrimPol$^{-/-}$ mice (n=4 mice per time point). PrimPol deficient mice present higher hyperplasia in all the time points. *p<0.05 according to Fisher t-test.

Importantly, UV-induced epidermal thickening in PrimPol$^{-/-}$ mice was caused by cell swelling and intercellular edema rather than an increase in cell number, as deduced from the lower number of epidermal cells per mm of linear skin (Figure 47A and XB).

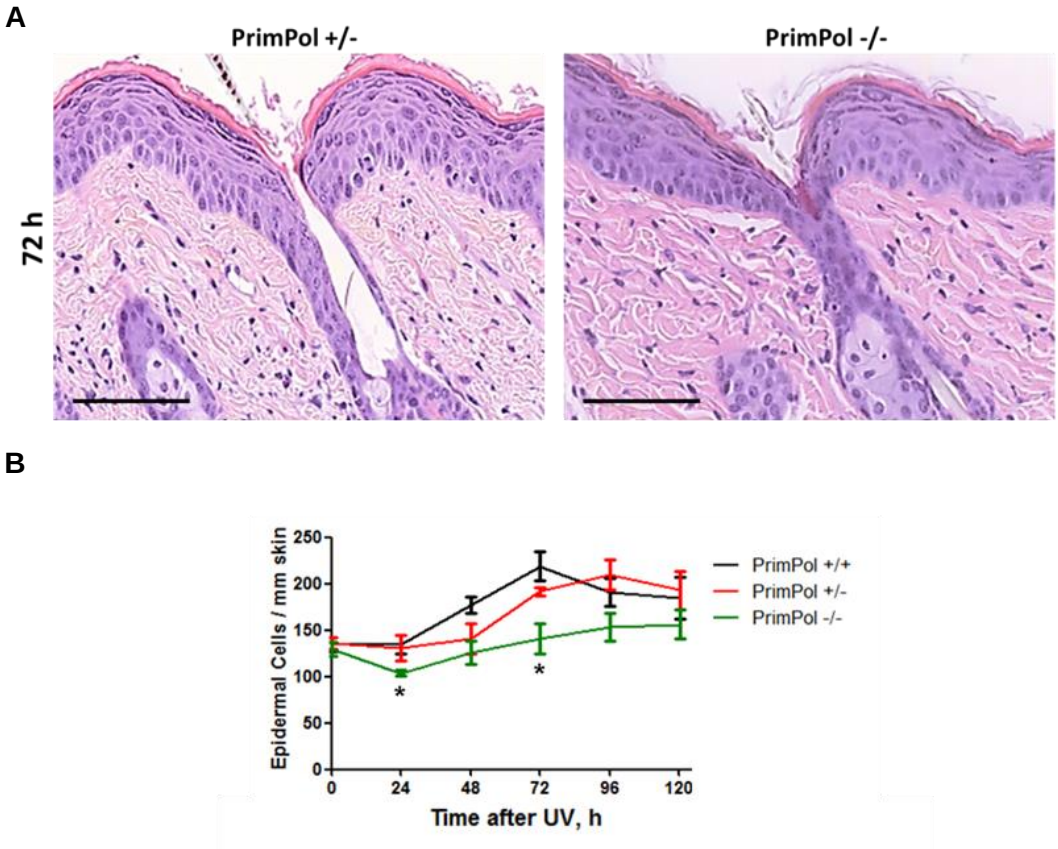

Figure 47. Reduced cellularity in the skin of PrimPol$^{-/-}$ mice after UV-B irradiation. A. Skin sections stained with H&E from PrimPol$^{+/-}$ and PrimPol$^{-/-}$ at 72h after UV. Red arrow indicates zones with low cellular density. Scale bar, 100 μm **B.** Quantification of total interfollicular epidermal cells per mm of linear skin (mean value +/- SEM) from the PrimPol$^{+/+}$, PrimPol$^{+/-}$ and PrimPol$^{-/-}$ mice described in Figure 46. PrimPol-deficient mice present less cellularity in all the time points. *p<0.05 according to Fisher t-test.

When BrdU incorporation was analyzed by IHC in interfollicular epidermal cells and follicular cells, we observed that PrimPol$^{+/+}$ and PrimPol$^{+/-}$ displayed a normal burst in DNA replication 48h after UV irradiation and a progressive decrease in later time points. In contrast, the same cells in PrimPol$^{-/-}$ mice failed to incorporate the BrdU at the same extent, explaining the lower cell density and suggesting a problem in the replacement of damaged skin cells (Figure 48A and B). To directly test the accumulation of cells with damaged DNA, we evaluated the presence of γH2AX by IHC. All mice tested presented a high percentage of positive cells for γH2AX upon 24h of UV irradiation, the percentage of γH2AX-positive cells in PrimPol$^{+/+}$ and PrimPol$^{+/-}$ skin decreased rapidly with time being almost undetectable by 96h (Figure 48B). Again, in contrast to PrimPol$^{+/+}$ and PrimPol$^{+/-}$ mice, PrimPol$^{-/-}$ skin displayed longer

persistence of the γH2AX DNA damage marker consistent with a delay in the replacement of damaged cells (Figure 48Cand D).

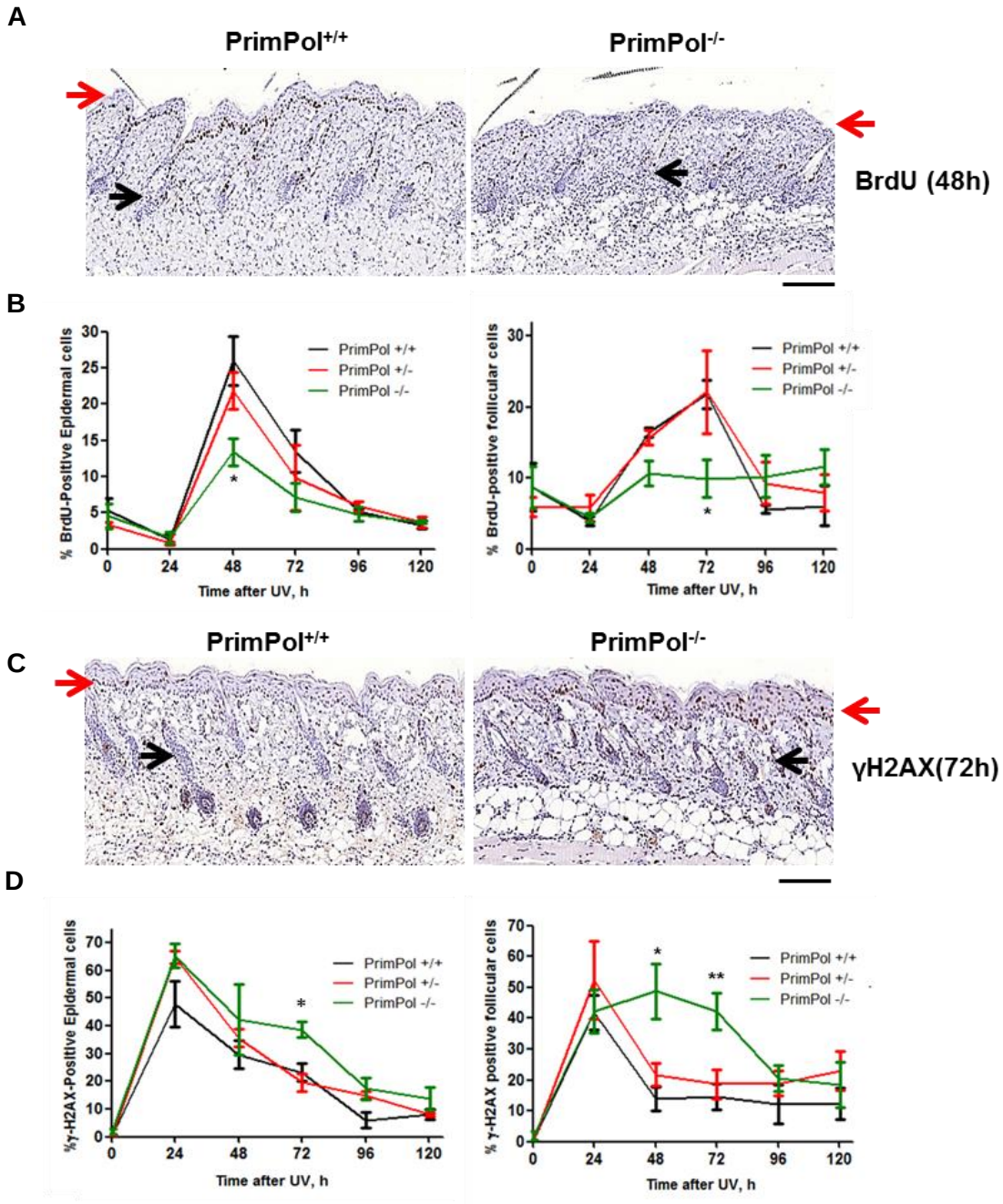

Figure 48. Limited cell proliferation in the epidermis of PrimPol-deficient mice following UV irradiation. A. Representative BrdU-stained skin sections from PrimPol$^{+/+}$and PrimPol$^{-/-}$ mice isolated 48 h after UV. Red arrows point interfollicular epidermal cells and black arrows point hair follicle cells. Scale bar, 100 μm. **B.** Percentage of BrdU-positive cells (mean value +/- SEM) in the basal layer of the epidermis (left) and hair follicle (right) of PrimPol$^{+/+}$, PrimPol$^{+/-}$ and PrimPol$^{-/-}$ mice at the indicated time points. *p<0.05 according to Fisher t-test (n=4 mice per genotype and time point). **C.** Representative of γH2AX-stained skin sections from PrimPol$^{+/+}$and PrimPol$^{-/-}$ mice isolated 48 h after UV. Scale bar, 100 μm. **D.** Percentage of γH2AX-positive cells (mean value +/- SEM) in the basal layer of the epidermis (left) and hair follicle (right) of PrimPol$^{+/+}$, PrimPol$^{+/-}$ and PrimPol$^{-/-}$ mice at the indicated time points. *p<0.05, **p<0.01, according to Fisher t-test (n=4 mice per genotype and time point).

In addition to the skin, PrimPol loss also had a negative impact in the eye. Three days after UV-B irradiation (3,000 J/m^2 and 3,500 J/m^2), a higher level of γH2AX in the cornea was observed by IHC in PrimPol$^{-/-}$ corneas compared to PrimPol$^{+/+}$ littermates (Figure 49A and B).

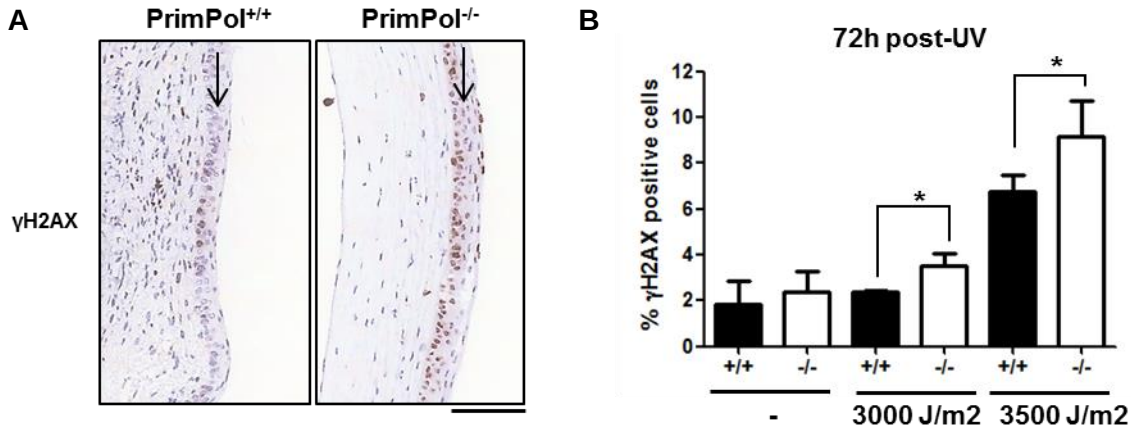

Figure 49. Accumulation of γH2AX in the cornea upon UV-irradiation. A. Representative immunohistochemical stainings γH2AX in eye sections from PrimPol$^{+/+}$and PrimPol$^{-/-}$ mice 72h after a single dose (3,000 J/m^2) of UV-B. Black arrows point the cornea. Scale bar, 100 μm. **B.** Percentage of γH2AX-positive cells (mean value +/- SEM) in the cornea from PrimPol$^{+/+}$ and PrimPol$^{-/-}$ mice (n=4 mice per genotype and condition). *p<0.05 according to Fisher t-test.

These results indicate that PrimPol plays an important role in the response to acute UV-B radiation.

3.2. PrimPol deficient mice are not hypersensitive to TPA

As discussed above, PrimPol deficiency leads to UV-light sensitivity. Due to the fact that PrimPol is also able to bypass non-UV light induced lesions such as 8-oxo-G, we tested whether PrimPol deficiency sensitizes the skin to other source of DNA damage, such as 12-O-tetradecanoylphorbol-13-acetate (TPA). TPA is a potent tumor promoter that induces cell proliferation, skin hyperplasia, moderate inflammation and the production of reactive oxygen species (Lange *et al.*, 2013). TPA (four doses of 3.4ng) was applied to the back skin of 8-week-old mice (Figure 50A). The degree of hyperplasia and cellularity was similar in PrimPol$^{+/+}$ and PrimPol$^{+/-}$. It was slightly reduced in PrimPol$^{-/-}$ mice although the differences did not reach stadistical significance (Figure 50B and C). In addition, no statistically differences were observed in terms of BrdU incorporation and γH2AX levels among the three genotypes (Figure 50C and D).

We conclude from this experiment that PrimPol deficiency does not affect the sensitivity of skin to TPA in the condition tested, although we cannot rule out that higher TPA concentrations might have produced some effects in PrimPol-deficient mice.

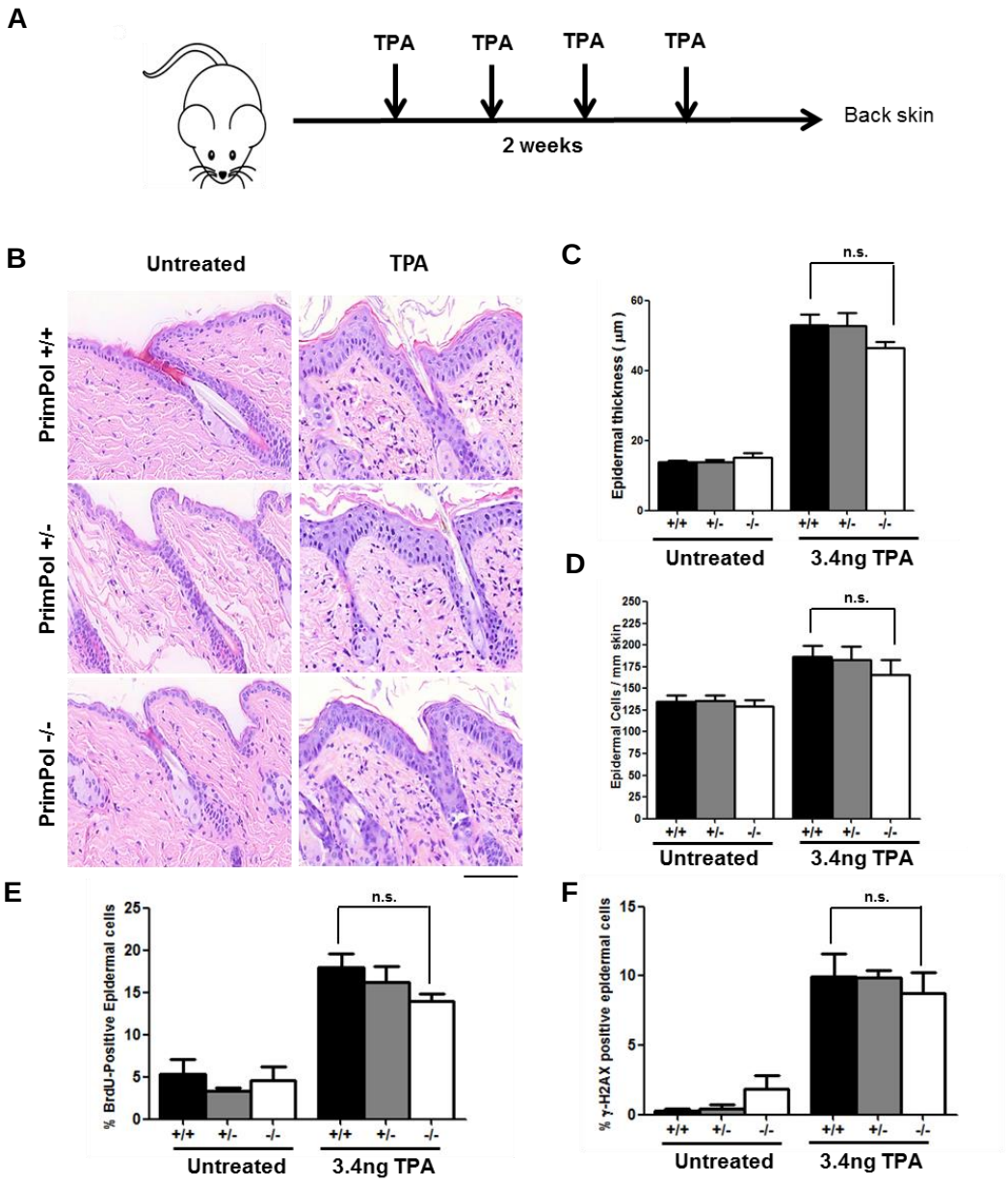

Figure 50. Normal response to TPA in PrimPol-deficient mice. A. Schematic of the experiment. PrimPol$^{+/+}$, PrimPol$^{+/-}$ and PrimPol$^{-/-}$ mice (2 males and 2 females) were treated with 3.4 ng TPA four times. BrdU was injected i.p. 30 min before euthanasia. **B.** Representative of H&E stainings of skin sections of PrimPol$^{+/+}$, PrimPol$^{+/-}$ and PrimPol$^{-/-}$ mice either untreated or 48h after the application of TPA in the back skin. Scale bar, 100 µm. **C.** Quantification of epidermal thickness (mean +/- SEM) of PrimPol$^{+/+}$, PrimPol$^{+/-}$ and PrimPol$^{-/-}$ mice (n=6). **D.** Quantification of total interfollicular epidermal cells per mm of linear skin (mean +/- SEM) from PrimPol$^{+/+}$, PrimPol$^{+/-}$ and PrimPol$^{-/-}$ mice (n=6). **E.** Percentage of BrdU-positive cells (mean value +/- SEM) in the basal layer of the epiderm of PrimPol$^{+/+}$, PrimPol$^{+/-}$ and PrimPol$^{-/-}$ mice (n=4). **F.** Percentage of γH2AX-positive cells (mean value +/- SEM) in the basal layer of the epidermis of PrimPol$^{+/+}$, PrimPol$^{+/-}$ and PrimPol$^{-/-}$ mice (n=4). n.s.: non-significant.

3.3. Chronic exposure to UV-B radiation sensitizes PrimPol$^{-/-}$ mice to tumor development

Other mouse models with deficiencies in genes responsible for NER, BER or TLS polymerases also show sensitivity to UV radiation. In most cases, these mice developed tumors after chronic UV exposure. As described above, PrimPol plays a protective role to an acute high dose of UV radiation, and we decided to test the effect of chronic UV in tumorigenesis. Young mice (from 8 to 10 weeks old) were irradiated (1,800 J/m^2 three times a week) during 40 weeks. Tumor formation was monitored for the duration of the experiment and mice were euthanized following the humane end points defined by the IUCAC guidelines of ISCIII ("standard"). When this protocol (Figure 51A) was applied PrimPol$^{-/-}$ developed more and bigger papillomas than the PrimPol$^{+/+}$ and PrimPol$^{+/-}$ mice (Figure 51B and C). Besides, several papillomas in PrimPol$^{-/-}$ mice displayed signs of malignity, although full progression towards SCC was not observed. This could be related to the fact that C57BL/6J genetic background is highly resistant to the malignization process from papilloma to SCC (Figure 51D).

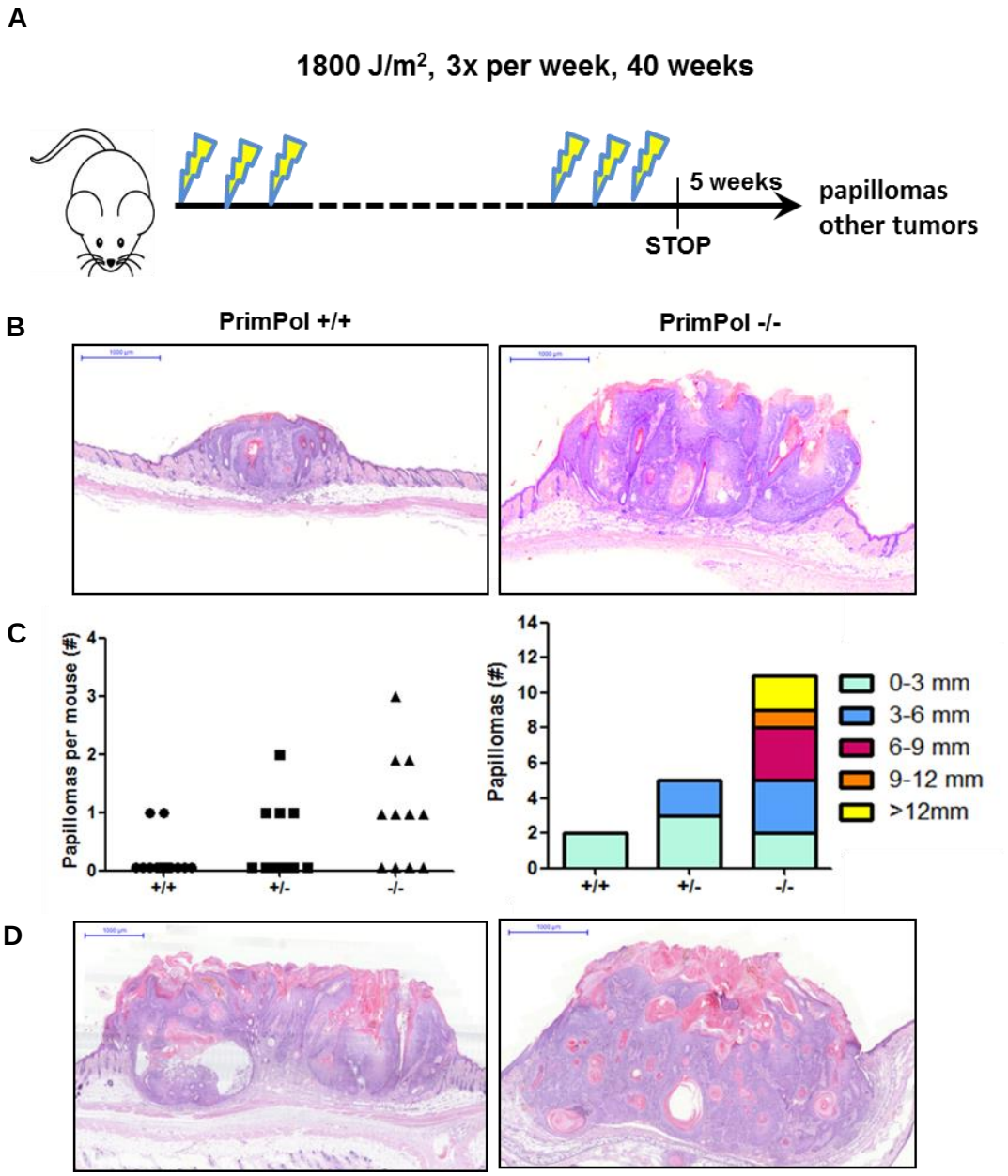

Figure 51. PrimPol deficient mice are susceptible to UV-induced carcinogenesis. A. Schematic of the experiment. PrimPol$^{+/+}$, PrimPol$^{+/-}$ and PrimPol$^{-/-}$ mice were irradiatiated at a dose of 1,800 J/m^2 three times per week during 40 weeks. After this chronic UV scheme, mice were kept five additional weeks without irradiation. **B.** Representative H&E stainings of papilloma lesions from PrimPol$^{+/+}$ and PrimPol$^{-/-}$ mice. **C.** Number of papillomas per mouse (left) and distribution of papilloma size (right) in PrimPol$^{+/+}$, PrimPol$^{+/-}$ and PrimPol$^{-/-}$ mice (n= 13 PrimPol$^{+/+}$, 11 PrimPol$^{+/-}$ and 11 PrimPol$^{-/-}$) **D.** Representative H&E stainings of skin papilloma sections from PrimPol$^{-/-}$ mice with a higher degree of malignancy.

Apart from papillomas (an epithelial tumor type), two PrimPol$^{-/-}$ mice developed sarcomas (a mesenchymal tumor type) (Figure 52A). Besides skin tumors, one PrimPol$^{+/-}$ and three PrimPol$^{-/-}$ mice developed hemangiomas in the eyes (Figure 52B).

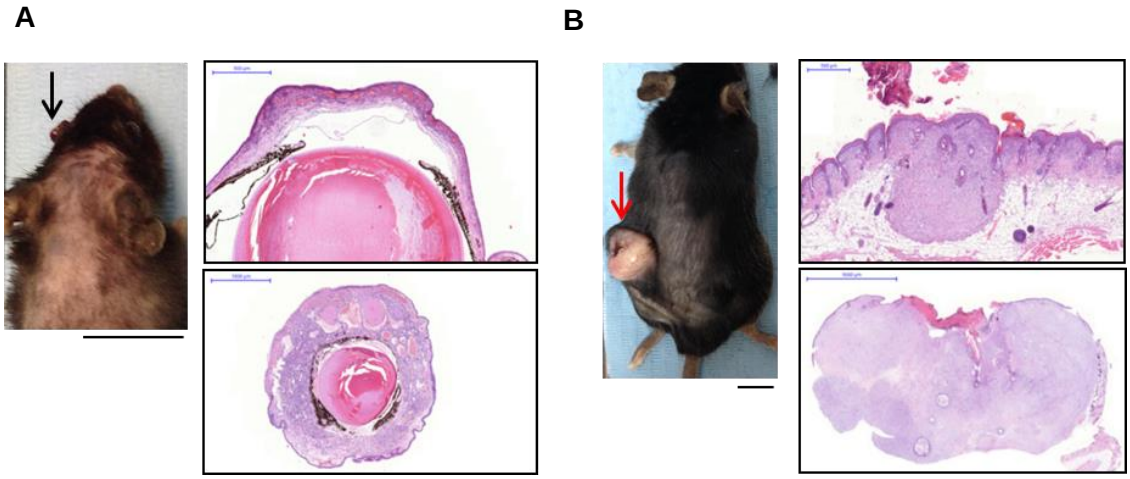

Figure 52. Mesenchymal tumor types in PrimPol-deficient mice. A. Representative picture of a hemangioma in the eye (black arrow; scale bar, 1 cm) and two H&E sections of eye hemangiomas in PrimPol$^{-/-}$ mice following chronic UV irradiation (see Figure 51A). Scale bar, 1 cm. **B.** Representative picture of a large sarcoma lesion (red arrow; scale bar, 1 cm). Right, H&E sections of two different sarcomas in PrimPol$^{-/-}$ mice.

In summary, PrimPol deficiency increased the sensitivity to UV-induced tumorigenesis. Most of the tumors were benign papillomas but notably, two other types of tumors (sarcomas and hemangiomas) were also detected.

3.4. Melanoma susceptibility in PrimPol-deficient mice?

The experiments described in the previous sections only tested the susceptibility at PrimPol-deficient mice to epithelial and mesenchymal tumors induced by UV-B-This excludes the cutaneous malignant melanomas (CMM), which in mice require a different regime of irradiation that combines UV-A and UV-B. In order to study the possible implication of PrimPol in preventing CMM development, cohorts of newborn mice (3.5d) was irradiated (3,310 J/m^2 UV-A and 6,240 J/m^2 UV-B) following a described protocol (Noonan *et al.*, 2001). This experiment is currently in progress. At the time of writing this thesis (18 weeks after irradiation) no CMMs had been observed.

DISCUSSION

DISCUSSION

1. Structure-function analysis in human PrimPol

1.1 Functional importance of the conserved WFYY motif of human PrimPol

Our initial interest in the conserved motif WFYY was driven by a study of exome sequencing that implicated a point mutation (Y89D) in PrimPol in the development of high myopia in human patients (Zhou *et al.*, 2013). Tyr89 is located within a conserved motif (WFYY) in higher eukaryotes. A detailed amino acid alignment revealed that Trp87 and Tyr90 residues, both located in the vicinity of Tyr89, are strictly invariant. In the first part of this dissertation, we have described a structure-function analysis that shows how the "pathological" mutation Y89D does not affect the activity of PrimPol either *in vitro* or *in vivo*. Controversially, a recent study claims that Y89D mutation affects negatively the DNA binding capacity and biochemical activities of PrimPol (Keen *et al.*, 2014). However, the authors in this report indicated that Y89D mutation induces structural changes in PrimPol. Therefore, its lower activity *in vitro* is likely a consequence of inefficient protein folding during expression and purification, rather than an effect of the mutation Y89D *per se*. Furthermore, Keen *et al.* (2014) report that the ability of Y89D mutant to reconstitute the loss of endogenous PrimPol was also compromised. In contrast, our results show that Y89D is perfectly capable of substituting for endogenous PrimPol in an unchallenged S phase and during the response to UV irradiation. The different results could be related to the fact that Keen *et al.* (2014) try to reconstitute the loss of endogenous PrimPol in avian DT40 cells with human PrimPol. This heterologous system may not be completely suitable to validate the activity of PrimPol mutations. More importantly, a subsequent genetic study has revealed that the Y89D is a common polymorphic variant that appears in the control population with similar frequency than in patients with high myopia (Li *et al.*, 2015). This study correctly points out that the conclusions of Keen *et al.* (2014) and Zhou *et al.* (2013) need to be re-evaluated.

While the analysis of Y89D mutation turned out to be a "red herring", it pointed us in the direction of the conserved WYFF motif. *In vitro* experiments conducted in the laboratory of Dr. Luis Blanco (CBMSO, Madrid) revealed that mutations in Trp87 (W87G) and Tyr90 (Y90D) rendered PrimPol protein completely inactive for both

primase and polymerase activities. In addition, PrimPol carrying a mutation in Phe88 (F88L) was still functional but with reduced activity. In this thesis, we tested the functionality of these PrimPol mutant versions in different conditions *in vivo*. Using single-molecule analysis of DNA replication in HeLa-shPrimPol cells, we found that W87G and Y90D mutants failed to compensate for the loss of endogenous PrimPol in all conditions tested. Interestingly, F88L mutant could substitute for the function of endogenous PrimPol in an unperturbed S-phase, but not when the forks were stalled by UV or HU. The ability to restart forks resides mainly in the primase activity of PrimPol (Mourón *et al.*, 2013). These results suggest that the partial primase activity left in the F88L mutant is capable of dealing with endogenous fork stalling, but fails to do so when DNA replication is extensively challenged with UV irradiation or dNTP attrition.

Mutations that affect the capacity of TLS polymerases to bind DNA have been described, such as mutation in Phe290 in human Polη that is linked to a variant of Xeroderma pigmentosum (Biertümpfel *et al.*, 2010). However, all the PrimPol mutants described here displayed normal binding to DNA in EMSA assays. Our results are consistent with the *in vitro* data generated in Dr. L. Blanco's laboratory, which indicate that amino acids within the WFYY motif are important for the formation of the (E:DNA:dNTP) preternary complex. In other AEP proteins involved in non-homologous end-joining (NHEJ), an invariant Phe residue plays a crucial role in the recognition and orientation of both the template and the incoming bases (preternary complex) into the active site (Pitcher *et al.*, 2007; Brisset *et al.*, 2010). In human PrimPol, W87G and Y90D mutations completely prevented the formation of this complex, and F88L affected it considerably. Even Y89D PrimPol mutant seemed to be slightly affected in preternary complex formation. We conclude that Trp87 and Tyr90 residues in human PrimPol, shown *in vitro* to participate in preternary complex formation, are essential *in vivo*.

1.2. Functional importance of Tyr100 in human PrimPol

Tyr100 is a conserved residue located between the A motif and the hydrophobic pocket WFYY in human PrimPol. This predicts that structurally, Tyr100 could be located close to the DNA/NTPs entrance channel. Sequence alignment shows that Tyr100 is substituted in other AEP primases, including Prim1, for a histidine. The identity of this

residue may influence the discrimination between NTPs and dNTPs. While a Tyr residue in the entrance seems to favor the incorporation of dNTPs over NTPs, primases with a His in this position insert preferentially NTPs. Moreover, the mutation Y100H has been found in a human cancer cell line (cBIOPORTAL; Cerami *et al.*, 2012; Gao *et al.*, 2013). Therefore, a Y100H human PrimPol variant was generated and analyzed. *In vitro* data provided by Dr. L. Blanco laboratory revealed that the Y100H mutant displayed primase and polymerase activity, but this specific Tyr to His change was sufficient to alter the balance of dNTPs vs NTPs insertion, favoring the insertion of NTPs. It should be noted that in the absence of NTPs, Y100H is still able to use dNTPs.

In our work, we tested whether Y100H PrimPol was able to substitute for endogenous PrimPol in HeLa cells. Interestingly, the mutant Y100H was active, displaying normal rates of fork progression in an unchallenged S phase and efficiently promoting fork restart after UV irradiation. These results suggest that this mutation does not prevent the normal functions of PrimPol in S phase. However, we still do not know whether these functions imply a higher incorporation of NTPs *in vivo*. Incorporation of ribonucleotides in the genome increases genomic instability and can lead to cancer if not properly repaired (reviewed in Williams and Kunkel, 2013). Future experiments will determine whether Y100H PrimPol protein causes genomic instability, and whether its activity can be tolerated only in the presence of efficient DNA repair pathways.

2. Role of PrimPol protein *in vivo*: characterization of a mouse KO model

2.1. PrimPol is not essential for mouse development

PrimPol-deficient mice are viable and born at Mendelian rates. Therefore, we first conclude that the functions of PrimPol are not essential during development. Adult mice do not display visible phenotypes until mid-age, when they start to gain weight and develop alopecia.

The obesity in old PrimPol KO mice suggests that the lack of PrimPol causes a metabolic syndrome. Several links have been established between enzymes that maintain genome instability and the development of metabolic syndrome. The accumulation of metabolic ROS is known to produce DNA damage in adipocytes and other cell types, mainly 8-oxo-G base modifications that could require the action of PrimPol or other enzymes involved in DDT or DNA repair. Furthermore, DDR key gene 'ataxia telangiectasia mutated' (ATM) mediates an antioxidant action that may be relevant to metabolic syndrome (Schneider *et al.*, 2006). Several mouse models in which DNA repair enzymes have been ablated are associated with metabolic syndrome and abnormal body weight, e.g. mice deficient in BER genes Neil1 or Ogg1 (Vartanian *et al.*, 2006; Sampath *et al.*, 2011; Sampath *et al.*, 2012). Interestingly, mice deficient in NER genes XP-A or ERCC1-XPF develop lipodystrophy, the contrary phenotype (Karakasilioti *et al.*, 2013; Fang *et al.*, 2014). Apart from DNA repair proteins, mice defective in DDT genes have also shown obesity: ablation of Polη causes adipose tissue senescence that eventually leads to metabolic syndrome (Chen *et al.*, 2015).

How PrimPol deficiency leads to obesity is still not clear. Given the antecedents with other mouse strains, it could be via a mechanism similar to DDT protein Polη. It could also be hypothesized that PrimPol participates in BER processes. Finally, since PrimPol is also a mitochondrial protein we cannot rule out that mitochondrial alterations cause problems with lipid metabolism. Indeed, the alterations in brown adipose tissues (BAT) observed in PrimPol-deficient mice could be linked to mitochondrial activity, as the mitochondrial complex III ROS regulates adipocyte differentiation in BAT (Tormos *et al.*, 2011) and deficient mitochondrial ATP production also produces alterations in BAT (Hao *et al.*, 2015). Indirectly, deficiency in the glucose metabolism that is also sustained

from mitochondrial activity also alters BAT composition and thermogenesis activity (Albert *et al.*, 2016). These possibilities are not mutually exclusive and all could contribute to the obese phenotype observed in the absence of PrimPol (Figure 53).

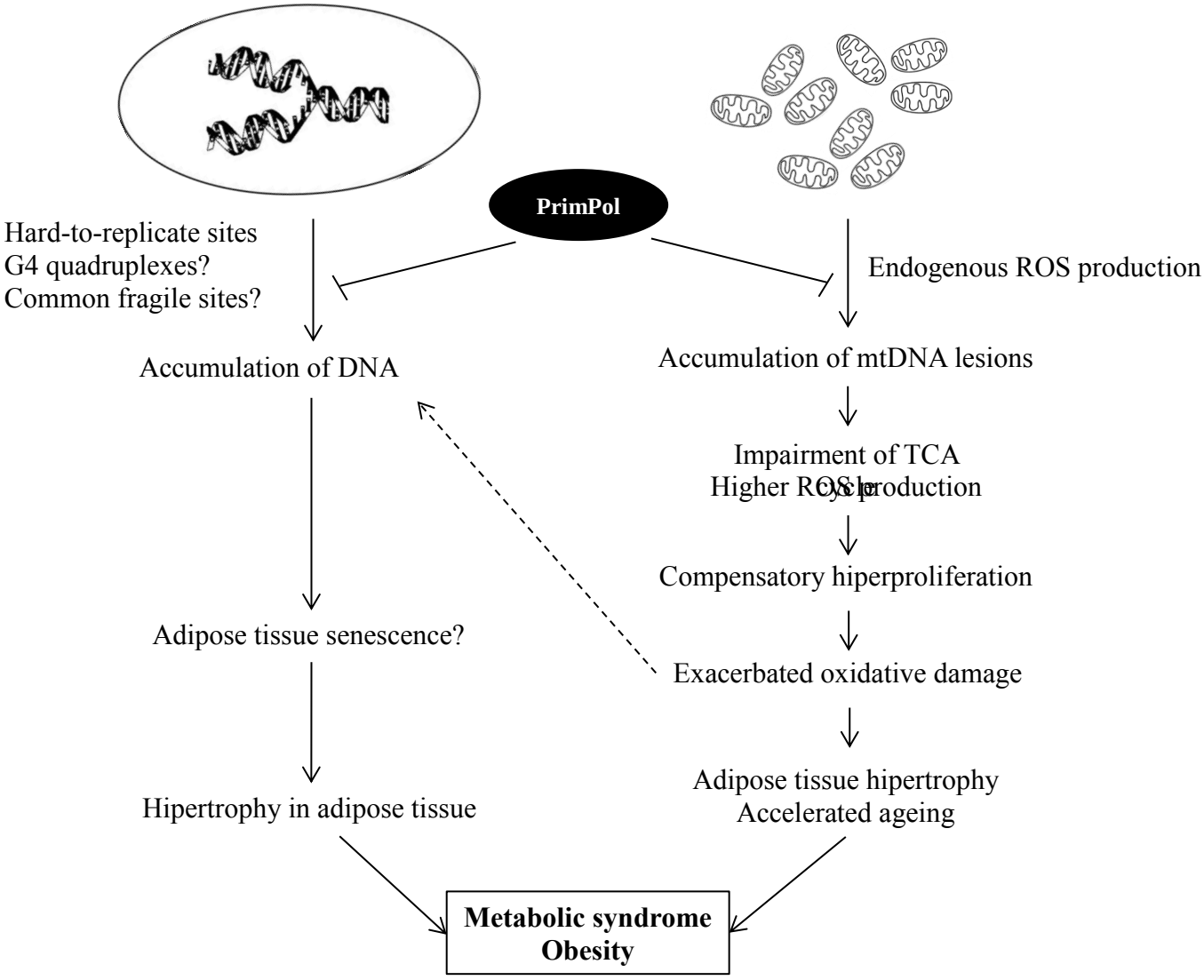

Figure 53. Hypothetical mechanisms that could link PrimPol to obesity. PrimPol facilitates nuclear and mitochondrial DNA replication by priming ahead of damaged sites. In its absence, inefficient replication causes an accumulation of lesions in the DNA that may lead to adipose tissue senescence and eventual obesity as reported in other mouse models with deficient DDT. In addition, the accumulation of mutations in mtDNA may impair the TCA cycle, increasing the production of ROS. In the absence of PrimPol there is a compensatory hiperproliferation in mitochondria that can further exacerbate oxidative damage and contribute to the hypertophy of adipose tissue.

The other obvious phenotype detected in the longevity studies was that PrimPol-deficient females developed alopecia. This phenotype has neither been described in NER- or BER-defective mice, nor in mice defective in other TLS polymerases such as

Polη or Polθ. Because mitochondrial ROS is known to promote epidermal differentiation and hair follicle development (Hamanaka *et al.*, 2013) it is likely that the alopecic phenotype in PrimPol is caused by defects in mitochondria. Besides PrimPol, Polζ is the only TLS polymerase described in mitochondria so far (García-Gómez *et al.*, 2013; Singh *et al.*, 2015). Interestingly, mice deficient in Polζ do not have hair because of an atrophy in the hair follicle (Lange *et al.*, 2013). Histopathology analysis of the skin sections of PrimPol-deficient mice revealed skin sections revealed the presence of "folded follicles", aberrant structures in which excessive keratinization prevents the release of hair from the follicle. This analysis also revealed the atrophy of sebaceous glands accompanied by a recruitment of mast cells.

In summary, PrimPol function seems important for the maintenance of hair growth in adult mice, possibly by maintaining proper mitochondrial activity around the hair follicles. More experiments will be required to characterize this phenotype and to understand why it is exclusive of female mice.

2.2. PrimPol: a tumor suppressor gene?

Our study revealed that the lifespan of PrimPol-deficient mice is slightly reduced, mainly due to the appearance of age-related tumors at an earlier stage. In fact, PrimPol KO mice developed more and different tumors than wt littermates. Aged C57BL/6 mice frequently develop hematological tumors, but their incidence was higher in PrimPol-deficient mice. Besides, the histopathological finding of lymphoma cells in more organs of PrimPol KO mice suggests an aggressive pattern. On the same token, rare tumor types have been detected in PrimPol KO mice, including hepatocellular carcinomas (HCC), hemangiomas, angiosarcomas and pulmonar adenomas. HCC and pulmonary adenomas have been linked to obesity. Moreover, hepatocarcinomas only appeared in males, as we observed. The mechanisms underlying the development of HCC remain poorly understood, but it is worth noting that mice defective in BER, e.g. Nth1- and Neil1-deficient strains, are also prone to HCC and pulmonary adenocarcinomas (Chan *et al.*, 2009).

At the cellular level, we have observed a higher efficiency of Ras-mediated transformation capacity in PrimPol-deficient MEFs. Combined with the *in vivo* tumorigenesis data, we strongly favor the idea that PrimPol is a tumor suppressor gene.

In agreement with this hypothesis, a cBioPortal analysis indicates that PrimPol is mainly mutated or homozigously deleted (Figure 54). It is worth noting that PrimPol gene is located next to the Caspase-3 gene, so PrimPol loss may be produced in some cases also as a consequence of the loss of heterozygozity (LOH) of this gene during cancer formation.

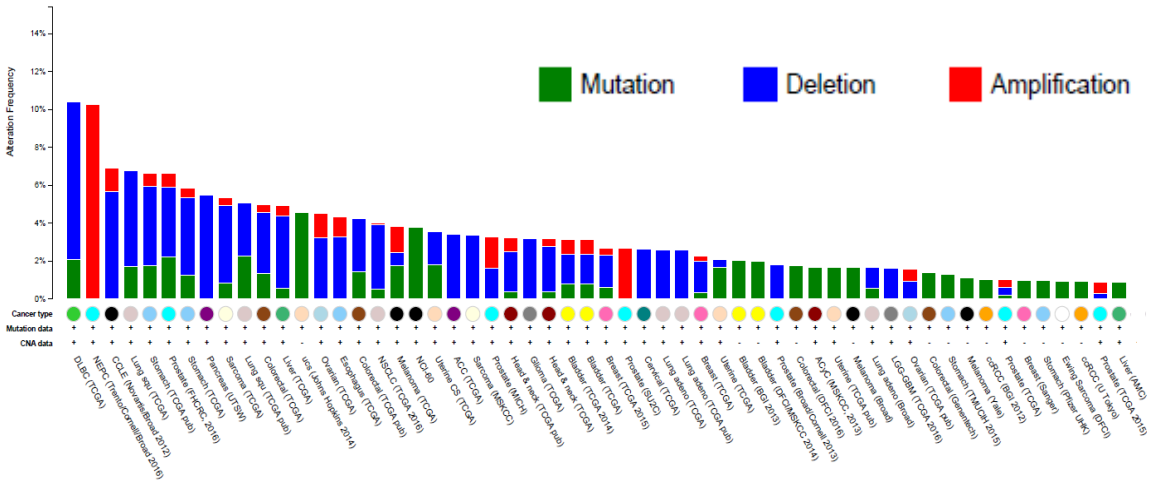

Figure 54. PrimPol alterations in human tumor samples. PrimPol is most frequently homozigously deleted (blue) or mutated (green). Many of the mutations are presumably inactivating. The type of cancer with the highest frequency of homozygous deletion of PrimPol is diffuse large B-cell lymphoma. In constrast to other tumors, all PrimPol alterations found in prostate cancer are amplifications.

In contrast, TLS polymerases are frequently overexpressed in tumors and are a poor-prognosis marker in chemotherapies based on cisplatin (Ceppi *et al.*, 2009; Wang *et al.*, 2010). Considering that PrimPol acts preferentially as a primase rather than a TLS polymerase during DDT, it is not surprising that it is not amplified or overexpressed in tumors like the TLS polymerases.

Whether DNA polymerases, particularly TLS polymerases, can prevent or contribute to cancer development is a complex issue. As summarized in the next few paragraphs, several DNA polymerase KO models are tumor-prone (Table 5).

Germline mutations in the proofreading domain of replicative Pold1 and Pole predispose to colorectal adenomas and carcinomas in humans (Palles *et al.*, 2013). This result underscores the notion that many point mutations in cancer cells stem from DNA polymerase errors that are not repaired. In addition, transgenic mice with an

exonuclease-deficient (exo) Pold1 developed thymic lymphomas, skin tumors, lung adenocarcinomas or teratomas within the first eight months of life. Pole$^{exo/exo}$ mice died prematurely of intestinal adenomas and adenocarcinomas. The combination of Pold1$^{exo/exo}$ and Pole$^{exo/exo}$ mice died even faster, mainly from thymic lymphomas (Goldsby *et al.*, 2002; Uchimura *et al.*, 2009; Albertson *et al.*, 2009).

DNA polymerase	Gene	Phenotype of knockout mice
Polα	Pola1	Embryonic lethality
Polε	Pole	Embryonic lethality. Tumorigenesis in Pole$^{exo/exo}$
Polδ	Pold1	Embryonic lethality after E4.5. Tumorigenesis in Pold1$^{exo/exo}$ and Pold1$^{exo/-}$ mice
Polζ	Rev3l	Embryonic lethality after E9.5. p53 deficiency cannot rescue the lethality. Spontaneous tumor development in condicional knock-out mice (constitutive or tissue-specific)
Polγ	Polg	Embryonic lethality after E7.5
Polθ	Polq	Viable and fertile. High micronuclei frequency in reticulocytes. Very low viability of Polq$^{-/-}$; Atm$^{-/-}$ mice
Polν	Poln	Unknown
Polη	Polh	Viable and fertile. Susceptible to UV radiation. Generation of A:T mutations during SHM. Obesity.
Polι	Poli	Viable and fertile. UV susceptibility
Polκ	Polk	Viable and fertile. Reduced life span. Increased mutations in tissues.
REV1	Rev1	Inviable on the C57BL/6 background, but viable on the 129/OLA background. Loss of C:G transversions during SHM.
Polβ	Polb	Exhibit apoptsosis in post-mitotic neuronal cells and die at birth. Loss of p53 rescues the phenotype. Polb$^{+/-}$ mice develop spontaneous lymphomas.
Polλ	Poll	Viable, fertile and display reduced Ig heavy chain junction viability
Polμ	Polm	Viable, fertile and display reduced Ig light chain junction viability
TDT	Dntt	Viable, fertile and display reduced Ig heavy chain junction viability

Table 5. DNA polymerase knockout mouse phenotypes. This table shows the phenotypes observed in knockout mice for the catalytic subunit of the indicated DNA polymerase. Atm, ataxia-telangiectasia mutated; E, embryonic day; exo: exonuclease-deficient; Pol, polymerase; TDT, terminal transferase; UV: Ultraviolet.

Interestingly, the Polα/Prim1 complex is amplified in many tumor types, except for a few cases (head and neck SCC, esophageal carcinoma and lung SCC, among others) in

which Pola1 appears to be deleted. Prim1 is also homozygously deleted in 42% of adenoid cystic breast carcinoma and 15% of adenoid carcinomas. These observations suggest that another enzyme, possibly PrimPol, could substitute for Polα/Prim1 function in the tumors. It is unlikely, however, that PrimPol can substitute for Polα/Prim1 in normal cells and tissues, because Polα$^{-/-}$ mice show an embryonic lethality phenotype.

A Pol ζ$^{-/-}$ (Rev3L$^{-/-}$) mouse model displays embryonic lethality at E9.5, suggesting that this TLS polymerase is essential in late embryonic development (Bemark *et al.*, 2000; Esposito *et al.*, 2000; Wittschieben *et al.*, 2000). A Pol ζ conditional KO developed mammary tumors; ablation of Pol ζ specifically in the skin developed Squamous Cell Carcinoma (SCC) in the absence of exogenous DNA damaging factors. To date, Polζ KO is the only TLS polymerase-deficient strain that shows an increase in spontaneous tumorigenesis (Wittschieben *et al.*, 2010; Lange *et al.*, 2013).

Heterozygous Polβ$^{+/-}$ mice develop normally but show an increased incidence of lymphomas with high infiltration capacity, similar to the tumor aggressiveness observed in PrimPol-deficient mice (Cabelof *et al.*, 2006). This intriguing parallelism would also be consistent with a possible role of PrimPol in BER, as Polβ. Indeed, a mass-spectrometry analysis of PrimPol interacting factors in UV-irradiated HeLa chromatin extracts showed that PrimPol interacts with BER proteins (Karolina Jodkowska and Silvana Mourón, unpublished data). Of note, PrimPol is highly expressed in lymphatic tissues, where BER occurs during SHM. One possibility is that PrimPol acts as a primase during DDT after exogenous DNA damage such as UV, but also plays a role in endogenous SHM. Indeed, it is been recently proposed that PrimPol serves as an anti-mutagenic factor in SHM. When AP sites are endogenously created, PrimPol primes ahead of these lesions leaving an unreplicated gap that is resolved preferentially by HR without introducing mutations. In the absence of PrimPol, AP sites are repaired by TLS, increasing the mutagenesis rate (Pilzecker *et al.*, 2016). PrimPol is needed to facilitate replication through special DNA structures such as G4 quadruplexes (Bailey *et al.*, 2016). In this sense, the aggressive pattern of the tumors in PrimPol$^{-/-}$ mice could be a consequence of the accumulation of mutations if TLS is preferred over HR during endogenous DNA repair processes.

Finally, the mitochondrial replicative polymerase Polγ is amplified in a large number of tumors (Cerami *et al.*, 2012; Gao *et al.*, 2013). As expected, KO mice are lethal during

embryogenesis (E7.5; Hance *et al.*, 2005). Polγ point mutations have been linked to other diseases and syndromes such as Progressive External Ophtalmoplegia (PEO), Alper's syndrome, ataxia-neuropathy, dysarthria, premature menopause and infertility (reviewed in Loed and Monnat, 2008).

2.3. PrimPol protects the skin from UV-induced DNA damage

Several antecedents suggested that PrimPol would play an important role in the cellular response to UV irradiation *in vivo*. First, cellular experiments showed that PrimPol association to chromatin was increased after UV, particularly to the damaged DNA sites. Single molecule analyses of DNA replication revealed that the primase activity of PrimPol was strictly required to mediate fork restart after UV-induced DNA damage (Mourón *et al.*, 2013).

We have found that MEFs deficient in PrimPol undergo difficulties to complete DNA replication after an UV challenge, which are eventually solved by other mechanisms. Avian DT40 cells lacking PrimPol accumulate in G2/M after UV irradiation and this block is resolved later on by other mechanisms (Bailey *et al.*, 2012). S-phase progression is also perturbed in Polη-, Polι-, Polκ- and Rev1-deficient MEFs after UV (Temviriyanukul *et al.*, 2012; Jansen *et al.*, 2014). Therefore, the lack of PrimPol, as that of TLS polymerases, makes the cells more susceptible to UV light.

Furthermore, PrimPol deficiency leads to an accumulation of CPD and (6,4)-pp lesions upon UV, a phenotype that had been also reported in Nrf2- or XPC-deficient skin cells (Tsaalbi-Shtylik *et al.*, 2009; Schäfer *et al.*, 2010). Therefore, PrimPol participates in the response to UV that facilitates the elimination of photoproducts in the DNA of damaged cells.

In this thesis we have characterized the UV susceptibility of PrimPol-deficient mice, using several approaches. First, we compared the skin response of PrimPol+/+, PrimPol$^{+/-}$ and PrimPol$^{-/-}$ mice to acute UV irradiation. In normal mice, a UV dosage of 3000J/m^2 induces DNA damage in the external layers of the epidermis that can be readily monitored by γH2AX. This is followed by a proliferative response in the basal layer to replace the damaged cells, causing a tissue hyperplasia that normally lasts 3-4 days. Cell proliferation in this stage can also be monitored by BrdU incorporation. Interestingly, PrimPol-deficient mice displayed a delayed, inefficient reaction to UV.

The proliferation response was incomplete (as seen by the lower percentage of BrdU-positive cells) and the epidermal thickening was caused by inflammation rather than by an increase in cellularity. As a consequence, the DNA damage was persistent for a longer time.

Strong susceptibility to UV has also been observed in mice deficient for XPA, XPC or Polζ. Polζ mice display a strong phenotype, as acute UV treatment causes skin ulceration after 10 days (Nakane *et al.*, 1995; Tsaalbi-Shtylik *et al.*, 2009; Lange *et al.*, 2013). In PrimPol-deficient mice, healing starts by five days post-UV, suggesting the participation of compensatory mechanisms.

We also studied how mice responded to a regime of chronic UV exposure, which is known to induce benign papillomas in wt mice. After 40 weeks of repeated UV exposure, the frequency of papilloma formation in PrimPol-deficient mice was significantly higher than in wt littermates. No progression towards squamous cell carcinomas (SCC) was observed, but it should be noted that the C57BL/6J background is particularly resistant to transformation from papillomas to SCC (Woodworth *et al.*, 2004). Albeit with lower frequency, mesenchymal tumors such as sarcomas and hemangiomas, were detected in PrimPol KO mice upon continued UV exposure. Therefore, PrimPol contributes to prevent cell transformation induced by UV-promoted DNA damage.

UV-induced skin tumors are common in mice deficient in DDT and DNA repair pathways. Polη or Polι KO strains (both TLS polymerases capable of bypassing CPD lesions) developed SCC and skin mesenchymal tumors, respectively (Lin *et al.*, 2006; Ohkumo *et al.*, 2006). Notably, Polι is also implicated in BER, so the tumor propensity could be caused by deficient lesion bypass or by defective BER pathway.

As shown in table 6, all mice strains deficient in the NER pathway (XPA, XPC or Ercc1) developed SCCs upon UV exposure (Berg *et al.*, 1997; Nakane *et al.*, 1995; de Vries *et al.*, 1998; van der Host *et al.*, 2002; Berg *et al.*, 2000; Tsaalbi-Shtylik *et al.*, 2009; Doig *et al.*, 2006; Cheo *et al.*, 1996; Sands *et al.*, 1995). Similarly, mice defective in genes responsible for Cockaine syndrome group A or B (Ercc8 and Ercc6, respectively) developed skin carcinomas by 40 weeks (Berg *et al.*, 2000; van der Host *et al.*, 2002). Furthermore, mice deficient in BER genes such as Ogg1 developed SCC and also mesenchymal tumors (Kunisada *et al.*, 2005).

The combined deficiency of DDT and DNA repair pathways leads to stronger phenotypes. For instance, the ablation of DDT polymerase REV1 expression in mice deficient in NER factor XPC accelerates SCC formation after chronic exposure to UV (Tsaalbi-Shtylik *et al.*, 2009).

Of note, other mice with high levels of RS such as telomeric TRF2-overexpressing mice are also more sensitive to UV-induced tumor formation and progression (Muñoz *et al.*, 2005; Stout *et al.*, 2009).

Function	Gene	Genetic Background	UVB dose (J/m^2)	Skin tumors
NER	Ercc1	Albino hairless (hr)	125 three times per week	SCC
	Xpa	Albino hairless (HRA/SKH) -129	32 daily // 80 daily	SCC
	Xpa	Albino hairless (HRA/SKH) -129	80 daily // 32 daily	SCC
	Xpa	129-C57Bl6 mix	2000 three times per week	SCC
	Xpa	129-C57Bl6 mix	1200 five times per week	SCC
	Xpc	129-C57Bl6 mix	1200 five times per week 600 five times per week	SCC
	Xpc	(HRA/SKH) -129-129-C57Bl6 mix	80 daily	SCC
	Xpc	(HRA/SKH) -129	40 daily	SCC
	Xpc	129-C57Bl6 mix	2500 daily	SCC
	Xpc	129-C57Bl6 mix	1200 daily	SCC
	Ercc6 (Csb)	Albino hairless (HRA/SKH) -129-C57Bl6 mix	80 daily	SCC
	Ercc8 (Csa)	129 C57Bl6 mix	1200 or 600 five times per week	SCC
TLS	Polh	C57Bl6	2000 daily	SCC
	Polh	C57Bl6 mix-129 mix	3750 three times per week	SCC
	Rev3L	C57BL/6 129 mixed or FVB	50 three times per week	None (ulceration)
TLS/BER	Poli	C57Bl6	2000 daily	Sarcoma and hemangioma.
TLS/NER	Xpc and Rev1	(HRA/SKH) -129 mixed	40 daily	SCC
BER	Ogg1	C57BL/6	2500 three times per week	SCC, sarcomas and hemangiomas
TLS-primase	PrimPol	C57BL/6	1800 three times per week	Papillomas, sarcomas and hemangiomas.

Table 6. UV-B radiation-induced carcinogenesis in DNA repair- or TLS- or a combination of both defective mouse models. SCC: Squamous cell carcinoma.

Altogether, we conclude that PrimPol is an important factor in the physiological response to UV-induced DNA damage. In our model (Figure 55), PrimPol promotes DDT by catalyzing the priming event downstream of a lesion. Efficient DDT in S-phase would favor later repair of the lesion by error-free HR-mediated mechanisms. In the absence of PrimPol, these lesions may be preferentially bypassed by TLS polymerases, which entail a higher risk of mutation, chromosomal instability and tumorigenesis. In the future, a *knock-in* mouse strain that encodes a mutant PrimPol version lacking the Zn finger domain (i.e. null for primase activity but with intact polymerase activity; Mourón *et al.*, 2013) could provide additional genetic evidence that the UV-induced tumorigenesis in PrimPol-deficient mice is mainly derived from the lack of primase activity.

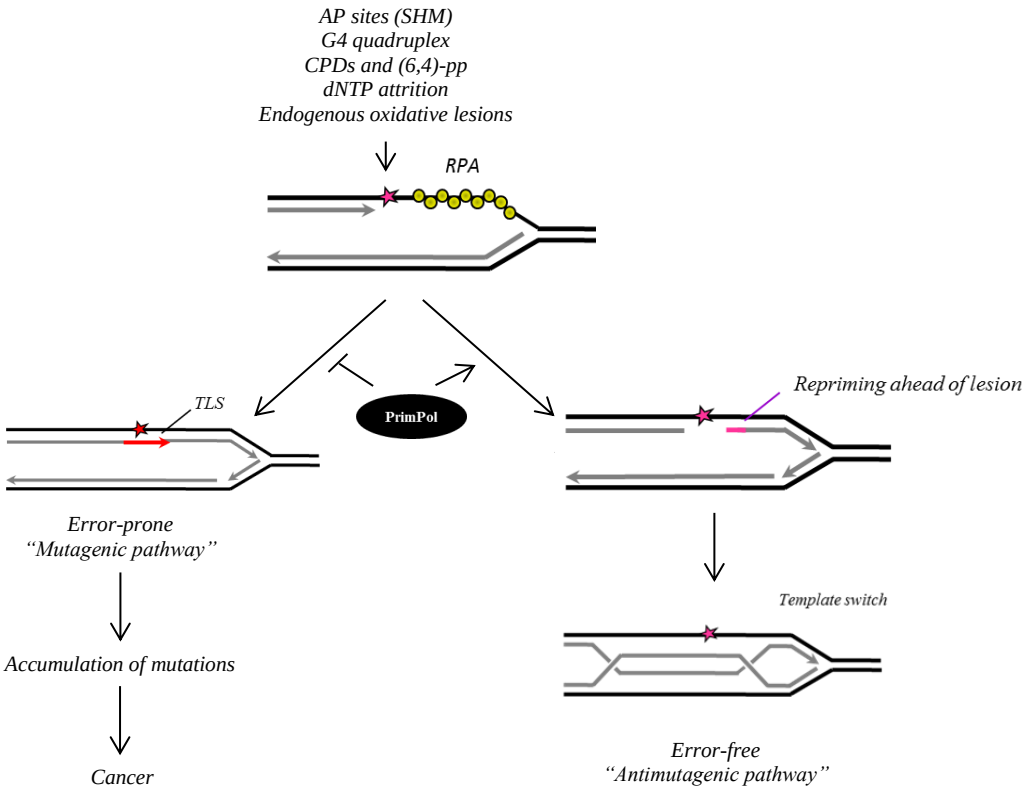

Figure 55. General antimutagenic role of PrimPol protein: a model. PrimPol is known to prime new DNA synthesis downstream of the indicated lesions. The unreplicated gap left behind is then repaired by homologous recombination, mainly an error free pathway. In the absence of PrimPol, DNA lesions would be mainly processed by TLS polymerases which are normally mutagenic.

Other interesting directions for future research could be to monitor the UV susceptibility of mice in which the loss of PrimPol is combined with a deficiency in Ogg1, Polη, or p53. It would also be interesting to learn whether the inefficient response

to UV in PrimPol KO mice could be alleviated or reverted in a mouse overexpressing photolyase, an enzyme with the ability to break UV photoproducts.

In summary, in this dissertation we have reported that PrimPol protein, involved in DDT, is necessary for the protection against UV damage, and its absence also leads to defects in fat tissue homeostasis and hair follicle growth. The higher frequency of tumorigenesis in PrimPol KO mice also indicates a tumor suppression function. Future studies will increase our knowledge about the possible participation of PrimPol in other processes, and the precise contributions of its mitochondrial and nuclear functions.

CONCLUSIONS

CONCLUSIONES

CONCLUSIONS

1. The point mutation in human PrimPol supposedly implicated in the development of high myopia (Y89D) yields a completely functional protein, *in vitro* and *in vivo*.

2. Trp87 and Tyr90 amino acids in the conserved WFYY motif are essential to preserve the functionality of PrimPol as a primase and a polymerase. *In vitro* studies carried out by our collaborators indicate that these amino acids are necessary for the formation of the enzyme-DNA-NTP preternary complex.

3. The mutation Y100H in hPrimPol, identified in cancer genomic studies, does not affect the functionality of PrimPol *in vivo*.

4. PrimPol-deficient MEFs show mild proliferation defects and UV-susceptibility.

5. PrimPol is not essential for mouse development or fertility.

6. The absence of PrimPol affects the regulation of adipose tissue and the hair follicle structure, by mechanisms that are not yet understood.

7. PrimPol plays a protective role against UV-induced DNA damage in vivo: PrimPol-deficient mice are more susceptible to short-term and long-term exposure to UV.

8. PrimPol-deficient mice present an increased incidence of late-onset tumors, which behave more aggressively, affecting the life expectancy by several weeks.

9. PrimPol acts like a tumor supressor protein *in vivo*.

CONCLUSIONES

1. La mutación puntual Y89D en la proteína PrimPol humana, supuestamente asociada al desarrollo de miopía magna, presenta una funcionalidad normal *in vitro* e *in vivo*.

2. Los aminoácidos Trp87 y Tyr90 del motivo WFYY son esenciales para las actividades bioquímicas primasa y polimerasa de PrimPol, así como para preservar su funcionalidad *in vivo*. Estudios llevados a cabo por nuestros colaboradores indican que estos dos aminoácidos participan en la formación del complejo preternario enzima-DNA-NTP.

3. La mutación Y100H en PrimPol, identificada en estudios genómicos de cáncer, no afecta a la funcionalidad de PrimPol *in vivo*.

4. MEFs deficientes en PrimPol muestran defectos sutiles en proliferación y una mayor susceptibilidad a la radiación UV.

5. PrimPol no es esencial para el desarrollo del ratón ni para su fertilidad.

6. La ausencia de PrimPol afecta la regulación del tejido adiposo y la estructura del folículo piloso, a través de mecanismos aún no conocidos.

7. PrimPol tiene un papel protector ante daños en el DNA inducidos por UV *in vivo*: los ratones deficientes en PrimPol son más susceptibles a la irradiación por UV.

8. Los ratones deficientes en PrimPol presentan una mayor frecuencia de tumores asociados al envejecimiento, que además presentan un comportamiento más agresivo y reducen la esperanza de vida en varias semanas.

9. PrimPol actua como un supresor de tumores *in vivo*.

REFERENCES

REFERENCES

Acharya, N., Johnson, J.E., Pagès, V., Prakash, L., Prakash, S. (2009). Yeast Rev1 protein promotes complex formation of DNA polymerase zeta with Pol32 subunit of polymerase delta. *Proc Natl Acad Sci USA* **106**, 9631-9636.

Akbari, M., Visnes, T., Krokan, H.E., Otterli, M. (2008). Mitochondrial base excision repair of uracil and AP sites takes place by single-nucleotide insertion and long-patch DNA synthesis. *DNA Repair* **7**, 605-616.

Albert, V., Svensson, K., Shimobayashi, M., Colombi, M., Muñoz, S., Jimenez, V., Handschin, C., Bosch, F., Hall, M.N. (2016). mTORC2 sustains thermogenesis via Akt-induced glucose uptake and glycolysis in brown adipose tissue. *EMBOMol Med* **8**, 232-246.

Albertson, T.M., Ogawa, M., Bugni, J.M., Hays, L.E., Chen, Y., Wang, Y., Treuting, P.M., Heddle, J.A., Goldsby, R.E., Preston, B.D. (2009). DNA polymerase epsilon and delta proofreading suppress discrete mutator and cancer phenotypes in mice. *Proc Natl Acad Sci USA* **106**, 17101-17104.

Almeida, K.H., Sobol, R.W. (2007). A unified view of base excision repair lesion dependent protein complexes regulated by post-translational modification. *DNA Repair* **6**, 695-711.

Augustin, M.A., Huber, R., Kaiser, J.T. (2001). Crystal structure of a DNA-dependent RNA polymerase (DNA primase). *Nat Struct Biol* **8**, 57-61.

Bailey, L.J., Bianchi, J., Hegarat, N., Hochegger, H., Doherty, A.J. (2016). PrimPol-deficient cells exhibit a pronounced G2 checkpoint response following UV damage. *Cell Cycle* **15**, 908-918.

Balajee, A.S., May, A., Bohr, V.A. (1999). DNA repair of pyrimidine dimers and 6-4 photoproducts in the ribosomal DNA. *Nucleic Acids Res* **27**, 2511-2520.

Bärtsch, S., Kang, L.E., Symington, L.S. (2000) Rad51 is required for the repair of plasmid double-stranded DNA gaps from either plasmid or chromosomal templates. *Mol Cell Biol* **20**, 1194-1205.

Bebenek, K., Tissier, A., Frank, E.G., McDonald, J.P., Prasad, R., Wilson S.H., Woodgate, R., Kunkel, T.A. (2001). 5'-Deoxyribose phosphate lyase activity of human DNA polymerase iota in vitro. *Science* **291**, 2156-2159.

Berg, R.J., de Vries, A., van Steeg, H., de Gruijl, F.R. (1997). Relative susceptibilities of XPA knockout mice and their heterozygous and wild-type littermates to UVB-induced skin cancer. *Cancer Res* **57**, 581-584.

Berg, R.J., Rebel, H., van der Horst, G.T., van Kranen, H.J., Mullenders, L.H., van Vloten, W.A., de Gruijl, F.R. (2000). Impact of global genome repair versus transcription-coupled repair on ultraviolet carcinogenesis in hairless mice. *Cancer Res* **60**, 2858-2863.

Berma, M., Kahmlichi, A.A., Davies, S.L., Neuberger, M.S. (2000). Disruption of mouse polymerase zeta (Rev3) leads to embryonic lethality and impairs blastocyst development in vitro. *Curr Biol* **10**, 1213-1216.

Berti, M., Vindigni, A. (2015) Replication stress: getting back on track. *Nat Struct Mol Biol* **23**, 103-109.

Bianchi, J., Rudd, S., Jozwiakowski, S., Bailey, L., Soura, V., Taylor, E., Stevanovic, I., Green, A., Stracker, T., Lindsay, H., Doherty, A. (2013). PrimPol bypasses UV photoproducts during eukaryotic chromosomal DNA replication. *Mol Cell* **52**, 566-573.

Biertümpfer, C, Zhao, Y., Kondo, Y., Ramón-Maiques, S., Gregory, M., Lee, L.Y., Masutani, C., Lehmann, A.R., Hanaoka, F., Yang, W. (2010). Structure and mechanism of human polymerase η. *Nature* **465**, 1044-1048.

Bowmaker, M., Yang, M.Y., Yasukawa, T., Reyes, A., Jacobs, H.T., Huberman, J.A., Holt, I.J. (2003). Mammalian mitochondrial DNA replicates bidirectionally from an initiation zona. *J Biol Chem* **278**, 50961-50969.

Braithwaite, E.K., Prasad, R., Shock.D.D., Hou, E.W., Beard, W.A., Wilson, S.H. (2005). DNA polymerase lambda mediates a back-up base excision repair activity in extracts of mouse embryonic fibroblasts. *J Biol Chem* **280**, 18469-18475.

Branzei, D. (2011). Ubiquitin family modifications and template switching. *FEBS Lett* **585**, 2810-2817.

Branzei, D., Vanoli, F., Foiani, M. (2008) SUMOylation regulates Rad18-mediated template switch. *Nature* **456**, 915-920.

Brisset, N.C., Martin, M.J., Pitcher, R.S., Bianchi, J., Juarez, R., Green, A.J., Fox, G.C., Blanco, L., Doherty, A.J. (2011). Structure of a preternary complex involving a prokaryotic NHEJ DNA polymerase. *Mol Cell* **41**, 221-231.

Brown, T.A., Cecconi, C., Tkachuk, A.N., Bustamante, C., Clayton, D.A. (2005). Replication of mitochondrial DNA occurs by strand displacement with alternative light-strand origins, not via a strand-coupled mechanism. *Genes Dev* **19**, 2466-2476.

Burgers, P.M.J., Gordeninm D., Kunkel, T.A. (2016). Who is leading the replication fork, Pol ε or Pol δ?. *Mol Cell* **61**, 492-493.

Byun, T.S., Pacek, M., Yee, M.C., Walter, J.C., Cimprich, K.A. (2005). Functional uncoupling of MCM helicase and DNA polymerase activities activates the ATR-dependent checkpoint. *Genes Dev* **19**, 1040-1052.

Cabelof, D.C., Ikeno, Y., Nyska, A., Busuttil, R.A., Anyangwe, N., Vijg, J., Matherly, L.H., Tucker, J.D., Wilson, S.H., Richardson, A., Heydari, A.R. (2006). Haploinsufficiency in DNA polymerase beta increases cancer risk with age and alters mortality rate. *Cancer Res* **66**, 7460-7465.

Callegari, A.J., Clark, E., Pneuman, A., Kelly, T.J. (2010). Postreplication gaps at UV lesions are signals for checkpoint activation. *Proc Natl Acad Sci USA* **107**, 8219-8224.

Callegari, A.J., Kelly, T.J. (2006). UV irradiation induces a postreplication DNA damage checkpoint. *Proc Natl Acad Sci USA* **103**, 15877-15886.

Ceppi, P.S., Novello, S., Cambieri, A., Longo, M., Monica, V., Lo Iacono, M., Giaj-Levra, M., Saviozzi, S., Volante, M., Papotti, M., Scagliotti, G. (2009). Polymerase eta mRNA expression predicts survival of non-small cell lung cáncer patients treated with platinum-based chemotherapy. *Clin Cancer Res* **15**, 1039-1045.

Cerami, E., Gao, J., Dogrusoz, U., Gross, B.E., Sumer, S.O., Aksoy, B.A., Jacobsen, A., Byrne, C.J., Heuer, M.L., Larsson, E., Antipin, Y., Reva, B., Goldberg, A.P., Sander, C., Schultz, N. (2012). The cBIO Cancer Genomics Portal: An Open Platform for Exploring Multidimensional Cancer Genomics Data. *Cancer Discov* **2**, 401-404.

Chan, M.K., Ocampo-Hafallla, M.T., Vartanian, V., Jaruga, P., Kirkali, G., Koeing, K.L., Brown, S., Lloyd, R.S., Dizdaroglu, M., Teebor, G.W. (2009). Targeted deletion of the genes encoding NTH1 and NEIL1 DNA N-glycosylases reveals the existence of novel carcinogenic oxidative damage to DNA. *DNA Repair* **8**, 786-794.

Chand, D.J., Cimprich, K.A. (2009). DNA damage tolerance: when it's OK to make mistakes. *Nat Chem Biol* **5**, 82-90.

Chen, Y., Harris, R.A., Hatahet, Z., Chou, K. (2015). Ablation of XP-V gene causes adipose tissue senescence and metabolic abnormalities. *Proc Natl Acad Sci USA* **112**, 4556-4564.

Cheng, X., Kanki, T., Fukuoh, A., Ohgaki, K., Takeya, R., Aoki, Y., Hamasaki, N., Kang, D. (2005). PDIP38 associates with proteins constituting the mitochondrial DNA nucleoid. *J Biochem* **138**, 673-678.

Cheo, D.L., Meria, L.B., Hammer, R.E., Burns, D.K., Doughty, A.T., Friedberg, E.C. (1996). Synergistic interactions between XPC and p53 mutations in double-mutant mice: Neural tube abnormalities and accelerated UV radiation-induced skin cancer. *Curr Biol* **6**, 1691-1694.

Clayton, D.A., Doda, J.N., Friedberg, E.C. (1974). The absence of a pyrimidine dimer repair mechanism in mammalian mitochondria. *Proc Natl Acad Sci USA* **71**, 2777-2781.

Copeland, W.C. (2010). The mitochondrial DNA polymerase in health and disease. *Subcell Biochem* **50**, 211-222.

Copeland, W.C., Tan, X. (1995). Active site mapping of the catalytic mouse primase subunit by alanine sanning mutagenesis. *J Biol Chem* **270**, 3905-3913.

Courdavault, S., Baudouin, C., Carveron, M., Canguilhem, B., Favier, A., Cadet, J., Douki, T. (2005). Repair of the three main types of bipyrimidine DNA photoproducts in human keratinocytes exposed to UVB and UVA radiations. *DNA Repair* **4**, 836-844.

Dantzer, F., Nasheuer, H.P., Vonesch, J.L., de Murcia, G., Menissier-de Murcia, J. (1998). Functional association of poly(ADP-ribose) polymerase with DNA polymerase alpha-primase complex: a link between DNA strand break detection and DNA replication. *Nucleic Acids Res* **26**, 1891-1898.

de Souza-Pinto, N.C., Mason, P.A., Hashiguchi, K., Weissman, L., Tian, J., Guay, D., Lebel, M., Stevnsner, T.V., Rasmussen, L.J., Bohr, V.A. (2009). Novel DNA mismatch-repair activity involving YB-1 in human mitochondria. *DNA Repair* **8**, 704-719.

de Vries, A., Berg, R.J., Wijnhoven, S., Westerman, A., Wester, P.W., van Krejil, C.F., Capel, P.J., de Gruijl, F.R., van Kranen, H.J., van Steeg, H. (1998). XPA-deficiency in hairless mice causes a shift in skin tumor types and mutational target genes after exposure to low doses of U.V.B. *P. Oncogene* **16**, 2205-2212.

Deans, A.J., West, S.C. (2011). DNA interstrand crosslink repair and cancer. *Nat Rev Cancer* **11**, 467-480.

Della, M., Palmbos, P.L., Tseng, H.M., Tonkin, L.M., Daley, J.M., Topper, L.M., Pitcher, R.S., Tomkinson, A.E., Wilson, T.E., Doherty, A.J. (2004). Mycobacterial Ku and ligase proteins constitute a two-component NHEJ repair machine. *Science* **306**, 683-685.

Doig, J., Anderson, C., Lawrence, N.J., Selfridge, J., Brownstein, D.G., Melton, D.W. (2006). Mice with skin-specific DNA repair gene (Ercc1) inactivation are hypersensitive to ultraviolet irradiation-induced skin cancer and show more rapid actinic progression. *Oncogene* **25**, 6229-6238.

Edmunds, C.E., Simpson, L.J., Sale, E.J. (2008). PCNA ubiquitination and REV1 define temporally distinct mechanisms for controlling translesion synthesis in the avian cell line DT40. *Mol Cell* **30**, 519-529.

Elyers, I., Johansson, F., Groth, P., Erixon, K., Helleday, T. (2011). UV stalled replication forks restart by re-priming in human fibroblasts. *Nucleic Acids Res* **39**, 7049-7057.

Esposito, G., Godindagger, I., Klein, U., Yaspo, M.L., Cumano, A., Rajewsky, K. (2000). Disruption of the Rev3L-encoded catalytic subunit of polymerase zeta in mice results in early embryonic lethality. *Curr Biol* **10**, 1213-1216.

Fang, E.F., Scheibye-Knudsen, M., Brace, L.E., Kassahun, H., SenGupta, T., Nilsen, H., Mitchell, J.R., Croteau, D.L., Bohr, V.A. (2014). Defective Mitophagy in XPA via PARP-1 Hyperactivation and NAD^+/SIRT1 Reduction. *Cell* **157**, 882-896.

Foiani, M., Lucchini, G., Plevani, P. (1997). The DNA polymerase alpha-primase complex couples DNA replication, cell-cycle progression and DNA-damage response. *Trends Biochem Sci* **22**, 424-427.

Frick, D.N., Richardson C.C. (2001). DNA primases. *Annu Rev Biochem* **70**, 39-80.

Fumasoni, M., Zwicky, K., Vanoli, F., Lopes, M., Branzei, D. (2015). Error-free DNA damage tolerance and sister chromatid proximity during DNA replication rely on the Polα/Primase/Ctf4 complex. *Mol Cell* **57**, 812-823.

Furnari, B., Blasina, A., Boddy, M.N., McGowan, C.H., Russell, P. (1999). Cdc25 inhibited in vivo and in vitro by checkpoint kinases Cds1 and Chk1. *Mol Biol Cell* **10**, 833-845.

Fuste, J.M, Wanrooij, S., Jemt, E., Granycome, C.E., Cluett, T.J., Shi, Y., Atanassova, N., Holt, I.J., Gustafsson, C.M., Falkenberg, M. (2010). Mitochondrial RNA polymerase is needed for activation of the origin of light-strand DNA replication. *Mol Cell* **37**, 67-78.

Friedberg, E.C. (2005). Suffering in silence: the tolerance of DNA damage. *Nat Rev Mol Cell Biol* **6**, 943-953.

Galal, W.C., Pan, M., Kelman, Z., Hurwitz, J. (2012). Characterization of DNA primase complex isolated from the archaeon, Thermococcus kodakaraensis. *J Biol Chem* **287**, 16209-16219.

Gao, J., Aksov, B.A., Dogrusoz, U., Dresdner, G., Gross, B., Sumer, S.O., Sun, Y., Jacobsen, A., Sinha, R., Larsson, E., Cerami, E., Sander, C., Schultz, N. (2013). Integrative analysis of complex cancer genomics and clinical profiles using the cBioPortal. *Sci Signal* **6**, pl1.

García-Gómez, S., Reyes, A., Martínez-Jiménez, M., Chocrón, S., Mourón, S., Terrados, G., Powell, C., Salido, E., Méndez, J., Holt, I., Blanco, L. (2013). PrimPol, an archaic primase/polymerase operating in human cells. *Mol Cell* **52**, 541-553.

Ge, X., Jackson, D., Blow, J. (2007). Dormant origins licensed by excess Mcm2-7 are required for human cells to survive replicative stress. *Genes Dev* **21**, 3331-3341.

Goldsby, R.E., Hays, L.E., Chen, X., Olmsted, E.A., Slayton, W.B., Spangrude, G.J., Preston, B.D. (2002). High incidence of epithelial cancers in mice deficient for DNA polymerase delta. *Proc Natl Acad Sci USA* **99**, 15560-15565.

Guilliam T.A., Bailey, L.J., Brissett, N.C., Doherty, A.J. (2016). PolDIP2 interacts with human PrimPol and enhances its DNA polymerase activities. *Nucleic Acids Res* **44**, 3317-3329.

Guilliam T.A., Keen, B.A., Brissett, N.C., Doherty, A.J. (2015). Primase-polymerases are a functionally diverse superfamily of replication and repair enzymes. *Nucleic Acids Res* **43**, 6651-6664.

Guilliam T.A., Jozwiakowski, S.K., Ehlinger, A., Barnes, R.P., Rudd, S.G., Bailey, L.J., Skehel, J.M., Eckert, K.A., Chazin, W.J., Doherty, A.J. (2015). Human PrimPol is a highly error-prone polymerase regulated by single-stranded DNA binding proteins. *Nucleic Acids Res* **43**, 1056-1068.

Guo, C., Fischhaber, P.L., Luk-Paszyc, M.J., Masuda, Y., Zhou, J., Kamiya, K., Kisker, C., Friedberg, E.C. (2003). Mouse Rev1 protein interacts with multiple DNA polymerases involved in translesion synthesis. *EMBO J* **22**, 6621-6630.

Guo, C., Sonoda, E., Tang, T.S., Parker, J.L., Bielen, A.B., Takeda, S., Ulrich, H.D., Friedberg, E.C. (2006). REV1 protein interacts with PCNA: significance of the REV1 BRCT domain in vitro and in vivo. *Mol Cell* **23**, 265-271.

Hamanaka, R.B., Glassauer, A., Hoover, P., Yang, S., Blatt, H., Mullen, A.R., Getsios, S., Gottardi, C.J., DeBerardinis, R.J., Lavker, R.M., Chandel, N.S. (2013). Mitochondrial Reactive Oxygen Species Promote Epidermal Differentation and Hair Follicle Development. *Science Sci* **6**, ra8.

Hampp, S., Kiessling, T., Buechle, K., Mansilla, S.F., Thomale, J., Rall, M., Ahn, J., Pospiech, H., Gottifredi, V., Wiesmüller, L. (2016). DNA damage tolerance pathway involving DNA polymerase ι and the tumor suppressor p53 regulates DNA replication fork progression. *Proc Natl Acad Sci USA* **113**, 4311-4319.

Hanawalt, P.C., Spivak, G. (2008). Transcription-coupled DNA repair: two decades of progress and surprises. *Nat Rev Mol Cell Biol* **9**, 958-970.

Hance, N., Ekstrand, M.I., Trifunovic, A. (2005). Mitochondrial DNA polymerase gamma is essential for mammalian embryogenesis. *Hum Mol Genet* **14**, 1775-1783.

Hao, Q., Yadav, R., Basse, A.L., Petersen, S., Sonne, S.B., Rasmussen, S., Zhu, Q., Lu, Z., Wang, J., Audouze, K., Gupta, R., Madsen, L, Kristiansen, K., Hansen, J.B. (2015). Transcriptome profiling of brown adipose tissue during cold exposure reveals extensive regulation of glucose metabolism. *Endocrinol Metab* **308**, 380-392.

Harlow, L., Lane, D. (1999). Using antibodies: a laboratory manual. New York: CSHL Press.

Heller, R.C., Marians, K.J. (2006). Replication fork reactivation downstream of a blocked nascent leading strand. *Nature* **439**, 557-562.

Heller, R.C., Marians, K.J. (2006). Replisome assembly and the direct restart of stalled replication forks. *Nat Rev Mol Cell Biol* **7**, 932-943.

Heyer, W.D., Ehmsen, K.T., Liu, J. (2010). Regulation of homologous recombination in eukaryotes. *Annu Rev Genet* **44**, 113-139.

Hoege, C., Pfander, B., Moldovan G.L., Pyrowolaskis, G., Jentsch, S. (2002). RAD6-dependent DNA repair is linked to modification of PCNA by ubiquitin and SUMO. *Nature* **419**, 135-141.

Holm, L., Sander, C. (1995). DNA polymerase beta belongs to an ancient nucleotidyltransferase superfamily. *Trends Biochem Sci* **20**, 345-347.

Ibarra, A., Schwob, E., Méndez, J. (2008). Excess MCM proteins protect human cells from replicative stress by licensing backup origins of replication. *Proc Natl Acad Sci USA* **105**, 8956-8961.

Ito, J., Braithwaite, D.K. (1991). Compilation and alignment of DNA polymerase sequences. *Nucleic Acids Res* **19**, 4045-4057.

Iyer, L.M., Koonin, E.V., Leipe, D.D., Aravind, L. (2005). Origin and evolution of the archaeo-eukaryotic primase superfamily and related palm-domain proteins: structural insights and new members. *Nucleic Acids Res* **33**, 3875-3896.

Jackson, D.A., Pombo, A. (1998). Replicon clusters are stable units of chromosome structure: evidence that nuclear organization contributes to the efficient activation and propagation of S phase in human cells. *J Cell Biol* **140**, 1285-1295.

Jackson, S., Bartek, J. (2009). The DNA-damage response in human biology and disease. *Nature* **461**, 1071-1078.

Jansen, J.G., Temviriyanukul, P., Wit, N., Delbos, F., Reynaud, C., Jacobs, H., de Wind, N. (2014). Redundancy of mammalian Y family DNA polymerases in cellular responses to genomic DNA lesions induced by ultraviolet light. *Nucleic Acids Res* **42**, 11071-11082

Johnson, R.E., Klassen, R., Prakash, L., Prakash, S. (2015). A major role of DNA polymerase δ in replication of both the leading and the lagging DNA strands. *Mol Cell* **59**, 163-175.

Johnson, R.E:, Washington, M.T., Prakash, S., Prakash, L. (2000). Fidelity of human DNA polymerase eta. *J Biol Chem* **275**, 7447-7450.

Kannouche, P.L., Stary, A. (2004). Xeroderma pigmentosium variant and error-prone DNA polymerases. *Biochimie* **85**, 1123-1132.

Karakasilioti, I., Kamileri, I., Chatzinikolaou, G., Kosteas, T., Vergadi, E., Robinson, A.R., Tsamadrinos, I., Rozgaja, T.A., Siakouli,, S., Tsatsanis, C., Niedernhofer, L.J., Garinis, G.A. (2013). DNA damage triggers a chronic autoinflammatory response, leading to fat depletion in NER progeria. *Cell Metab* **18**, 403-415.

Kasiviswanathan, R., Gustafson, A., Copeland, W.C., Meyer, J.N. (2012). Human mitochondrial DNA polymerase gamma exhibits potential for bypass and mutagenesis at UV-induced cyclobutane thymine dimers. *J Biol Chem* **287**, 9222-9229.

Keen, B.A., Bailey, L.J., Jozwiakowski, S.K., Doherty, A.J. (2014). Human PrimPol mutation associated with high myopia has a DNA replication defect. *Nucleic Acids Res* **43**, 1056-1068.

Keen, B.A., Jozwiakowski, S.K., Bailey, L.J., Bianchi, J., Doherty, A.J. (2014). Molecular dissection of the domain architecture and catalytic activites of human PrimPol. *Nucleic Acids Res* **42**, 5830-5845.

Kidane, D., Jonason, A.S., Gorton, T.S., Mihaylov, I., Pan, J., Keeney, S., Rooij, D.G., Ashley, T., Keh, A., Liu, Y., Banerjee, U., Zelterman, D., Sweasy, J.B. (2010). DNA polymerase beta is critical for mouse meiotic synapsis. *EMBO J* **29**, 410-423.

Kirk, B.W., Kuchta, R.D. (1999). Arg304 of human DNA primase is a key contributor to catlysis and NTP binding: primase and the family X polymerases share significant sequence homology. *Biochenistry* **38**, 7727-7736.

Knobel, P.A., Marti, T.M. (2011). Translesion DNA synthesis in the context of cancer research. *Cancer Cell Int* **11**, doi: 10.1186/1475-2867-11-39.

Kobayashi, K., Guilliam, T.A., Tsuda, M., Yamamoto, J., Bailey, L.J., Iwai, S., Takeda, S., Doherty, A.J., Hirota, K. (2016). Repriming by PrimPol is critical for DNA replication restart downstream of lesions and chain-terminating nucleosides. *Cell Cycle* **15**, 1997-2008.

Kuchta, R.D., Stengel, G. (2010). Mechanism and evolution of DNA primases. *Biochim Biophys Acta* **1804**, 1180-1189.

Kukimoto, I., Igaki, H., Kanda, T. (1999). Human CDC45 protein binds to minichromosome maintenance 7 protein and the p70 subunit of DNA polymerase alpha. *Eur J Biochem* **265**, 936-943.

Kunisada, M., Sakumi, K., Tominaga, Y., Budiyanto, A., Ueda, M., Ichihashi, M., Nakabeppu, Y., Nishigori, C. (2005). 8-Oxoguanine formation induced by chronic UVB exposure makes Ogg1 Knockout mice susceptible to skin carcinogenesis. *Cancer Res* **65**, 6006-6010.

Kunkel, T.A., Erie, D.A. (2015). Eukaryotic mismatch repair in relation to DNA replication. *Annu Rev Genet* **49**, 291-313.

Kusumoto, R., Masutani, C., Sugasawa, K., Iwai, S., Araki, M., Uchida, A., Mizukoshi, T., Hanaoka, F. 2001. Diversity of the damage recognition step in the global genomic nucleotide excision repair in vitro. *Mutat Res* **485**, 219-227.

Labib, K., Tercero, J.A., Diffley, J.F. (2000). Uninterrupted MCM2-7 function required for DNA replication fork progression. *Science* **288**, 1643-1647.

Lange, S., Takata, K., Wood, R.D. (2011). DNA polymerases and cancer. *Nat Rev Cancer* **11**, 96-110.

Lange, S., Bedford, E., Reh, S., Wittschieben, J., Carbajal, S., Kusewitt, D., DiGiovanni, J., Wood, R. (2013). Dual role for mammalian DNA polymerase ζ in maintaining genome stability and proliferative responses. *Proc Natl Acad Sci USA* **110**, 687-696.

Langston, L.D., O'Donnell, M. (2006). DNA replication : keep moving and don't mind the gap. *Mol Cell* **23**, 155-160.

Lao-Sirieix, S.H., Nookala, R.K., Roversi, P., Bell, S.D., Pellegrini, L. (2005). Structure of the heterodimeric core primase. *Nat Struct Biol* **12**, 1137-1144.

Lao-Sirieix, S.H., Pellegrini, L., Bell, S.D. (2005). The promiscuous primase. *Trends Genet* **21**, 568-572.

Li, J., Zhang, Q. (2015). PRIMPOL mutation: Functional Study Does Not Always Reveal The Truth. *Invest Ophtalmol Vis Sci* **56**, 1181-1182.

Lin, Q., Clark, A.B., McCulloch, S.D., Yuan, T., Bronson, R.T., Kunkel, T.A., Kucherlapati, R. (2006). Increased susceptibility to UV-induced skin carcinogenesis in polymerase η-deficient mice. *Cancer Res* **66**, 87-94.

Lindahl, T. (1993). Instability and decay of the primary structure of DNA. *Nature* **362**, 709-715.

Lipps, G., Röther, S., Hart, C., Krauss, G. (2003). A novel type of replicative enzyme harbouring ATPase, primase and DNA polymerase activity. *EMBO J* **22**, 2516-2525.

Lipps, G., Weinzierl, A.O., von Scheven, G., Buchen, C., Cramer, P. (2004). Structure of a bifunctional DNA primase-polymerase. *Nat Struct Biol* **11**, 157-162.

Livneh, Z., Ziv, O., Shachar, S. (2010). Multiple two-polymerase mechanisms in mammalian translesion DNA synthesis. *Cell Cycle* **9**, 729-735.

Loeb. L.A., Monnat, R.J. (2008). DNA polymerases and human diseases. *Nat Rev Genet* **9**, 594-604.

Lommel, L., Hanawalt, P.C. (1993). Increased UV resistance of a xenoderma pigmentosium revertant cell line is correlated with selective repair of the transcribed strand of an expressed gene. *Mol Cell Biol* **13**, 970-976.

Longley, M.J., Pierce, A.J., Modrich, P. (1997). DNA polymerase delta is required for human mismatch repair in vitro. *J Biol Chem* **18**, 10917-10921.

Lopes, M., Foiani, M., Sogo, J.M. (2006). Multiple mechanisms control chromosome integrity after replication fork uncoupling and restart at irreparable UV lesions. *Mol Cell* **21**, 15-27.

Lu, Y., Lou, Y., Yen, P., Mitchell, D., Huang, M., Conney, A. (1999). Time course for early adaptive responses to ultraviolet B light in the epidermis of SKH-1 mice. *Cancer Res* **59**, 4591-4602.

Lui, L., Rodriguez-Belmonte, E.M., Mazloum, N., Xie, B., Lee, M.Y. (2003). Identification of a novel protein, PDIP38, that interacts with the p50 subunit of DNA polymerase delta and proliferating cell nuclear antigen. *J Biol Chem* **278**, 10041-10047.

Lujan, S.A., Williams, J.S., Kunkel, T.A. (2016). DNA polymerases divide the labor of genome replication. *Trends Cell Biol* **26**, 640-654.

Maga, G., Crespan, E., Markkanen, E., Imhof, R., Furrer, A., Villani, G., Hbscher, U., Van Loon, B. (2013). DNA polymerase δ-interacting protein 2 is a processivity factor fo DNA polymerase λ during 8-oxo-1,8-dihydroguanine bypass. *Proc Natl Acad Sci USA* **110**, 18850-18855.

Mailand, N., Falck, J., Lukas, C., Syljuasen, R.G., Welcker, M., Bartek, J., Lukas, J. (2000). Rapid destruction of human Cdc25A in response to DNA damage. *Science* **288**, 1425-1429.

Mailand, N., Podtelejnikov, A.V., Groth, A., Mann, M., Bartek, J., Lukas, J. (2002). Regulation of G(2)/M events by Cdc25A through phosphorylation-dependent modulation of its stability. *EMBO J* **21**, 5911-5920.

Malumbres, M., Mangues, R., Ferrer, N., Lu, S., Pellicer, A. (1997). Isolation of high molecular weight DNA for reliable genotyping of transgenic mice. *Biotechniques* **22**, 1114-1119.

Martínez-Jiménez, M.I., García-Gómez, S., Bebenek, K., Sastre-Moreno, G.., Calvo, P.A., Díaz-Talavera, A., Kunkel, T.A., Blanco, L. (2015). Alternative solutions and new scenarios for translesion DNA synthesis by human PrimPol. *DNA Repair (Amst)* **29**, 127-138.

Mendez, J., Stillman, B. (2000). Chromatin association of human origin recognition complex, cdc6, and minichromosome maintenance proteins during the cell cycle: assembly of prereplication complexes in late mitosis. *Mol Cell Biol* **20**, 8602-8612.

Michael, W.M., Ott, R., Fanning, E., Newport, J. (2000). Activation of the DNA replication checkpoint through RNA synthesis by primase. *Science* **289**, 2133-2137.

Mitchell, D.L., Cleaver, J.E., Epstein, J.H. (1990). Repair of pyrimidine (6-4) pyrimidone photoproducts in mouse skin. *J Investig Dermatol* **95**, 55-59.

Mourón, S., Rodríguez-Acebes, S., Martínez-Jiménez, M., García-Gómez, S., Chocrón, S., Blanco, L., Méndez, J. (2013). Repriming of DNA synthesis at stalled replication forks by human PrimPol. *Nat Struct Mol Biol* **20**, 1383-1389.

Muñoz, P., Blanco, R., Flores, J.M., Blanco, M.A. (2005). XPF nuclease-dependent telomere loss and increased DNA damage in mice overexpressing TRF2 result in premature aging and cancer. *Nat Genet* **37**, 1063-1071.

Muñoz, S., Méndez, J. (2016). DNA replication stress: from molecular mechanisms to human disease. *Chromosoma* doi: 10.1007/s00412-016-0573-x.

Murakumo, Y, Ogura, Y., Ishii, H., Numata, S., Ichihara, M., Croce, C.M., Fishel, R., Takahashi, M. (2001). Interactions in the error-prone postreplication repair proteins hREV1, hREV3 and hREV7. *J Biol Chem* **276**, 35644-35651.

Muzi-Falconi, M., Giannattasio, M., Foiani, M., Plevani, P. (2003). The DNA Polymerase α-Primase Complex : Multiple Functions and Interactions. *Sci World J* **3**, 21-33.

Nakane, H., Takeuchi, S., Yuba, S., Saijo, M., Nakatsu, Y., Murai, H., Nakatsuru, Y., Ishikawa, T., Hirota, S., Kitamura, Y., Kato, Y., Tsunoda, Y., Miyauchi, H., Horlo, T., Tokunaga, T., Matsunaga, T., Nikaido, O., Nishimune, Y., Okada, Y., Tanaka, K.

(1995). High incidence of ultraviolet-B- or chemical-carcinogen-induced skin tumours in mice lacking the xenoderma pigmentosum group A gene. *Nature* **377**, 165-168.

Narayanan, D.L., Saladi, R.N., Fox, J.L. (2010). Ultraviolet radiation and skin cancer. *Int J Dermatol* **49**, 978-986.

Noonan, F.P., Recio, J.A., Takayama, H., Duray, P., Anver, M.R., Rush, W.L., De Fabo, E.C., Merlino, G. (2001). Neonatal sunburn and melanoma in mice. *Nature* **413**, 271-272.

Ogawa, T., Baker, T.A., van der Ende, A., Kornberg, A. (1985). Initiation of enzymatic replication at the origin of the Escherichia coli chromosome: contributions of RNA polymerase and primase. *Proc Natl Acad Sci USA* **82**, 3562-3566.

Ogi, T., Limsirichaikul, S., Overmeer, R.M., Volker, M., Takenaka, K., Cloney, R., Nakazawa, Y., Niimi, A., Miki, Y., Jaspers, N.G., Mullenders, L.H.F., Yamashita, S., Fousteri, M.I., Lehmann, A.R. (2010). Three DNA polymerases, recruited by different mechanisms, carry out NER repair synthesis in human cells. *Mol Cell* **37**, 714-727.

Ohashi, E., Murakumo, Y., Kanjo, N., Akagi, J., Masutani, C., Hanaoka, F., Ohmori, H. (2004). Interactions of hREV1 with three Y-family DNA polymerases, *Genes Cells* **9**, 523-531.

Ohkumo, T., Kondo, Y., Yokoi, M., Tsukamoto, T., Yamada, A., Sugimoto, T., Kanao, R., Higashi, Y., Kondoh, H., Tatematsu, M., Masutani, C., Hanaoka, F. (2006). UV-B radiation induces epithelial tumors in mice lacking DNA polymerase η and mesenchymal tumors in mice deficient for DNA polymerase ι. *Mol Cell Biol* **6**, 7696-7706.

Ollis, D.L., Brick, P., Hamlink, R., Xuong, N.G., Steitz, T.A. (1985). Structure of large fragment of Escherichia coli DNA polymerase I complexed with dTMP. *Nature* **6**, 762-766.

Palles, C., Cazier, J.B., Howarth, K.M., Domingo, E., Jones, A.M., Broderick, P., Kemp, Z., Spain, S.L., Guarino, E., Salguero, I., Sherbome, A., Chubb, D., Carvajal-Carmona, L.G., Ma, Y., Kaur, K., Dobbin, S., Barclay, E., Gorman, M., Martin, L., Kovac, M.B., Humphray, S. *et al.*. (2013). Germline mutations affecting the

proofreading domains of POLE and POLD1 predispose to colorectal adenomas and carcinomas. *Nat Genet* **45**, 136-144.

Petermann, E., Helleday, T. (2010). Pathways of mammalian replication fork restart. *Nat Rev Mol Cell Biol* **11**, 683-687.

Petermann, E., Woodcock, M., Helleday, T. (2010). Chk1 promotes replication fork progression by controlling replication initiation. *Proc Natl Acad Sci USA* **107**, 16090-16095.

Petta, T.B., Nakajima, S., Zlatanou, A., Despras, E., Couve-Privat, S., Ishchenko, A., Sarasin, A., Yasui, A., Kannouche, P. (2008). Human DNA polymerase iota protects cells against oxidative stress. *EMBO J* **27**, 2883-2895.

Pilzecker, B., Buoninfante, O.A., Pritchard, C., Blomberg, O.S., Huijbers, I., J., van den Berk, P.C.M., Jacobs, H. (2016). PrimPol prevents APOBEC/AID family mediated DNA mutagenesis. *Nucleic Acids Res* **44**, 4734-4744.

Pitcher, R.S., Brisset, N.C., Picher, A.J., Andrade, P., Juarez, R., Green, A.J., Fox, G.C., Blanco, L., Doherty, A.J. (2007). Structure and function of a mycobacterial NHEJ DNA repair polymerase. *Mol Cell* **41**, 221-231.

Prasad, R., Longley, M.J., Sharief, F.S., Hou, E.W., Copeland, W.C., Wilson, S.H. (2009). Human DNA polymerase theta possesses 5'-dRP lyase activity and functions in single-nucleotide base excision repair in vitro. *Nucleic Acids Res* **37**, 1868-1877.

Rastogi, R.P., Richa, Kumar, A., Tyagi, M.B., Sinha, R.P. (2010). Molecular mechanisms of ultraviolet radiation-induced DNA damage and repair. *J Nucleic Acids* **2010**: 592980.

Raynard, S., Buseen, W., Sung, P. (2006). A double Holliday junction dissolvasome comprising BLM, topoisomerase III alpha and BLAP75. *J Biol Chem* **281**, 13861-13864.

Renkawitz, J., Lademann, C.A., Jentsch, S. Mechanisms and principles of homology search during recombination. *Nat Rev Mol Cell Biol* **15**, 369-383.

Sale, J.E. (2012) Competition, collaboration and coordination-determining how cells bypass DNA damage. *J Cell Sci* **125**, 1633-1643.

Sampath, H., Batra, A.K., Vartanian, V., Carmical, J.R., Prusak, D., King, I.B., Lowell, B., Earley, L.F., Wood, T.G., Marks, D.L., McCullough, A.K., Lloyd, R.S. (2011). Variable penetrance of metabolic phenotypes and development of high-fat diet-induced adiposity in NEIL1-deficient mice. *Am J Physiol Endocrinol Metab* **300**, 724-734.

Sampath, H., Vartanian, V., Rollins, M.R., Sakumi, K., Nakabeppu, Y., Lloyd, R.S. (2012). 8-Oxoguanine DNA Glycosylase (OGG1) Deficiency Increases Susceptibility to Obesity and Metabolic Dysfunction. *PLOS ONE* **7**, e51697.

Sands, A.T., Abuin, A., Sanchez, A., Conti, C.J., Bradley, A. (1995). High susceptibility to ultraviolet-induced carcinogenesis in mice lacking XPC. *Nature* **377**, 162-165.

Schäfer, M., Dütsch, S., auf dem Keller, U., Navid, F., Schwarz, A., Johnson, D.A., Johnson, J.A., Werner, S. (2010). Nrf2 establishes a glutathione-mediated gradient of UVB cytoprotection in the epidermis. *Genes Dev* **24**, 1045-1058.

Schiavone, D., Jozwiakowski, S.K., Romanello, M., Guilbaud, G., Guilliam, T.A., Bailery, L.J., Sale, J.E., Doherty, A.J. (2016). PrimPol is required for replicative tolerance of G Quadruplexes in Vertebrate Cells. *Mol Cell* **61**, 161-169.

Schmidt, J.C., Cech, T.R. (2015). Human telomerase: biogenesis, trafficking, recruitment and activation. *Genes Dev* **29**, 1095-1105.

Schneider, J.G., Finck, B.N., Ren, J., Standley, K.N., Takagi, M., Maclean, K.H., Bernal-Mizrachi, C., Muslin, A.J., Kastan, M.B., Semenkovich, C.F. (2006). ATM-dependent suppression of stress signaling reduces vascular disease in metabolic syndrome. *Cell Metab* **18**, 403-415.

Seki, M., Masutani, C., Yang, L.W., Schuffert, A., Iwai, S., Bahar, I., Wood, R.D. (2004). High-efficiency bypass of DNA damage by human DNA polymerase Q. *EMBO J* **23**, 4484-4494.

Seki, M., Wood, R.D. (2008). DNA polymerase theta (POLQ) can extend mismatches and from bases opposite a (6-4) photoproduct. *DNA Repair* **7**, 119-127.

Shachar, S., Ziv, O., Avkin, S., Adar, S., Wittschieben, J., Reissner, T., Chaney, S., Friedberg, E.C., Wang, Z., Carell, T., Geacintov, N., Livneh, Z. (2009). Two-

polymerase mechanisms dictate error-free and error-prone translesion DNA synthesis in mammals. *EMBO J* **28**, 383-393.

Sheaff, R.J., Kuchta, R.D. (1994). Misincorporation of nucleotides by calf thymus DNA primase and elongation of primers containing multiple noncognate nucleotides by DNA polymerase alpha. *J Biol Chem* **269**, 19225-19231.

Singh, B., Li, X., Owens, K.M., Vanniarajan, A., Liang, P., Singh, K.K. (2015). Human Rev3 DNA Polymerase Zeta localizes to mitochondria and protects the mitochondrial genome. *PLOS One* **13**, e0140409.

Sonoda, E., Sasaki, M.S., Morrison, C., Yamaguchi-Iwai, Y., Takata, M., Takeda, S. (1999). Sister chromatid exchanges are mediated by homologous recombination in vertebrate cells. *Mol Cell Biol* **19**, 5166-5169.

Steitz, T.A., Smerdon, S.J., Jäger, J., Joyce, C.M. (1994). A unified polymerase mechanism for nonhomologous DNA and RNA polymerases. *Science* **266**, 2022-2025.

Steitz, T.A., Steitz, J.A. (1993). A general two-metal-ion mechanism for catalytic RNA. *Proc Natl Acad Sci USA* **90**, 6498-6502.

Stillman, B. (2015). Reconsidering DNA polymerases at the replication fork in eukaryotes. *Mol Cell* **59**, 139-141.

Stojkovic, G., Makarova, A.V., Wanrooij, P.H., Forslund, J., Burgers, P.M., Wanrooij, S. (2016). Oxidative DNA damage stalls the human mitochondrial replisome. *Sci Rep* **6** doi: 10.1038/srep28942.

Stout, G.J., Blasco, M.A. (2009). Genetic dissection of the mechanisms underlying telomere-associated diseases: impact of the TRF2 telomeric protein on mouse epidermal stem cells. *Dis Model Mec* **2**, 139-156.

Stucki, M.B., Pascucci, B., Parlanti, E., Fortini, P., Wilson, S.H., Hubscher, U., Dogliotti, E. (1998). Mammalian base excision repair by DNA polymerases delta and epsilon. *Oncogene* **17**, 835-843.

Sugasawa, K., Okamoto, T., Shimizu, Y., Masutani, C., Iwai, S., Hanaoka, F. (2001). A multiple damage recognition mechanism for global genomic nucleotide excision repair. *Genes Dev* **15**, 507-521.

Temviriyanukul, P., van Hees-Stuivenberg, S., Delbos, F., Jacobs, H., de Wind, N., Jansen, J. (2012). Temporally distinct translesion synthesis pathways for ultraviolet light-induced photoproducts in the mammalian genome.*DNA Repair* **11**, 550-558.

Terret, M.E., Sherwood, R., Rahman, S., Qin, J., Jallepalli, P.V. (2009). Cohesin acetylation speeds the replication fork. *Nature* **462**, 231-234.

Tissier, A., Janel-Bintz, R., Coulon, S., Klaile, E., Kannouche, P., Fuchs, R.P., Cordonnier, A.M. (2010). Crosstalk between replicative and translesional DNA polymerases : PDIP38 interacts direclty with Pol eta. *DNA Repair* **9**, 922-928.

Tormos, K.V., Anso, E., Hamanaka, R.B., Eisenbart, J., Joseph, J., Kalyanaraman, B., Chandel, N.S. (2011). Mitochondrial Complex III ROS Regulate Adipocyte Differentation. *Cell Metab* **14**, 537-544.

Tsaalbi-Shtylik, A., Verspuj, J.W., Jansen, J.G., Rebel, H., Carlée, L.M., van der Val, M.A., Jonkers, J., de Gruijl, F.R., de Wind, N. (2009). Error-prone translesion replication of damaged DNA suppresses skin carcinogenesis by controlling inflammatory hyperplasia. *Proc Natl Acad Sci USA* **106**, 21836-21841.

Uchimura, A., Hidaka, Y., Hirabayashi, T., Hirabayashi, M., Yagi, T. (2009). DNA polymerase delta is required for early mammalian embryogenesis. *PLOS One* **4**, e4184.

Vallerga, M.B., Mansilla, S.F., Federico, M.B., Bertolin, A.P., Gottifredi, V. (2015). Rad51 recombinase prevents Mre11 nuclease-dependent degradation and excessive PrimPol-mediated elongation of nascent DNA after UV irradiation. *Proc Natl Acad Sci USA* **112**, 6624-6633.

van der Ende, A., Baker, T.A., Ogawa, T., Kornberg, A. (1985). Initiation of enzymatic replication at the origin of the Escherichia coli chromosome: primase as the sole priming enzyme. *Proc Natl Acad Sci USA* **82**, 3954-3958.

van de Horst, G.T., Meira, L., Gorgels, T.G., de Wit, J., Velasco-Miguel, S., Richardson, J.A., Kamp, Y., Vreeswijk, M.P., Smit, B., Bootsma, D., Hoeijmakers, J.H., Friedberg, E.C. (2002). UVB radiation-induced cáncer predisposition in Cockayne síndrome group A (Csa) mutant mice. *DNA Repair* **1**, 143-157.

Vartanian, V., Lowell, B., Minko, I.G., Wood, T.G., Ceci, J.D., George, S., Ballinger, S.W., Corless, C.L., McCullough, A.K., Lloyd, R.S. (2006). The metabolic syndrome resulting from a knockout of the NEIL1 DNA glycosylase. *Proc Natl Acad Sci USA* **103**, 1864-1869.

Vreeswijk, M.P., van Hoffen, A., Westland, B.E., Vrieling, H., van Zeeland, A.A., Mullenders, L.H. (1994). Analysis of repair of cyclobutane pyrimidine dimers and pyrimidine 6-4 pyrimidone photoproducts in transcriptionally active and inactive genes in Chinese hamster cells. *J Biol Chem* **269**, 31858-31863.

Walker, L., Minesinger, B., Wiltrout, M., D'Souza, S., Woodruff, G. (2009). Eukaryotic translesion polymerase and their roles and regulation in DNA damage tolerance. *Microbiol Mol Biol Rev* **73**, 134-154.

Wan, L.m Lou, J., Xia, Y., Su, B., Liu, T., Cui, J., Sun, Y., Lou, H., Huang, J. (2013). hPrimPol1/CCDC111 is a human DNA primase-polymerase required for the maintenance of genome integrity. *EMBO Rep* **14**, 1104-1112.

Wang, H., Wu, W., Wang, H.W., Wang, S., Chen, Y., Zhang, X., Yang, J., Zhao, S., Ding, H.F., Lu, D. (2010). Analysis of specialized DNA polymerases expression in human gliomas: association with prognostic significance. *Neuro Oncol* **12**, 679-686.

Wanrooij, S., Fuste, J.M., Farge, G., Shy, Y., Gustafsson, C.M., Falkenberg, M. (2008). Human mitochondrial RNA polymerase primes lagging-strand DNA synthesis in vitro. *Proc Natl Acad Sci USA* **105**, 11122-11127.

Williams, J.S., Kunkel, T.A. Ribonucleotides in DNA: origins, repair and consequences. *DNA Repair* **19**, 27-37.

Weisshart, K., Forster, H., Kremmer, E., Schlott, B., Grosse, F., Nasheuer, H.P. (2000). Protein-protein interactions of the primase subunits p58 and p48 with simian virus 40 T antigen are required for efficient primer synthesis in a cell-free system. *J Biol Chem* **275**, 17328-17337.

Wigler, M., Silverstein, S., Lee, L.S., Pellicer, A., Cheng, Y., Axel, R. (1977). Transfer of purified herpes virus thymidine kinase gene to cultured mouse cells. *Cell* **11**, 223-232.

Wittschieben J.P., Patil, V., Glushets, V., Robinson, L.J., Kusewitt, D.F., Wood, R.D. (2010). Loss of DNA polymerase ζ enhances spontaneous tumorigenesis. *Cancer Res* **70**, 2770-2778.

Wittschieben, J.P., Shivji, M.K., Lalani, E., Jacobs, M.A., Marini, F., Gearhart, P.J., Rosewell, I., Stamp, G., Wood, R.D. (2000). Disruption of the developmentally regulated Rev3L gene causes embryonic lethality. *Curr Biol* **10**, 1217-1220.

Wood, R.D., Doublié, S. (2016). DNA polymerase θ (POLQ), double-strand break repair, and cancer. *DNA repair* **44**, 22-32.

Woodworth, C.D., Michael, E., Smith, L., Vijayachandra, K., Glick, A., Hennings, H., Yuspa, S.H. (2004). Strain-dependent differences in malignant conversion of mouse skin tumors is an inherent property of the epidermal keratinocyte. *Carcinogenesis* **25**, 1771-1778.

Xie, B., Li, H., Wang, Q., Xie, S., Rahmeh, A., Dai, W., Lee, M., M.Y.W.T. (2005). Further characterization of human DNA polymerase delta interacting protein 38. *J Biol Chem* **280**, 22375-22384.

Yan, S., Michael, W.M. (2009). TopBP1 and DNA polymerase-α directly recruit the 9-1-1 complex to stalled DNA replication forks. *J Cell Biol* **184**, 793-804.

Yasukawa, T., Reyes, A., Cluett, T.J., Yang, M.Y., Bowmaker, M., Jacobs, H.T., Holt, I.J. (2006). Replication of vertebrate mitochondrial DNA entails transient ribonucleotide incorporation throughout the lagging strand. *EMBO J* **25**, 5358-5371.

Yoon, J.H., Park, J., Conde, J., Wakami, M., Prakash, L., Prakash, S. (2015). Rev1 promotes replication through UV lesions in conjunction with DNA polymerases η, ι, and κ but not DNA polymerase ζ. *Genes Dev* **29**, 2588-2602.

Yousefzadeh, M.J., Wyatt, D.W., Takata, K., Mu, Y., Hensley, S.C., Tomida, J., Bylund, G.O., Doublié, S., Johansson, E., Ramsden, D.A., McBride, K.M., Wood, R.D. (2014). Mechanism of suppression of chromosomal instability by DNA polymerase POLQ. *PLOS Genet* **10**, e1004654.

Zaidi, M.R., De Fabo, E.C., Noonan, F.P., Merlino, G. (2012). Shedding light on melanocyte pathobiology in vivo. *Cancer Res* **4**, 1591-1595.

Zafar, M..K., Ketkar, A., Lodeiro, M.F., Cameron, C.E., Eoff, R.L. (2014). Kinetic analysis of human PrimPol DNA polymerase activity reveals a generally error-prone enzyme capable of accurately bypassing 7,8-dihydro-8-oxo-2'-deoxyguanosine. *Biochemistry* **53**, 6584-6594.

Zeman, M.K., Cimprich, K.A. (2014). Causes and consequences of replication stress. *Nat Cell Biol* **16**, 2-9.

Zhou, F., Wu, J., Xue, A., Su, Y., Wang, X., Lu, X., Zhou, Z., Qu, J., Zhou, X. (2013). Exome sequencing reveals CCDC111 mutation associated with high myopia. *Hum Genet* **132**, 913-921.

Zou, L., Cortez, D., Elledge, S.J. (2002). Regulation of ATR substrate selection by Rad17-dependent loading of Rad9 complexes onto chromatin. *Genes Dev* **16**, 198-208.

ANNEX I

ANNEX I

Tables containing all the tumors found in the longevity studies according to the histopathology analysis are shown below.

PrimPol +/+	Case	Age (weeks)	Tumor	Location	Staining	IHC
Males	FCB00136	83	B-cell Lymphoma	Mesenteric glangyons	H&E	
	FCB00086	121	Histiocytic sarcoma	Spleen	H&E	
				Liver	H&E	
				Bone Marrow	H&E	
				Pleura	H&E	
				Thymus	H&E	
				Kidney	H&E	
	FCB00066	146	Lymphoma	Intestine	H&E	
				Mesenteric glangyons	H&E	
				Pancreas	H&E	
				Spleen	H&E	
				Salivary gland nodes	H&E	
	FCB00135	141	Lymphoma	Mesenteric glangyons	H&E	
				Spleen	H&E	
				Peyer's Patches	H&E	
	FCB00129	98	Lymphoma	Spleen	H&E	
				Salivary gland nodes	H&E	
				Salivary gland	H&E	
Females	FCB00063	78	B-cell Lymphoma	Spleen	H&E	
				Liver	H&E,	PAX5,CD3
				Adipose tissue	H&E	
				Lymphatic node	H&E	
	FCB00130	83	Lymphoma	Spleen	H&E	PAX5/CD3
				Liver	H&E	
				Lymphatic ganglyons	H&E	
				Adipose tissue	H&E	
				Uterus	H&E	

				Lung	H&E	
	FCB00037	120	Hystiocitic sarcoma	Spleen	H&E	
				Intestine	H&E	
				Bone Marrow	H&E	
				Salivary glands	H&E	
	FCB00065	108	Lymphoma	Spleen	H&E	
				Intestine	H&E	
				Mesenteryc nodes	H&E	
	FCB00062	97	Lymphoma	Spleen	H&E	
	FCB00042	101	Histiocytic sarcoma	Liver	H&E	F4/F80
				Salivary glands	H&E	F4/F80
	FCB00132	116	Lymphoma	Spleen	H&E	
				Liver	H&E	
				Mesenteryc nodes	H&E	
				Nerve ganglion	H&E	
				Lung	H&E	
				Intestine	H&E	

Supplementary Table 1. Tumors found in PrimPol$^{+/+}$ mice in longevity studies.

PrimPol +/-	Case	Age (weeks)	Tumor	Location	Staining	IHC
Males	FCB28	93	Hyperplasia	Red pulp Spleen	H&E	
			Histiocytic sarcoma	Lung	H&E	F4/F80
				Liver	H&E	F4/F81
	FCB81	71	Adenoma	Accesory ocular gland	H&E	
			B-cell Lymphoma	Spleen	H&E	Pax5/CD3
				Lymphatic ganglyons	H&E	
				Kidney	H&E	
				Bone Marrow	H&E	
				Lung	H&E	
				Intestine	H&E	
				Testis	H&E	
	FCB212	56	Hystiocitic sarcoma	Salivary glands	H&E	F4/F80
				Spleen	H&E	
				Bone Marrow	H&E	
	FCB35	96	Hystiocitic sarcoma	Liver	H&E	
				Testis	H&E	
				Epididium	H&E	
	FCB51	113	Adenoma	Lung	H&E	
	FCB72	121	Histiocytic sarcoma	Liver	H&E	F4/F80
			Lymphoma	Salivary glands	H&E	Pax5/CD3
	FCB26	120	Lymphoma	Spleen	H&E	
	FCB44	120	Adenoma	Intestine	H&E	
			Histiocytic sarcoma	Spleen	H&E	
	FCB71	117	Histiocytic sarcoma	Spleen	H&E	
				Liver	H&E	
			Adenoma X2	Lung	H&E	
	FCB213	132	Hepatocarcinoma	Liver	H&E	aFP
					H&E	
					H&E	
					H&E	
Females	FCB00061	78	Lymphoma	Spleen	H&E	Pax5/CD3
				Bone Marrow	H&E	
				Salivary glands	H&E	
				Lymphatic ganglyons	H&E	

				Adipose tissue	H&E	
	FCB79	110	Lymphoma	Spleen	H&E	
				Kidney	H&E	
	FCB68	100	Follicular lymphoma	Spleen	H&E	
	FCB38	93	Histiocytic sarcoma	Spleen	H&E	
				Mesenteryc node	H&E	
				Kidney	H&E	
				Liver	H&E	
				Intestine	H&E	
				Uterus	H&E	
				Lung	H&E	
				Salivary glands nodes	H&E	
				Pancreas	H&E	
	FCB70	126	Lymphoma	Mesenteryc node	H&E	
				Adipose tissue	H&E	
				Bladder	H&E	
				Lung	H&E	
				Kidney	H&E	
				Liver	H&E	
				Spleen	H&E	
				Serous stomach	H&E	
	FCB130	83	Follicular lymphoma	Liver	H&E	
				Kidney	H&E	
				Spleen	H&E	
				Bone Marrow	H&E	
				Lung	H&E	
				Stomach	H&E	
				thyroid gland	H&E	
				Salivary gland	H&E	
				Salivary gland nodes	H&E	
				Traquea	H&E	
				Adipose tissue	H&E	
				Mesenteryc node	H&E	

Supplementary Table 2. Tumors found in PrimPol$^{+/-}$ mice in longevity studies.

PrimPol -/-	Case	Age (weeks)	Tumor	Location	Staining	IHC
Males	FCB00027	86	B-cell lymphoma	Spleen	H&E	CD3/PAX5/F4/80
				Liver	H&E	CD3/PAX5/F4/81
				Kidney	H&E	
			Chronic pancreatitis	Pancreas	*H&E*	
			Enteritis	Intestine	*H&E*	
	FCB00088	58	B-cell lymphoma	Lymphatic ganglyons	H&E	CD3, PAX5
				Spleen	H&E	CD3, PAX5
				Bone Marrow	H&E	
				Thymus	H&E	
				Liver	H&E	
				Lung	H&E	
				Intestine	H&E	
				Testis	H&E	
				Pancreas	H&E	
	FCB00034	101	Adenoma	Lung	H&E	
	FCB93	111	Hepatocarcinoma	Liver	H&E	
	FCB231	94	Angiosarcoma	Salivary glands	H&E	CD31
	FCB73	131	Adenoma	Lung	H&E	
	FCB75	135	Hepatocarcinoma	Liver	H&E	F4/80
			Hystiocitic sarcoma	Spleen	H&E	
	FCB00089	75	Hepatocarcinoma	Liver	H&E	aFP
	FCB90	128	Histiocytic sarcoma	Spleen	H&E	
			Hemangiosarcoma	Intesinte	H&E	
	FCB84	129	Hepatocarcinoma	Liver	H&E	aFP
			Adenoma	Lung	H&E	
Females	FCB00080	87	Fibrosarcoma	Muscle	H&E	
				Mammary glands	H&E	
				Adipose tissue	H&E	
			Lymphoma	Spleen	H&E	CD3/PAX5
				Bone Marrow	H&E	CD3/PAX5
			Plasmacytoma ??	Spleen	H&E	
	FCB00094	71	B-cell lymphoma	Spleen	H&E	CD3/PAX5
				Liver	H&E	
				Lymphatic ganglyons	H&E	
				Salivary	H&E	

				glands		
				Bone Marrow	H&E	
				Intestine	H&E	
				Lung	H&E	
				Stomach	H&E	
				Uterus	H&E	
				Muscle	H&E	
	FCB000241	89	B-cell lymphoma	Lymphatic nodes	H&E	
				Liver	H&E	
	FCB00114	108	Lymphoma	Spleen	H&E	
				Kidney	H&E	
				Liver	H&E	
				Lymphatic nodes	H&E	
				Lung	H&E	
				Thymus	H&E	
				Bone Marrow	H&E	
				Salivary glands	H&E	
				Thyroid	H&E	
				Traquea	H&E	
				Serous Stomach	H&E	
				Intesinte	H&E	
			Histiocytic sarcoma	Spleen	H&E	
				Bone Marrow	H&E	
				Liver	H&E	
	FCB00050	85	Lymphoma	Spleen	H&E	
				Liver	H&E	
	FCB00125	107	B-cell lymphoma	Spleen	H&E	
				Liver	H&E	
				Lymphatic nodes	H&E	
				Heart (auricula)	H&E	
				Traquea	H&E	
				Lung	H&E	
				Salivary glands	H&E	
				Thyroid	H&E	
				Kidney	H&E	
				Ovary	H&E	
				Adipose tissue	H&E	
				Bone Marrow	H&E	

				Intestine	H&E	
				Stomach (Serous)	H&E	
	FCB53	89	Lymphoma	Spleen	H&E	
				Kidney	H&E	
				Pancreas	H&E	
				Lung	H&E	
				Heart (ventricle)	H&E	
				Thymus	H&E	
				Salivary glands	H&E	
				Bone Marrow	H&E	
				Muscle	H&E	
				Intestine	H&E	
				Adipose tissue	H&E	
				Mesenteric nodes	H&E	
				Uterus	H&E	
				Liver	H&E	
				Serous Stomach	H&E	
				Skin	H&E	
	FCB226	94	Papillomas	Stomach	H&E	
			Lymphoma	Intesinte	H&E	
				Mesenteric nodes	H&E	
				Adipose tissue	H&E	
				Kidney	H&E	
				Salivary glands	H&E	
	FCB129	128	Papilloma	Ovary	H&E	
			Lymphoma	Spleen	H&E	

Supplementary Table 3. Tumors found in PrimPol$^{-/-}$ mice in longevity studies.

ANNEX II

ANNEX II

During this Doctoral Thesis I contributed in the following publications:

1. Alvarez, S., **Díaz, M.**, Flach, J., Rodríguez-Acebes, S., López-Contreras, A.J., Martínez, D., Cañamero, M., Fernández-Capetillo, O., Isern, J., Passegué, E., Méndez, J. (2015). "Replication stress caused by low MCM expression limits fetal erythropoiesis and hematopoietic stem cell funcionality". *Nature Communications* **6**, 8548. doi: 10.1038/ncomms9548, 2015.

2. Murga, M., Lecona, E., Kamileri, I., **Díaz, M.**, Lugli, N., Sotiriou, S.K., Anton, M.E., Méndez, J., Halazonetis, T.D., Fernandez-Capetillo, O. (2016). "POLD3 is haploinsufficient for DNA replication in mice". *Molecular Cell* **63**, 877-883.